Functional analysis of Mushroom body miniature's RGG-box and its role in neuroblast proliferation in *Drosophila melanogaster*

Dissertation zur Erlangung des wissenschaftlichen Doktorgrades

der Julius-Maximilians-Universität Würzburg

Vorgelegt von

Heiko Hartlieb

aus Heilbronn

Würzburg, 2019

Eingereicht am: ……………………………………………………………………

Mitglieder der Promotionskommission:

Vorsitzender:

Gutachter: Prof. Dr. Thomas Raabe

Gutachter: Prof. Dr. Peter Gallant

Tag des Promotionskolloquiums: …………………………………………….

Doktorurkunde ausgehändigt am: …………………………………………..

Eidesstattliche Erklärungen nach §7 Abs. 2 Satz 3, 4, 5
der Promotionsordnung der Fakultät für Biologie

Eidesstattliche Erklärung

Hiermit erkläre ich an Eides statt, die Dissertation: „**Funktionelle Analyse der RGG-Box von Mushroom body miniature und deren Rolle in der Neuroblastenproliferation in *Drosophila melanogaster***", eigenständig, d. h. insbesondere selbständig und ohne Hilfe eines kommerziellen Promotionsberaters, angefertigt und keine anderen, als die von mir angegebenen Quellen und Hilfsmittel verwendet zu haben.

Ich erkläre außerdem, dass die Dissertation weder in gleicher noch in ähnlicher Form bereits in einem anderen Prüfungsverfahren vorgelegen hat.

Weiterhin erkläre ich, dass bei allen Abbildungen und Texten bei denen die Verwertungsrechte (Copyright) nicht bei mir liegen, diese von den Rechtsinhabern eingeholt wurden und die Textstellen bzw. Abbildungen entsprechend den rechtlichen Vorgaben gekennzeichnet sind sowie bei Abbbildungen, die dem Internet entnommen wurden, der entsprechende Hypertextlink angegeben wurde.

Affidavit

I hereby declare that my thesis entitled: „**Functional analysis of Mushroom body miniature's RGG-box and its role in neuroblast proliferation in *Drosophila melanogaster***" is the result of my own work. I did not receive any help or support from commercial consultants. All sources and / or materials applied are listed and specified in the thesis.

Furthermore I verify that the thesis has not been submitted as part of another examination process neither in identical nor in similar form.

Besides I declare that if I do not hold the copyright for figures and paragraphs, I obtained it from the rights holder and that paragraphs and figures have been marked according to law or for figures taken from the internet the hyperlink has been added accordingly.

Würzburg, den 11.11.2019

_____

Signature PhD-student

Table of Contents

1. Summary

Development of the central nervous system in *Drosophila melanogaster* relies on neural stem cells called neuroblasts. Neuroblasts divide asymmetrically to give rise to a new neuroblast as well as a small daughter cell which eventually generates neurons or glia cells. Between each division, neuroblasts have to re-grow to be able to divide again. In previous studies, it was shown that neuroblast proliferation, cell size and the number of progeny cells is negatively affected in larvae carrying a P-element induced disruption of the gene *mushroom body miniature* (*mbm*). This *mbm* null mutation called *mbm^{SH1819}* is homozygously lethal during pupation. It was furthermore shown that the nucleolar protein Mbm plays a role in the processing of ribosomal RNA (rRNA) as well as the translocation of ribosomal protein S6 (RpS6) in neuroblasts and that it is a transcriptional target of Myc. Therefore, it was suggested that Mbm might regulate neuroblast proliferation through a role in ribosome biogenesis.

In the present study, it was attempted to further elucidate these proposed roles of Mbm and to identify the protein domains that are important for those functions. Mbm contains an arginine/glycine rich region in which a di-RG as well as a di-RGG motif could be found. Together, these two motifs were defined as Mbm's RGG-box. RGG-boxes can be found in many proteins of different families and they can either promote or inhibit protein-RNA as well as protein-protein interactions. Therefore, Mbm's RGG-box is a likely candidate for a domain involved in rRNA binding and RpS6 translocation. It could be shown by deletion of the RGG-box, that Mbm^{dRGG} is unable to fully rescue survivability and neuroblast cell size defects of the null mutation *mbm^{SH1819}*. Furthermore, Mbm does indeed rely on its RGG-box for the binding of rRNA *in vitro* and in *mbm^{dRGG}* as well as *mbm^{SH1819}* mutants RpS6 is partially delocalized. Mbm itself also seems to depend on the RGG-box for correct localization since Mbm^{dRGG} is partially delocalized to the nucleus. Interestingly, protein synthesis rates are increased in *mbm^{dRGG}* mutants, possibly induced by an increase in TOR expression. Therefore, Mbm might possess a promoting function in TOR signaling in certain conditions, which is regulated by its RGG-box. Moreover, RGG-boxes often rely on methylation by protein arginine methyltransferases (in *Drosophila*: Darts – *Drosophila* arginine methyltransferases) to fulfill their functions. Mbm might be symmetrically dimethylated within its RGG-box, but the results are very equivocal. In any case, Dart1 and Dart5 do not seem to be capable of Mbm methylation.

Additionally, Mbm contains two C_2HC type zinc-finger motifs, which could be involved in rRNA binding. In an earlier study, it was shown that the mutation of the zinc-fingers, *mbm^{ZnF}*, does not lead to changes in neuroblast cell size, but that Mbm^{ZnF} is delocalized to the cytoplasm. In the present study, *mbm^{ZnF}* mutants were included in most experiments. The results, however, are puzzling since *mbm^{ZnF}* mutant larvae exhibit an even lower viability than the *mbm* null mutants and Mbm^{ZnF} shows stronger binding to rRNA than wild-type Mbm. This suggests an unspecific interaction of Mbm^{ZnF} with either another protein, DNA or RNA, possibly leading to a dominant negative effect by disturbing other interaction partners. Therefore, it is difficult to draw conclusions about the zinc-fingers' functions.

In summary, this study provides further evidence that Mbm is involved in neuroblast proliferation as well as the regulation of ribosome biogenesis and that Mbm relies on its RGG-box to fulfill its functions.

2. Zusammenfassung

Die Entwicklung des zentralen Nervensystems von *Drosophila melanogaster* beruht auf neuronalen Stammzellen genannt Neuroblasten. Neuroblasten teilen sich asymmetrisch und bringen dabei sowohl einen neuen Neuroblasten als auch eine kleinere Tochterzelle hervor, die wiederum letztlich Neuronen oder Gliazellen generiert. Zwischen jeder Zellteilung müssen die Neuroblasten wieder auf ihre ursprüngliche Größe wachsen, sodass sie zur erneuten Teilung in der Lage sind. In vorhergehenden Studien konnte gezeigt werden, dass sowohl die Proliferation der Neuroblasten, deren Zellgröße als auch die Anzahl ihrer Tocherzellen reduziert ist in Larven, die eine P-Element-induzierte Unterbrechung des Gens *mushroom body miniature* (*mbm*) tragen. Diese *mbm*-Nullmutation, genannt *mbm^{SH1819}*, ist homozygot letal während des Puppenstadiums. Es konnte außerdem gezeigt werden, dass das nucleoläre Protein Mbm eine Rolle in der Prozessierung ribosomaler RNA (rRNA), sowie der Translokation des ribosomalen Proteins S6 (RpS6) in Neuroblasten erfüllt und dass seine Transkription durch Myc reguliert wird. Daher wurde geschlussfolgert, dass Mbm die Proliferation von Neuroblasten durch eine Funktion in der Ribosomenbiogenese regulieren könnte.

In der vorliegenden Studie wurde das Ziel verfolgt, weitere Hinweise auf diese möglichen Funktionen von Mbm zu finden und die Proteindomänen zu identifizieren, die dafür benötigt werden. Mbm beinhaltet einen Arginin/Glycin-reichen Abschnitt, der ein di-RG sowie ein di-RGG Motiv enthält. Diese beiden Motive wurden zusammen zu Mbms RGG-Box definiert. RGG-Boxen finden sich in vielen Proteinen verschiedener Familien und sie können sich sowohl verstärkend als auch inhibierend auf Protein-RNA- sowie Protein-Protein-Interaktionen auswirken. Somit stellt Mbms RGG-Box einen vielversprechenden Kandidaten dar für eine Proteindomäne, die in die rRNA-Bindung sowie die Translokation von RpS6 involviert ist. Es konnte gezeigt werden, dass Mbm mit deletierter RGG-Box (Mbm^{dRGG}) nicht in der Lage ist, die Überlebensfähigkeit und die Neuroblastengröße der Nullmutation *mbm^{SH1819}* vollständig zu retten. Des Weiteren benötigt Mbm die RGG-Box, um rRNA *in vitro* zu binden und in *mbm^{dRGG}* sowie *mbm^{SH1819}* Mutanten konnte eine partielle Delokalisation von RpS6 beobachtet werden. Die korrekte Lokalisation von Mbm selbst scheint auch von der RGG-Box abzuhängen, da Mbm^{dRGG} teilweise in den Nukleus delokalisiert ist. Interessanterweise ist außerdem die Proteinsyntheserate in *mbm^{dRGG}* Mutanten erhöht, was möglicherweise in einer Erhöhung der TOR-Expression begründet ist. Somit könnte Mbm unter bestimmten Bedingungen eine verstärkende Funktion im TOR-

Signalweg erfüllen, die durch seine eigene RGG-Box reguliert wird. Des Weiteren sind RGG-Boxen hinsichtlich ihrer Funktion häufig von der Methylierung durch Protein-Arginin-Methyltransferasen (in *Drosophila*: Darts – *Drosophila* arginine methyltransferases) abhängig. Mbm könnte innerhalb seiner RGG-Box symmetrisch dimethyliert sein, allerdings sind die Ergebnisse in dieser Hinsicht sehr zweifelhaft. Jedenfalls scheinen Dart1 und Dart5 nicht imstande zu sein, Mbm zu methylieren.

Außerdem beinhaltet Mbm zwei Zink-Finger-Motive des C_2HC-Typs, die in die Bindung von rRNA involviert sein könnten. Eine vorhergehende Studie konnte zeigen, dass die Mutation der Zink-Finger, mbm^{ZnF}, zwar nicht zu einer Veränderung der Neuroblastengröße führt, allerdings, dass Mbm^{ZnF} ins Zytoplasma delokalisiert vorliegt. In der vorliegenden Studie wurden die mbm^{ZnF} Mutanten in die meisten Experimente mit einbezogen. Allerdings sind die Ergebnisse rätselhaft, da mbm^{ZnF}-mutierte Larven sogar eine geringere Überlebensrate zeigen als die mbm Nullmutanten und da Mbm^{ZnF} eine stärkere Bindungsaffinität zu rRNA zeigt als wildtypisches Mbm. Dies weist auf eine unspezifische Interaktion zwischen Mbm^{ZnF} und einem anderen Protein, RNA oder DNA hin, was einen dominant-negativen Effekt auslösen könnte, indem andere Interaktionspartner gestört werden. Somit gestaltet es sich schwierig, Schlussfolgerungen zur Funktion der Zink-Finger zu ziehen.

Zusammengefasst liefert die vorliegende Studie weitere Anhaltspunkte, dass Mbm in der Neuroblastenproliferation sowie der Regulation der Ribosomenbiogenese involviert ist und dass Mbm seine RGG-Box benötigt, um seine Funktionen zu erfüllen.

3. Introduction

3.1. Neurogenesis in *Drosophila melanogaster*

Drosophila melanogaster is a widely used model organism for developmental and neurobiology research. It found its way into laboratories as early as around 1900 and it has since become the number one genetic system due to being easy to maintain and to modify genetically (Kohler, 1994; Tolwinski, 2017). Therefore and due to the key features of neuronal development of higher species being present in *Drosophila*, it is a very good model organism to study brain development (Homem and Knoblich, 2012). The brain or central nervous system (CNS) of *Drosophila* consists of the central brain (CB), the optic lobes (OL) and the ventral nerve cord (VNC). It is built up during neurogenesis in the embryonic and larval stages by neural progenitor cells called neuroblasts (NBs). NBs are the neural stem cells in *Drosophila* and are therefore studied to shed light into stem cell biology (Homem & Knoblich, 2012). Early during the embryonal development – between embryonic stages 8 and 11 – the NBs from which the CB and VNC arise delaminate from the neuro-ectoderm in the embryo's ventrolateral region (Campos-Ortega & Hartenstein, 1997; Homem and Knoblich, 2012). In the case of the VNC, the NB fate is decided for only one cell in a neural equivalence group of 5 to 6 cells (Egger et al., 2008) by a positive feedback loop in Delta/Notch signaling and expression of *achaete-scute* (*ac/sc*) genes. *ac/sc* genes which promote the NB fate (Villares and Cabrera, 1987; Gonzalez et al., 1989) induce Delta signaling to neighboring cells, thereby activating Notch which leads to *ac/sc* down-regulation in these cells and induction of the epidermal cell fate (Skeath and Carroll, 1992). Thus, the cell that initially exhibits the highest *ac/sc* expression levels within an equivalence group will acquire the NB cell fate (Martin-Bermudo et al., 1991; Cubas et al., 1991; Skeath and Carroll, 1991; reviewed in Skeath and Thor, 2003; Figure 1). Approximately 50 % of NBs, however, lack *ac/sc* function meaning that other NB cell fate determinants must exist (Jimenez and Campos-Ortega, 1990) with *seven-up* and *huckebein* being potential candidates (Doe, 1992).

In the case of the central brain, NB delamination is more complex. The procephalic neuroectoderm is divided into several mitotic domains within which the cell cycle entry of all cells is synchronized (Foe, 1989). These mitotic domains also exhibit different modes of NB delamination (Urbach et al., 2003; Urbach and Technau, 2004). In mitotic domain B, instead of producing NBs by division, neuroectodermal cells enlarge on the basal side and then delaminate as NBs (Figure 2A). In mitotic domains 1, 2 and 5, cells divide in parallel to the ectodermal layer and then one of the daughter cells delaminates as a NB (Figure 2B). In
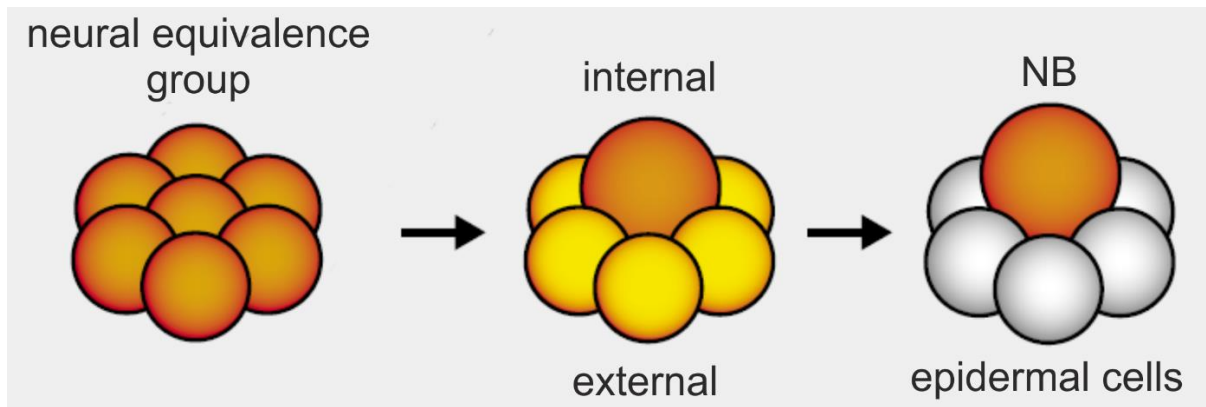
Figure 1: Neuroblast cell fate decision
In a neural equivalence group, *achaete-scute* (*ac/sc*) genes are at first approximately evenly expressed (orange). The cell with the highest *ac/sc* expression laterally inhibits *ac/sc* expression in the other cells of the group through Delta/Notch signaling (yellow) and becomes the only neuroblast of the cell cluster (figure modified from Skeath and Thor (2003) with permission from Elsevier).

mitotic domain 9, there are two different modes of NB formation. In one case, neuroectodermal cells delaminate from the layer in apical direction, then reintegrate and either delaminate in basal direction as NBs or remain in the layer as epidermoblasts (Figure 2Ca). In the other case, the cells divide along the apical-basal axis with the basal daughter cell becoming a NB while the apical daughter cell integrates into the ectodermal layer as an epidermoblast (Figure 2Cb; Urbach et al., 2003; Urbach and Technau, 2004). Like in the VNC, the NB fate is decided in cell clusters which express proneural genes of the *ac/sc* group, but these clusters significantly vary in size. While the small clusters of five to seven cells only produce one NB similar to the clusters in the VNC, in the larger clusters several adjacent cells can adopt the NB fate due to less efficient lateral inhibition by Delta/Notch signaling (Urbach et al., 2003). Unlike CB and VNC neuroblasts, the ~800 OL NBs were long believed to arise from neuroepithelial cells during larval stages only (Egger et al., 2007; Harding and White, 2018). Newer results, however, show that OL NBs are already generated by the neuroepithelium during embryonic stages (Hakes et al., 2018). In mid-larval stages, the neuroepithelial cells then transform into OL NBs (Yasugi et al., 2008).

After delamination, the NBs start to divide in a self-renewing manner (Reichert, 2011), generating a new NB as well as ganglion mother cells (GMC) or intermediate neural progenitors (INP) which in the end generate neurons or glia cells (reviewed in Homem and Knoblich, 2012). This phase in brain development is known as the first wave of neurogenesis during which all cells composing the larval CNS, but only about 10 % of the adult CNS are generated (Prokop and Technau, 1991; Green et al., 1993; Homem and Knoblich, 2012). In the embryonic stages, the NBs do not regrow between each division and therefore become
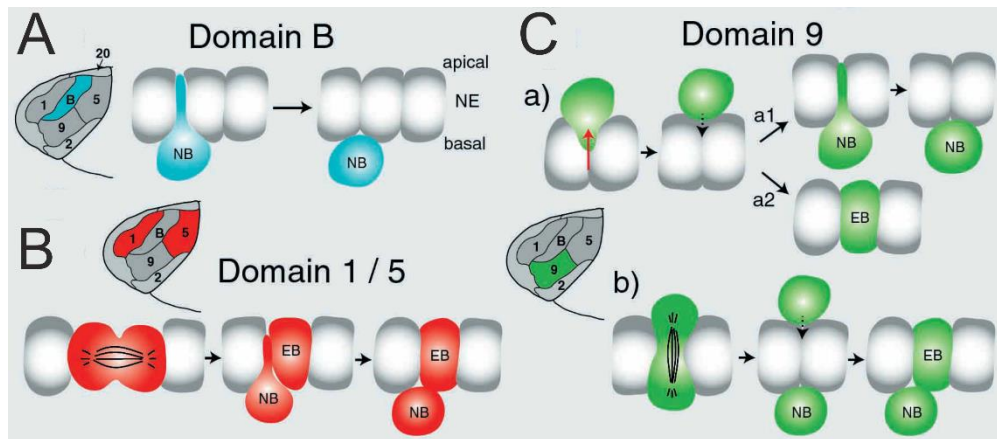
Figure 2: Neuroblast formation in the procephalic neuroectoderm
NB formation differs between mitotic domains. **A** In domain B, neuroectodermal cells enlarge on the apical side and delaminate as NBs. The scheme on the left shows the positions of the mitotic domains in the procephalic ectoderm in lateral view. **B** In domains 1, 2 and 5, the ectodermal cells divide parallel to the layer and one daughter cell delaminates as a NB. **C** In mitotic domain 9, two modes of NB formation can occur. **Ca)** Neuroectodermal cells move to the apical side, then re-enter the layer and either delaminate as a NB or stay as an epidermoblast (EB). **Cb)** Neuroectodermal cells divide along the apical-basal axis. The apical daughter cell re-enters the layer as an EB, the basal progeny delaminates as a NB (figure modified from Urbach et al. (2003) with permission from The Company of Biologists Ltd.).

progressively smaller until they enter a quiescent state or undergo apoptosis before larval hatching (Figure 3). Quiescence might be initiated by the reduction in NB cell size between each division (Hartenstein et al., 1987) and apoptosis is induced by the *reaper* gene (Peterson et al., 2002). A newer study could show that NB quiescence is initiated by a pulse of transient nuclear Prospero, a protein that is otherwise known as a cell fate determinant in asymmetric NB division (see 3.1.2.), but the exact mechanism remains unclear (Lai and Doe, 2014; Harding and White, 2018). The ratio of NBs entering quiescence versus those undergoing programmed cell death differs between embryonal segments: out of 30 abdominal NBs only three enter quiescence while 20 out of 30 thoracic NBs persist into the larval stages (Truman and Bate, 1988; Prokop and Technau, 1991; White et al., 1994). Recently, it was shown that 75 % of NBs enter quiescence during the G2 phase of the cell cycle while the remaining 25 % exit the cell cycle in G0 phase (Otsuki and Brand, 2018). Entry into G2 quiescence as well as maintaining the quiescent state into larval stages is regulated by the pseudokinase *tribbles*. Furthermore, it was found that NBs in G2 quiescence are reactivated more quickly than those in G0 quiescence which might be important for producing neural circuits in the correct order (Otsuki and Brand, 2018). The NBs re-enter the cell cycle after larval hatching (ALH), starting the second wave of neurogenesis during which the remaining 90 % of the CNS are generated. The exact point in time at which the NBs re-enter the cell cycle differs between tissues with CB NBs starting between eight and ten hours ALH, followed by OL NBs after ten to twelve hours, the thoracic NBs after 28 hours and the abdominal NBs ~50 hours ALH

(Truman and Bate, 1988; Prokop and Technau, 1991; Ebens et al., 1993; Green et al., 1993; Datta, 1995; Sousa-Nunes et al., 2011). Cell cycle re-entry depends on nutrient sensing pathways and does not occur under lack of amino acid intake (Sousa-Nunes et al., 2011; Chell and Brand, 2010; Harding and White, 2018). Glia cells in close proximity to the neuroblasts regulate NB reactivation through secretion of insulin-like peptides 2/6 (dILP2/6), thereby initiating cell cycle re-entry through Akt signaling (Chell and Brand, 2010). However, it was noted that dILP2/6 secretion alone is not sufficient for full NB reactivation. It was furthermore shown that glial cells regulate NB quiescence and proliferation through secretion of *anachronism*, *terribly reduced optic lobes* and *dally-like*, but the respective mechanisms remain unclear (Ebens et al., 1993; Datta, 1995; Voigt et al., 2002; Kanai et al., 2018; Harding and White, 2018). Following reactivation, NBs regrow between each division, which enables them to divide more often. During the pupal stages, however, the NBs become smaller once again and while abdominal NBs eventually are eliminated by apoptosis through expression of *reaper*, *grim* and *sickle*, thoracic and CB NBs undergo a final symmetrical division (Ito and Hotta, 1992; Maurange et al., 2008; Peterson et al., 2002; Tan et al., 2011 Siegrist et al., 2010; Harding and White, 2018; Figure 3). This final differentiation is initiated by the nuclear accumulation of Prospero, leading to differentiation by down-regulation of self-renewal genes (Maurange et al., 2008; Choksi et al., 2006).
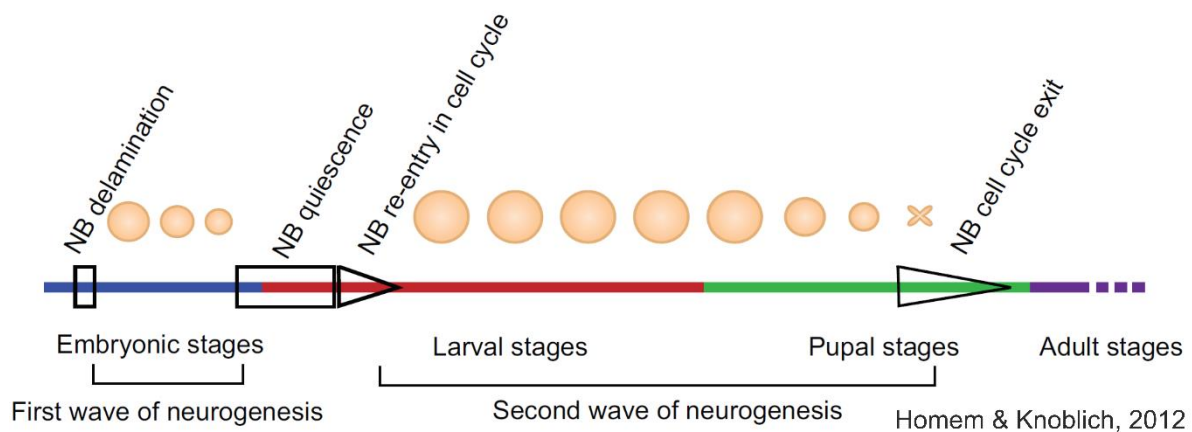
Figure 3: Neurogenesis in *Drosophila melanogaster*
During the first wave of neurogenesis in embryonic stages 8 to 11 the neuroblasts (NB) delaminate from the neuro-ectoderm and start dividing growing progressively smaller until they undergo apoptosis or enter quiescence. Early in the larval stages the NBs re-enter the cell cycle now re-growing between each division. This second wave of neurogenesis ends in the pupal stage when NBs become smaller once again and undergo apoptosis or final differentiation (figure from Homem & Knoblich (2012) with permission from The Company of Biologists Ltd).

Many neuroblast cell fate decisions like apoptosis or final differentiation are regulated by the so-called temporal series, which is characterized by sequentially expressed transcription

factors (Maurange et al., 2008; Harding and White, 2018). The exact temporal transcription factor (TTF) series, however, varies between different NB populations (reviewed in Doe, 2017). Most embryonic type I NBs, for example, sequentially express Hunchback (Hb) → Krüppel (Kr) → Pdm → Castor (Cas) → Grainyhead (Grh) and each of these TTFs specifies the identity of NB progeny and thus ensures the generation of the correct neurons in their respective time frame (Figure 4). Grh, however, has also been shown to regulate apoptosis as well as proliferation of NBs, which might in turn be regulated by Hox genes (Cenci and Gould, 2005; Almeida and Bray, 2005; Harding and White, 2018). Furthermore, some of these TTFs are repressed by their respective successor in the series: Kr is repressed by Pdm, Pdm is repressed by Cas and Cas is repressed by Grh (Grosskortenhaus et al., 2006; Tran and Doe, 2008; Kambadur et al., 1998; Tsuji et al., 2008; Baumgardt et al., 2009). Thereby, the unidirectional cascade of TTF expression is ensured (Doe, 2017).
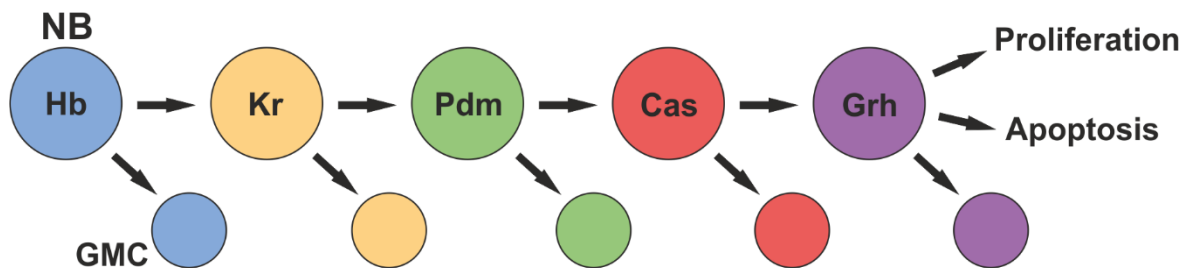
Figure 4: The temporal transcription factor (TTF) series
The TTF expression sequence in embryonic type I neuroblasts (NB). Each TTF specifies the cell fate of the progeny in the respective time frame (HB = Hunchback; Kr = Krüppel; Cas = Castor; Grh = Grainyhead; GMC = ganglion mother cell). Grainyhead also regulates proliferation and apoptosis in neuroblasts (figure adapted from Harding and White (2018), licensed under CC BY 4.0).

3.1.1. Neuroblasts in the 3rd instar larval central brain

In the 3rd instar larval CB there are around 105 neuroblasts per brain hemisphere (Urbach et al., 2003; Urbach and Technau, 2003a; Urbach and Technau, 2003b). There are, however, not a single but three different types of NBs: approximately 90 type I and eight type II neuroblasts which differ in their mode of division (reviewed in Homem and Knoblich, 2012) as well as four mushroom body neuroblasts (MBNBs). The MBNBs build up the MB and do not enter quiescence between the first and second wave of neurogenesis (Ito and Hotta, 1992; Figure 5).

Type I NBs divide asymmetrically into a new neuroblast and a ganglion mother cell (GMC). Type II NBs, in contrast, divide into a new NB and an immature intermediate neural progenitor (INP). The immature INP then matures by changes in gene transcription and divide asymmetrically for three to five times (Bello et al., 2008), generating a new INP as well as a GMC. The GMCs in both the type I and type II NB lineages divide symmetrically into two neurons or glia cells (Homem & Knoblich, 2012; Figure 6). Thereby, each type II NB on average generates 450 neural cells while type I NB lineages comprise only about 100 to 120 neural cells on average (Izergina et al., 2009; Bello et al., 2008). However, there is an additional mode of NB division in the embryonic VNC, leaving out the GMC intermediate: type 0 NBs divide into a new NB and a terminally differentiated neuron (Baumgardt et al., 2014; Karcavich and Doe, 2005, Baumgardt et al., 2009). Type 0 NBs previously divide in type I mode and then undergo a switch to type 0, which is suggested to be regulated by the temporal series (Harding and White, 2018).

Type I and type II NB lineages can be distinguished by several differentially expressed transcription factors (Figure 6). Both NB types express Deadpan (Dpn) which plays an important role in self-renewing neural precursors in *Drosophila* (Homem and Knoblich, 2012; Wallace et al., 2000), but only type I NBs express Asense (Ase; Bowman et al., 2008). In type II NBs, Ase expression is assumed to be suppressed by an isoform of Pointed (PntP1) which induces the type II NB cell fate and therefore is absent in type I NBs (Zhu et al., 2011). Furthermore, it was recently shown that PntP1 and other components of the epidermal growth factor (EGF) signaling pathway are also required for the specification of type II NBs during

embryogenesis (Walsh and Doe, 2017; Alvarez and Diaz-Benjumea, 2018; Harding and White, 2018). In contrast to NBs, immature INPs lack both Ase as well as Dpn. During maturation, which takes four to six hours, INPs do not divide but re-start expression of Ase and Dpn and then start dividing asymmetrically (Bayraktar et al., 2010). Furthermore, maturing INPs start to express Earmuff (Erm) which is suggested to limit proliferation and eventually promote terminal differentiation of INPs (Li et al., 2016; Homem and Knoblich, 2012; Weng et al., 2010). Both the type I NBs and the INPs in the type II NB lineage give rise to GMCs which lack expression of all the transcription factors mentioned above (Bayraktar et al., 2010). In summary, type I NBs are Dpn$^+$, Ase$^+$, Erm$^-$ and PntP1$^-$, type II NBs are Dpn$^+$, Ase$^-$, Erm$^-$ and PntP1$^+$, only mature INPs are Dpn$^+$, Ase$^+$ and Erm$^+$ and GMCs show no expression of these transcription factors (Figure 6).
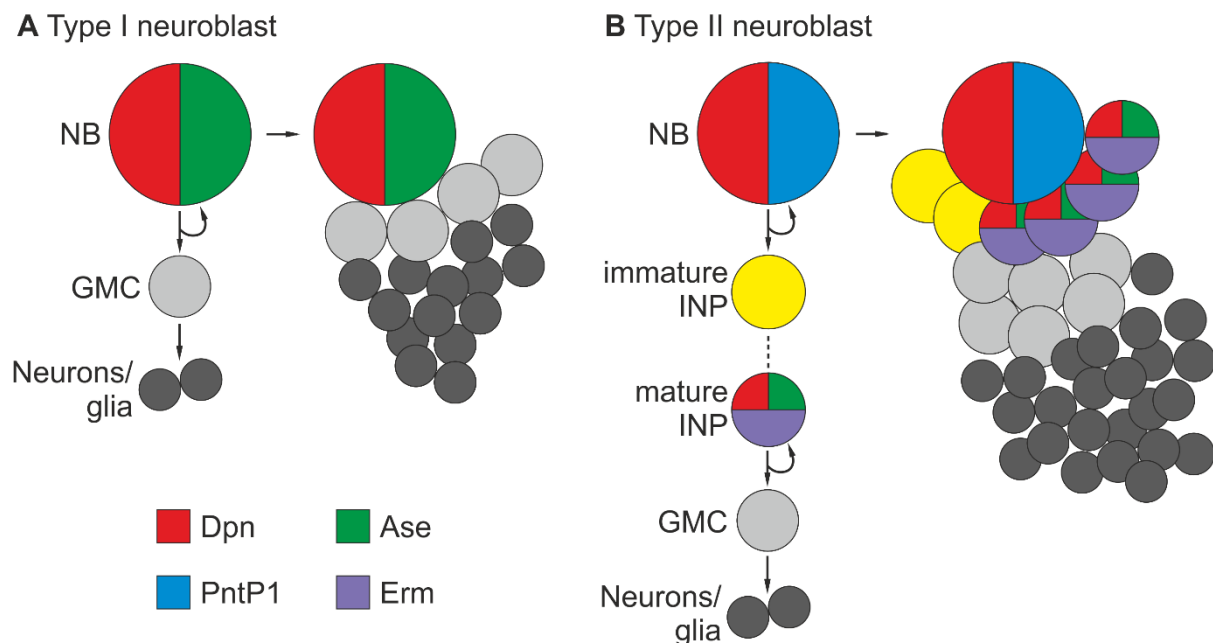
Figure 6: Type I and type II neuroblast lineages
A Type I neuroblasts (NBs) are Dpn$^+$ (red) and Ase$^+$ (green) and divide asymmetrically into a new NB and a ganglion mother cell (GMC; light grey) which divides symmetrically into neurons or glia cells (dark grey). **B** Type II NBs are Dpn$^+$ (red) and PntP1$^+$ (blue) and divide symmetrically into a new NB and an immature intermediate neural progenitor (INP; yellow) which then matures and expresses Dpn (red), Ase (green) as well as Erm (purple). Mature INPs divide asymmetrically to self-renew and produce a GMC (light gray) which divides symmetrically into neurons or glia cells (dark grey). The coloring of NBs and INPs does not indicate polarized localization of the mentioned transcription factors (figure adapted from Homem & Knoblich (2012) with permission from The Company of Biologists Ltd).

3.1.2. Asymmetric division of neuroblasts

Self-renewing asymmetric division and the generation of all cell types in their respective tissue is a feature characteristic for stem cells (Hall and Watt, 1989; Potten and Loeffler, 1990; Morrison et al., 1997). As mentioned earlier, neuroblasts are the neural stem cells in *Drosophila* and are being used as a model to study stem cell biology (Homem & Knoblich, 2012). In contrast to germline stem cells, for example, the asymmetric division of NBs does not depend on extrinsic signals or an external axis and they are therefore capable of self-renewing asymmetric divisions even in cell culture (Homem & Knoblich, 2012; Datta, 1999; Ceron et al., 2006; Rebollo et al., 2007). However, the correct orientation of the cortical polarity relative to the neuroepithelium was shown to depend on extrinsic signaling in embryonic NBs (Siegrist and Doe, 2006; Yoshiura et al., 2012). The intrinsic signals defining the apical-basal axis and inducing asymmetric divisions are conducted by several protein complexes and cell fate determinants (Figure 7).
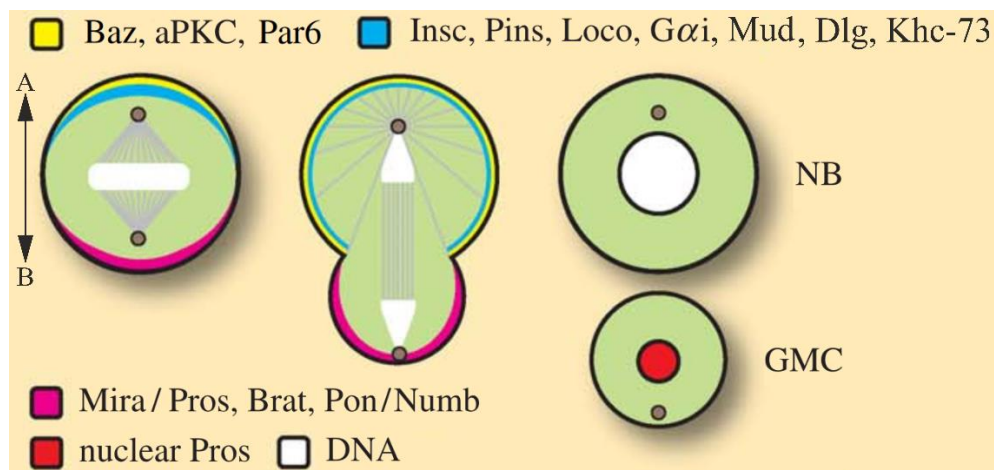
Figure 7: Asymmetric division of neuroblasts
Asymmetric division of neuroblasts is induced by protein complexes on the apical side of the cell. The Par complex (Bazooka (Baz), atypical protein kinase C (aPKC) and Par6; yellow) directs the cell fate determinants Prospero (Pros), Brat (Brain tumor) and Numb as well as their adaptor proteins Miranda (Mira) and Partner of Numb (Pon; magenta) to the basal side where they are segregated into the small daughter cell and lead to the ganglion mother cell (GMC) fate. The other protein complex consisting of Inscuteable (Insc), Partner of Inscuteable (Pins), Loco and Gαi recruits Mud, which attracts one of the spindle poles to the apical side. In a second pathway, Pins recruits Dlg and Khc-73, which links astral microtubules to the apical cortex. A: apical, B: basal (figure modified from Egger et al. (2008), licensed under CC BY 4.0).

The apical-basal axis of NBs is inherited from the epithelial cells during delamination in the embryonic stages by retaining the apical localization of the Par complex (Schober et al., 1999; Wodarz et al., 1999; Homem & Knoblich, 2012). This complex consists of the proteins Bazooka (Baz), Par6 and atypical protein kinase C (aPKC; Betschinger and Knoblich, 2004). The Par complex then recruits Inscuteable (Insc) which binds to Baz and in turn recruits

Partner of Inscuteable (Pins). Pins contains three GoLoco domains which bind to the heterotrimeric G protein subunit Gαi (Knoblich, 2008). This induces a conformational change of Pins leading to recruitment of Mud which in turn is capable of binding microtubules and attracting one of the spindle poles to the apical side (Bowman et al., 2006; Knoblich, 2008; Dewey et al., 2016). There is, however, a second pathway of spindle orientation in which Pins binds to Discs Large (Dlg), which subsequently recruits kinesin motor protein Khc-73. Khc-73 is capable of binding the plus ends of microtubules and therefore, the complex Pins – Dlg – Khc-73 is suggested to link astral microtubules to the apical cortex (Siegrist and Doe, 2005; Gallaud et al., 2017).

Following the initial asymmetric division, the apical localization of the Par complex and its partners and consequently the spindle orientation is setup during interphase. The basal localization of cell fate determinants (CFDs) that are segregated into the small daughter cell, however, takes place during metaphase. An important factor for the basal localization of CFDs is Lethal (2) of giant larvae (Lgl; Peng et al., 2000; Ohshiro et al., 2000), which is phosphorylated by aPKC (Plant et al., 2003; Yamanaka et al., 2003; Betschinger et al., 2003). Since aPKC localization is restricted to the apical side and overexpression of aPKC leads to loss of function of *lgl*, it is suggested that Lgl is inactivated by aPKC-mediated physphorylation and is therefore only active on the basal side of the NB (Betschinger et al., 2005; Knoblich, 2008). However, it is not known how Lgl is essential for CFD localization, especially since none of the CFDs bind to Lgl (Knoblich, 2008).

The cell fate determinants that are segregated into the small daughter cell inducing the GMC fate are Numb, Prospero (Pros) and Brain tumor (Brat) (Spana et al., 1995; Hirata et al., 1995; Bello et al., 2006). Numb binds to the endocytic protein α-Adaptin and thereby represses signal transduction in the Notch pathway (Berdnik et al., 2002; Le Borgne et al., 2005; Schweisguth, 2004). Upon Numb mutation, NBs show a tumor-like phenotype (Lee et al., 2006a; Wang et al., 2006) caused by NB-specific gene expression and proliferation pattern in both daughter cells (Knoblich, 2008). Similarly, mutation of Pros leads to the expression of NB markers and multiple divisions of GMCs in the embryo (Choksi et al., 2006) and to tumor formation in larval NBs (Betschinger et al., 2006; Lee et al., 2006b; Bello et al., 2006). Pros is nuclear only in GMCs (Betschinger and Knoblich, 2004) where it acts as a transcription factor regulating over 700 genes including cell cycle related and pro-neural genes (Knoblich, 2008; Choksi et al., 2006; Southall and Brand, 2009). The third important cell fate determinant, Brat, interacts with Pros during embryogenesis to induce GMC formation, but while the single

mutation of *pros* only affects a small portion of GMCs they are almost completely lost in *pros*/*brat* double mutants (Betschinger et al., 2006). In larval type II NB lineages, Brat binds to Deadpan and Zelda in the small daughter cell and mediates their degradation, thereby inducing the INP cell fate (Reichardt et al., 2018). Brat loss of function therefore leads to formation of multiple type II NB-like cells and tumor formation. However, type II NBs lack Pros and are therefore more sensitive to loss of tumor suppressors. Interestingly, overexpression of Pros reverts the *brat* mutant phenotype (Knoblich, 2008).

Numb, Pros and Brat are segregated to the basal side by the adaptor proteins Partner of Numb (Pon) and Miranda (Mira) (Betschinger and Knoblich, 2004). Pon binds to Numb and mediates its basal localization. In Pon mutants, however, the asymmetric localization of Numb is only delayed to anaphase and telophase, meaning that other factors have to be involved (Knoblich, 2008). Yet, delayed segregation of Numb causes defects in NB self-renewal (Wang et al., 2007). Pros and Brat on the other hand bind to Mira which mediates their segregation to the basal side. Mira is furthermore capable of binding Staufen, a protein that can bind and transport *pros* RNA. Loss of Staufen, however, does not influence the induction of the GMC cell fate. In *mira* mutants, in contrast, Pros and Brat localization is defective leading to a uniformly cytoplasmic dispersion and therefore an equal segregation into both daughter cells (Knoblich, 2008).

Interestingly, NBs in the inner proliferating center of larval optic lobes were recently shown to switch to symmetric amplifying divisions in a temporal pattern (Mora et al., 2018). In these cells, the cell fate determinants Numb, Pros and Brat are no longer segregated asymmetrically and thus do not lead to asymmetric division. This temporal switch is induced by the pro-neural gene *atonal*, but the exact mechanism of the induction of symmetric divisions is still unclear (Mora et al., 2018; Harding and White, 2018).

3.2. Mushroom body miniature

In *Drosophila melanogaster* there are several known genes which, when mutated, negatively influence the development of the CNS or certain brain structures. One of these genes is *mushroom body miniature* (*mbm*) which was found in a genetic screen of mutant flies exhibiting defects in the neuropil known as mushroom body (MB) (Heisenberg et al., 1985). The MB is built up by the four equipotent MBNBs and consists of about 2000 intrinsic MB neurons per brain hemisphere, the Kenyon cells (Ito and Hotta, 1992; Aso et al., 2009). The

Kenyon cells (KC) form the different substructures of the MB: the calyx, which consists of dendrites of the cell bodies at the dorsal posterior surface, and the peduncle, which is formed by axons projecting ventrally toward the anterior end of the brain (Figure 8 A, B; Lee et al., 1999). The peduncle bifurcates into five terminal lobes, the γ-, α'/β'- and α/β-neurons (Figure 8 C, D), which are born in this order throughout development (Crittenden et al., 1998; Jefferis et al., 2002; Lee et al., 1999). The γ-neurons arise during early larval stages while α'/β'-neurons are born during the second half of the 3rd instar larval stage and lastly the α/β-neurons arise during pupal stages (Lee et al., 1999). The larval γ-neurons bifurcate toward the medial and dorsal lobe, but then undergo extensive remodeling during the pupal stages resulting in the branching pattern of the adult MB (Technau and Heisenberg, 1982; Lee et al., 1999; Yu and Schuldiner, 2014). Then, the γ-neurons only project toward the medial lobe, while the α'/β'- and α/β-neurons bifurcate toward the dorsal surface (α, α') as well as the medial lobe (β, β') (Crittenden et al., 1998; Ito et al., 1998; Aso et al., 2009).
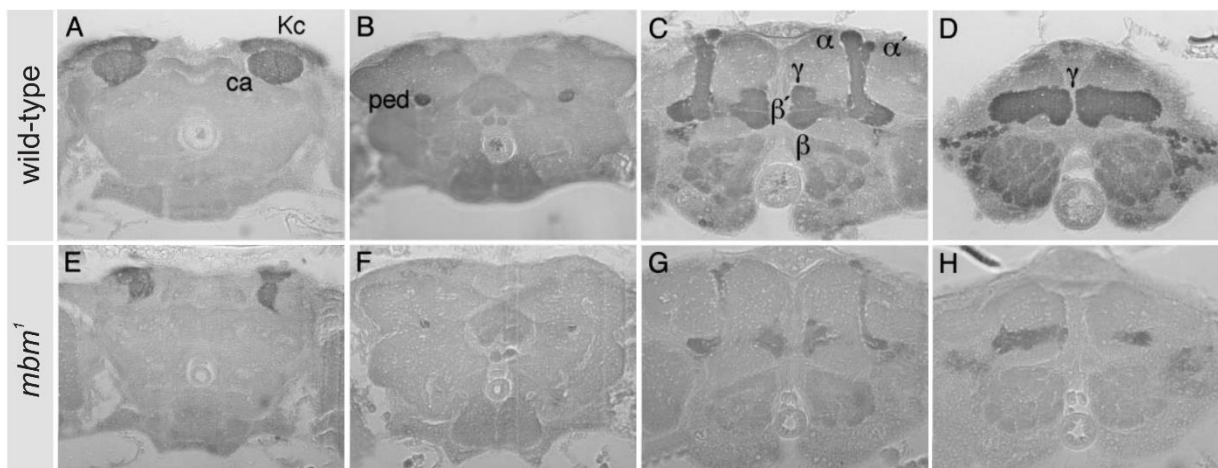
Figure 8: Mushroom bodies in wild-type and *mbm^1* mutant female flies
Cross-sections through wild-type (A – D) and *mbm^1* (E – H) female fly brains. In *mbm^1*, all compartments (α, α', β, β' and γ lobes as well as the calyx (ca) and peduncle (ped)) of the mushroom bodies (MB) are still present but grossly reduced compared to wild-type flies (figure modified from Raabe et al. (2004); Copyright (2004) National Academy of Sciences).

In female flies carrying the hypomorphic mutation *mbm^1*, the MB is greatly reduced (Figure 8) and the flies show reduced odor-learning capabilities (Heisenberg et al., 1985; Raabe et al., 2004; de Belle and Heisenberg, 1996). This is consistent with additional findings that the mushroom body is involved in olfactory learning and memory (Zars et al., 2000; reviewed in Cognigni et al., 2018), besides other functions including control of locomotor activity and courtship behavior (Heisenberg, 2003; Ferveur et al., 1995; O'Dell et al., 1995). The reason for the sexual dimorphism in *mbm^1* flies is not known so far. In contrast, the homozygous *mbm* null mutation called *mbm^{SH1819}*, in which *mbm* is disrupted by a P-element insertion, is

lethal after pupation in both female and male flies. However, the exact role of Mbm remains elusive.

Even though the effect of the *mbm^1* mutation is observed in the mushroom bodies, *mbm* expression is not exclusive to MBNBs, but Mbm can be found in all NB types. Furthermore, in *mbm^SH1819* mutant 3rd instar larvae the whole brain is visibly smaller than in wild-type. As Hovhanyan et al. (2014) could show, Mbm localizes to the nucleolus during interphase and its absence (in *mbm^SH1819* mutant larval brains) leads to a decrease in NB cell size and fewer progeny cells. The asymmetric division of NBs, however, is not affected. It was suggested that Mbm plays a role in NB proliferation, supported by results showing effects on the localization of ribosomal protein S6 (RpS6) and defects in rRNA processing as well as decreased protein synthesis rates in *mbm^SH1819* mutant NBs. It was furthermore shown that *mbm* expression is regulated by dMyc (Hovhanyan et al., 2014) which is known to be involved in the expression of ribosome modifying enzymes and ribosomal components (Gallant, 2013; Teleman et al., 2008; Li et al., 2010).

Since Mbm features two C_2HC zinc-finger motifs, it was suggested that Mbm might have a function involving the binding of nucleic acids (Raabe et al., 2004; Figure 9). In conjunction with Mbm's possible role in rRNA processing, the question arose whether these zinc-fingers enable Mbm to bind ribosomal RNA. First experiments showed that Mbm does indeed bind to rRNA and DNA, however independent of the two zinc-fingers (Cornelia Engert, Master Thesis, 2015). Thus, there has to be another protein domain with the ability to bind nucleic acids. In Mbm's N-terminal half there is an arginine/glycine (R/G) rich region (Figure 9) which might contain an RG/RGG-box and thus another possible nucleic acid binding domain (see 3.3.). The acidic clusters 1 (AC-1) and 2 (AC-2) shown in Figure 9 contain phosphorylation sites for casein kinase 2 (CK2). Mutation of these sites leads to a decrease in overall phosphorylation of Mbm and a partial delocalization to the cytoplasm can be observed (Hovhanyan et al., 2014). AC-3 was suggested to contain additional CK2 phospho sites, but so far, no experimental evidence exists.
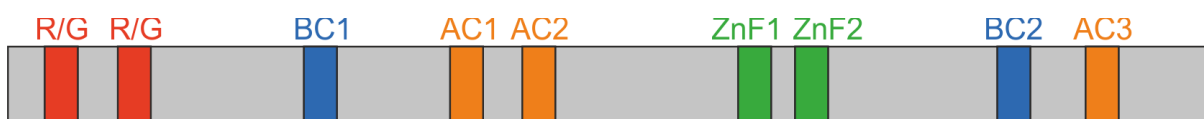
Figure 9: Features of the Mbm protein
Mbm features three clusters of acidic amino acids (AC1-3, orange) which contain phosphorylation sites for casein kinase 2 as well as two basic clusters (BC1/2, blue). The two zinc-finger domains (ZnF1/2, green) could not be shown to play a role in nucleic acid binding. Two arginine/glycine rich regions (R/G, red) may contain RNA binding RG or RGG domains (figure adapted from Anna Hovhanyan, PhD Thesis, 2014).

In summary, Mbm is a transcriptional target of dMyc and gets phosphorylated by CK2 and might therefore be involved in ribosome biogenesis (Hovhanyan et al., 2014). CK2 is known to phosphorylate proteins involved in ribosome biogenesis (e.g. B23; Louvet et al., 2006; Negi and Olson, 2006; Szebeni et al., 2003) as well as components of the rRNA transcription machinery (Filhol and Cochet, 2009; St-Denis and Litchfield, 2009). Mbm's relation with dMyc furthermore implies a possible role in growth control mediated by the TOR pathway (Hovhanyan et al., 2014; Sousa-Nunes et al., 2011). While loss of Mbm leads to NB cell size decrease, fewer progeny, delocalization of RpS6 and defective rRNA processing, its exact function remains elusive. The idea that Mbm might bind to DNA or rRNA could be confirmed, but the zinc-finger domains are not involved. Thus, a potential RG or RGG domain in the arginine/glycine rich region would be a promising candidate.

3.3. RGG/RG-boxes and their RNA binding capabilities

The RGG motif was first described by Lischwe et al., 1985 as a binding site for protein arginine methyltransferases (PRMTs) leading to the dimethylation of the domain's arginines. Seven years later, the RNA binding capabilities of RGG motifs were found in the case of heterogenous nuclear ribonucleoprotein U (hnRNP U) (Kiledjian and Dreyfuss, 1992). They found a sequence of three arginine-glycine-glycine (RGG) repeats in close proximity, which is conserved in RNA binding proteins of different species, and named it RGG-box. Some of these proteins are mammalian nucleolin (human, mouse and hamster), yeast fibrillarin 1 and RNA helicase of fruit flies. However, an extensive study of proteins containing RGG and RG repeats revealed that RGG motifs are not constricted to three repeats and that there are also cases of tri-RG motifs in proteins involved in RNA biogenesis and mRNA translation (Thandapani et al., 2013). In this study, these motifs were defined as follows: tri-RGG motifs are three arginine-glycine-glycine repeats separated from each other by 0 – 4 random amino acids (Figure 10). Accordingly, the RGG or RG repeats in di-RGG, tri-RG and di-RG motifs also have 0 – 4 random amino acids in between. di-RG motifs, however, are very common and can be found in many proteins of different families, e.g. in the transcription factor E2F-1, in lysine methyltransferase SETD5 or ubiquitin ligase RBBP6. Furthermore, RGG/RG motifs often appear in close proximity to each other, possibly functioning together as a motif of a higher order (Thandapani et al., 2013).

tri-RGG: RGG-(X_{0-4})-RGG-(X_{0-4})-RGG

di-RGG: RGG-(X_{0-4})-RGG

tri-RG: RG-(X_{0-4})-RG-(X_{0-4})-RG

di-RG: RG-(X_{0-4})-RG

Figure 10: Definition of RGG and RG motifs
RGG and RG motifs are two or three RGG (red) or RG (green) repeats separated by 0 – 4 random amino acids.

Besides RNA binding, RGG/RG motifs were also found to be important for protein-protein interactions as well as protein localization. For example, RGG/RG motifs are implicated in the interaction of nucleolin with the hepatitis C virus protein NS5B or of RNA helicase A with β-actin (Kusakawa et al., 2007; Tang et al., 2009). Nucleolin furthermore depends on its tri-RGG motif for correct localization to the nucleolus (Ginisty et al., 1999; Pellar and DiMario, 2003). Important for RGG/RG motifs' functions, however, is the methylation status of their arginines mediated by PRMTs.

3.3.1. Arginine methylation in RGG/RG motifs

Posttranslational modification by arginine methylation was shown to be an important regulator for protein-protein as well as protein-RNA interactions (Bedford and Clarke, 2009; Bedford and Richard, 2005; Bedford, 2007). This is also the case for RGG/RG motifs. For example, methylation of the tri-RGG motif in yeast Npl3 inhibits interaction with Tho2 (Yu et al., 2004). However, RGG/RG motifs also positively influence protein-protein interactions (Cote and Richard, 2005; Friesen et al., 2001; Selenko et al., 2001). Likewise, Blackwell et al. (2010) could show that arginine methylation of human FMRP within its RGG-box was essential for RNA binding. Furthermore, they found out that methylation of different arginine residues was necessary for the binding of different RNA molecules. In contrast, RNA binding of human CNBP is inhibited by arginine methylation (Wei et al., 2014). It was suggested that the inhibiting effect of arginine methylation on RNA binding might be caused by steric hindrance or by the loss of a possible hydrogen bond between the protein and the RNA molecule (McBride and Silver, 2001). Promotion of protein-RNA interaction, on the other hand, might be induced by the arginine residue becoming more hydrophobic upon methylation, thereby facilitating an association (Bedford and Richard, 2005).

In eukaryotes, arginine methylation is carried out by protein arginine methyltransferases (PRMTs). So far, eleven members of the PRMT family have been identified, with PRMT1-9

showing methyltransferase activity. PRMTs 10 and 11 are homologs to PRMT 7 and 9, respectively, but their functions are still unclear (Harada et al., 2015; Jahan and Davie, 2015; Krause et al., 2007). PRMTs are capable of different modes of arginine methylation classified into type I-III. Type I PRMTs (PRMT1, 2, 3, 4, 6 and 8; PRMT4 is also known as CARM1) add two methyl groups to the same amino residue of the arginine, leading to an asymmetric dimethylation (Gary and Clarke, 1998; Blackwell et al., 2010). Type II PRMTs (PRMT5 and 9), in contrast, methylate two different amino groups, thereby causing symmetric dimethylation (Branscombe et al., 2001; Cook et al., 2006; Yang et al., 2015; Figure 11). Both type I and type II PRMTs do this in two steps, first monomethylating then dimethylating the arginine (Thandapani et al., 2013). Type III PRMTs are suggested to only be capable of monomethylation. There are, however, conflicting reports about PRMT7 and which group it belongs to. For example, Lee et al., 2005 suggested human PRMT7 to be a type II PRMT, but a later study could only detect (human) PRMT7-mediated monomethylation of a specific substrate which could be asymmetrically and symmetrically dimethylated by PRMTs 1 and 5, respectively (Zurita-Lopez et al., 2012). Thus, PRMT7 was classified as the only type III PRMT (Thandapani et al., 2013). Arginines within RGG/RG motifs are methylated by type I PRMTs 1, 3, 6 and 8 as well as PRMT5 (type II) (Thandapani et al., 2013). It was shown in cell culture that human PRMT1 methylates FMRP, a protein which depends on methylation of its RGG-box for regulation of RNA binding (Blackwell et al., 2010), while an *in vitro* study found a direct connection between rat PRMT1-mediated RGG methylation and RNA binding in human CNBP (Wei et al., 2014).
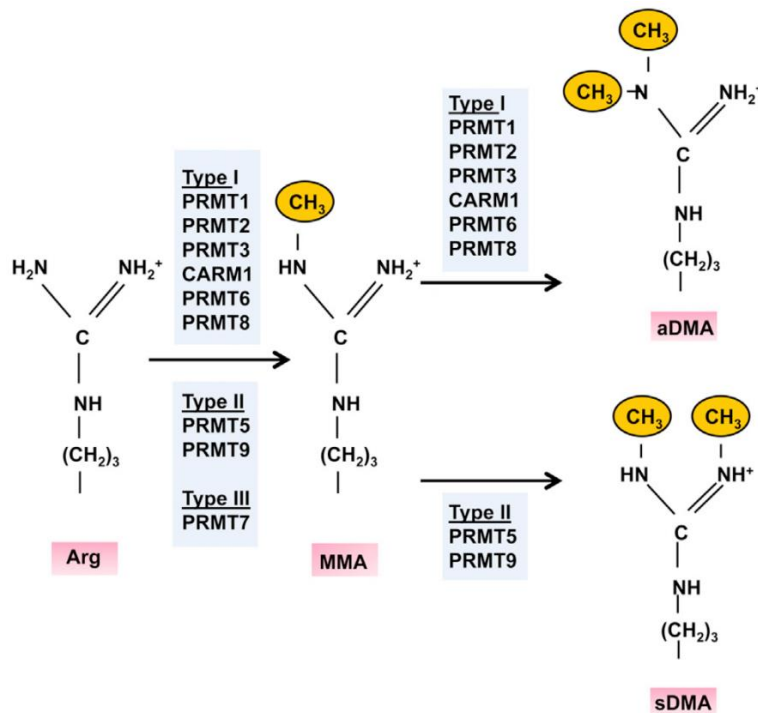
Figure 11: Arginine methylation by protein arginine methyltransferases (PRMTs)
Type I, II and III PRMTs monomethylate one of the arginine's amino groups, generating monomethyl-arginine (MMA). In a second step, type I PRMTs add another methyl group to the same amino residue, leading to asymmetric dimethylation (aDMA). Type II PRMTs catalyze symmetric dimethylation (sDMA). PRMT7 (type III) is only capable of monomethylation (figure modified from Thandapani et al. (2013) with permission from Elsevier).

In *Drosophila*, 9 homologs to the mammalian PRMTs have been identified and termed accordingly DART1-9 (*Drosophila* arginine methyltransferase) by Boulanger et al. (2004). They found highly conserved domains known for arginine methyltransferases and high homologies between DART1/PRMT1, DART4/PRMT4, DART5/PRMT5 and DART7/PRMT7. The remaining DARTs 2, 3, 6, 8 and 9 showed the highest similarity with PRMT1. Furthermore, DART1 and 4 were shown to asymmetrically dimethylate arginines (Boulanger et al., 2004), while DART5 and 7 are capable of symmetric dimethylation (Gonsalvez et al., 2008). In conjunction with the knowledge about mammalian PRMTs, DARTs 1 and 5 are probably the most promising candidates for regulation of RGG/RG-mediated RNA binding in *Drosophila*.

3.4. Ribosome biogenesis – an overview

As explained earlier, the decreased growth and proliferation in *mbm* null mutant neuroblasts may be caused by defects in ribosome biogenesis (Hovhanyan et al., 2014). During the biogenesis of eukaryotic ribosomes, the small (40S) and large (60S) ribosomal subunits are assembled which together consist of four (in *Drosophila*: five) ribosomal RNAs (rRNAs) and 79 ribosomal proteins (RPs) (Klinge et al., 2012; Pavlakis et al., 1979; Yusupova and Yusupov, 2014). Ribosome biogenesis starts in the fibrillar center (FC) of the nucleolus or at the border of the FC and the dense fibrillar component (DFC) with the transcription of the

ribosomal DNA (rDNA) genes by RNA polymerase I (RNA Pol. I; Boisvert et al., 2007; Figure 13). In *Drosophila*, however, the FC and DFC are substituted by the nuclear core which exhibits both component's features (Knibiehler et al., 1982). Onset of rDNA transcription is indirectly promoted by dMyc-induced expression of RNA Pol. I cofactors (Grewal et al., 2005). dMyc expression, in turn, is regulated on the post-transcriptional level by TOR (Teleman et al., 2008; see 3.5.). Once transcribed from the rDNA genes, the pre-rRNA consists of the 5' and 3' external transcribed spacer (ETS), the 18S rRNA, the internal transcribed spacer 1 (ITS1), the 5.8S rRNA, the internal transcribed spacer 2 (ITS2) and the 28S rRNA (25S in lower eukaryotes like *Saccharomyces cerevisiae*) (Long and Dawid, 1980; Henras et al., 2015; Figure 12). In *Drosophila*, there is an additional 2S rRNA fragment which was found to be homologous to the 3' end of 5.8S rRNAs of other species (Pavlakis et al., 1979; Figure 12). Together, the 2S and 5.8S fragments form a 5.8S molecule equivalent to that of other species. The pre-rRNA is then processed by several steps of exo- and endonucleolytic cleavage, thereby cutting out the 18S, 5.8S, 2S and 28S rRNAs (see Long and Dawid, 1980 for a detailed description of the two possible processing pathways in *Drosophila*). The remaining 5S rRNA is transcribed separately and later joins the large ribosomal subunit in complex with ribosomal proteins L5 and L11 (reviewed in Klinge and Woolford, 2019).
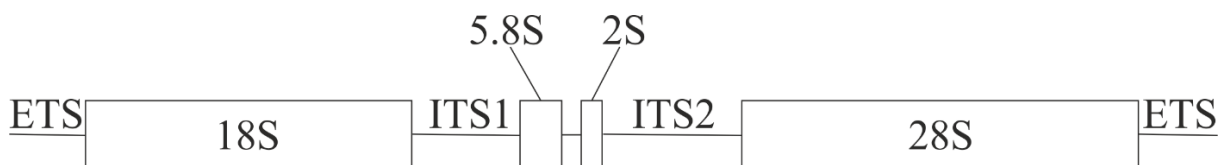
Figure 12: Structure of the pre-ribosomal RNA in *Drosophila*
The pre-ribosomal RNA (pre-rRNA) includes the 5' and 3' external transcribed spacer (ETS), 18S rRNA, internal transcribed spacer 1 (ITS1), 5.8S rRNA, 2S rRNA, internal transcribed spacer 2 (ITS2) and the 28S rRNA.

During rRNA processing, the intermediate rRNA fragments associate with small nucleolar ribonucleoproteins (snoRNPs), pre-ribosomal factors (PRFs) and ribosomal proteins (RPs). This happens in the DFC and the granular compartment (GC) of the nucleolus (Henras et al., 2015; Boisvert et al., 2007; Figure 13). The RPs, e.g. RpS6, are synthesized in the cytoplasm and then transported into the nucleus or the nucleolus where assembly of the ribosomal subunits takes place (Schlosser et al., 2003; Bohnsack and Bohnsack, 2019). In the large RNPs that are formed in the nucleolus, the rRNAs get folded, modified and assembled with RPs, finally resulting in the pre-60S and pre-40S particles which are subsequently transported into the nucleoplasm to mature. There, additional RPs are assembled into the pre-ribosomal

particles. The final assembly of 40S (consisting of 18S rRNA and 33 RPs) and 60S (consisting of 5S, 5.8S, (2S,) 28S and 46 RPs) ribosomal subunits takes place in the cytoplasm, forming mature ribosomes (Bohnsack and Bohnsack, 2019; Klinge and Woolford, 2019; Henras et al., 2015; Tschochner and Hurt, 2003; Figure 13).
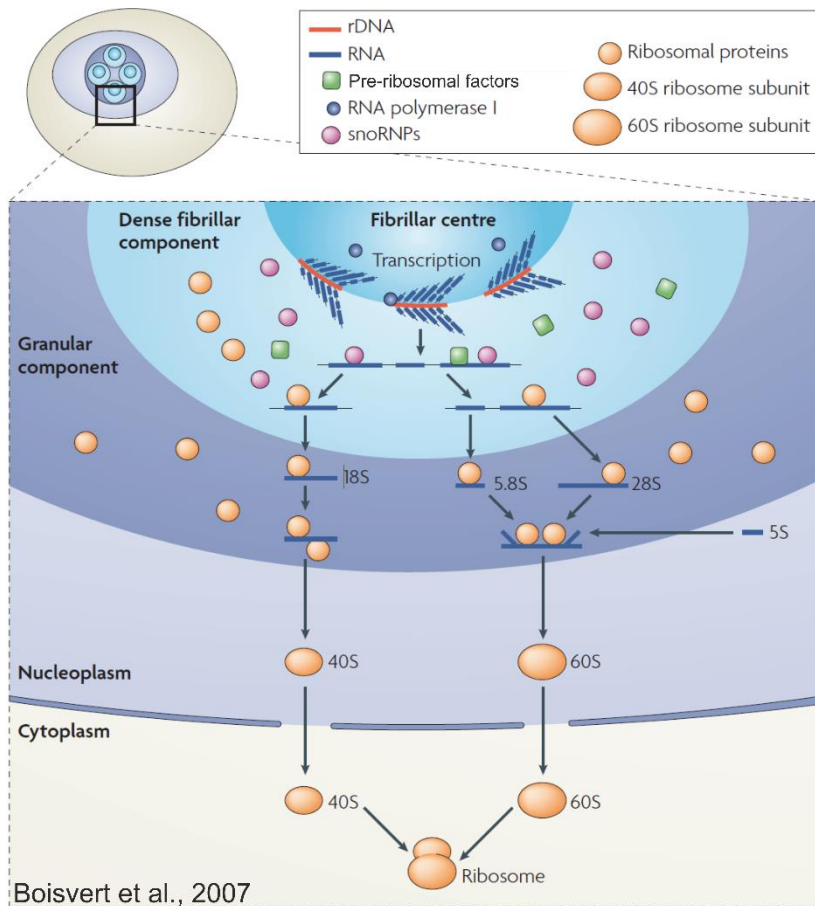
Figure 13: Ribosome biogenesis in eukaryotes
The rDNA genes are transcribed in the fibrillar center (FC) or at the border between the FC and the dense fibrillar component (DFC). Processing of the pre-rRNA takes place in the DFC and the granular component (GC) by interaction with pre-ribosomal factors (PRFs), small nucleolar ribonucleoproteins (snoRNPs) and ribosomal proteins (RPs). The 40S and 60S ribosomal subunits are assembled in the GC and transported to the nucleoplasm to mature. They finally join in the cytoplasm and form mature ribosomes (figure from Boisvert et al. (2007) with permission from Springer Nature).

3.4.1. Ribosome heterogeneity and ribosomopathies

Even though the process of ribosome biogenesis is highly conserved among eukaryotes, an increasing number of species-specific or even cell type-specific differences are found (reviewed in Brombin et al., 2015; Mills and Green, 2017). During assembly and maturation of the ribosomal subunits, numerous ribosomal biogenesis factors (RBFs) are involved in the structural remodeling of the pre-ribosomal particles. Functions of RBFs involve mediation of protein-protein interactions, the binding of RNA or enzymatic activity (Bohnsack and Bohnsack, 2019). RBFs are still studied extensively with new ones being discovered regularly. For example, Badertscher et al. (2015) found approximately 300 RBFs in human cells which are involved in the maturation of the small ribosomal subunit and Farley-Barnes et al. (2018) identified 139 potential human RBFs while screening for regulators of nucleolar

number. However, RBFs vary among eukaryotes and even among cell types. For example, Mbm was shown to be a *Drosophila-* as well as a neuroblast-specific RBF involved in the translocation of RpS6 (Hovhanyan et al., 2014) and Notchless, a maturation factor for the large ribosomal subunit in mice, is essential in hematopoietic stem cells but not in mature hematopoietic cells (Le Bouteiller et al., 2013; Brombin et al., 2015). Furthermore, stem cells generally exhibit higher rDNA transcription rates than their progeny, which is believed to be important for stem cell survival, and the down-regulation of rDNA transcription is even suggested to induce differentiation (Brombin et al., 2015; Hayashi et al., 2014; Zhang et al., 2014). Moreover, ribosomes of different cell types can vary regarding the isoforms or post-translational modifications of their RPs as well as post-transcriptional modifications of their rRNAs, which might be important to determine stem cell identity (Xue and Barna, 2012; Brombin et al., 2015; Mills and Green, 2017).

Defects in ribosome biogenesis that lead to disease are termed ribosomopathies. Ribosomopathies are caused by mutations of RBFs, RPs or components of the rDNA transcription machinery (Bohnsack and Bohnsack, 2019). For example, mutations in eleven RPs of the 40S and 60S ribosomal subunit are associated with the human disease known as Diamond-Blackfan anemia, which is caused by inhibition of the differentiation of hematopoietic stem cells (Boria et al., 2010; Bohnsack and Bohnsack, 2019). In *Drosophila*, knock-out of the nucleolar and Cajal body protein Nopp140, which is considered an RBF, leads to intracellular ribosomopathies including the loss of RpL34 and a significant decrease in protein synthesis (He et al., 2015). Cell type-specific defects in ribosomopathies may be caused by alterations in the rRNA modification machinery or of the levels of certain RPs, affecting the expression of proteins required in the respective cell type. Moreover, many tissue-specific ribosomopathies are linked to increased levels of tumor suppressor p53, which causes cell cycle arrest and apoptosis (Mills and Green, 2017; Bohnsack and Bohnsack, 2019).

3.5. Ribosome biogenesis is regulated by the insulin/TOR pathway

In *Drosophila*, the insulin/TOR (target of rapamycin) pathway is important for translational control, e.g. during starvation stress, for autophagy, endocytosis and hypoxia responses as well as for the control of ribosome biogenesis (reviewed in Grewal, 2009). The effects of insulin/TOR signaling are tissue-specific and still studied intensively. In the brain, for example, the insulin/TOR signaling pathway is involved in the regulation of organismal stress

responses whereas in the fat body it influences larval growth and adult aging (Wang et al., 2008; Colombani et al., 2003; Giannakou and Partridge, 2007).

In starving *Drosophila* larvae, insulin/TOR signaling is reduced and thereby ribosome synthesis is decreased, leading to reduced protein synthesis rates (Grewal et al., 2007; Hall et al., 2007). Secretion of insulins and subsequent binding to the insulin receptor at the cell surface activates a downstream signaling cascade including the kinases PI3K and Akt. The Akt kinase inhibits FOXO which in turn results in the activation of ribosome biogenesis (Oldham and Hafen, 2003; Burgering, 2008). Additionally, Akt can indirectly activate TORC1, a complex consisting of the TOR kinase, raptor and mLST8 (De Virgilio and Loewith, 2006). Both FOXO and TOR regulate Myc expression which in turn is an important expression regulator of many genes involved in ribosome biogenesis (Grewal et al., 2005; Teleman et al., 2008; Li et al., 2010; Figure 14). TOR furthermore limits cell growth in a nutrient-dependent manner by regulating the expression of the RNA Pol. I transcription factor TIF-IA. Thereby, rRNA synthesis and ribosome biogenesis is inhibited and cell as well as tissue growth is impeded (Grewal et al., 2007). Moreover, TIF-IA is regulated by Myc at the mRNA level which is another way for Myc to influence ribosome biogenesis (Grewal et al., 2005).
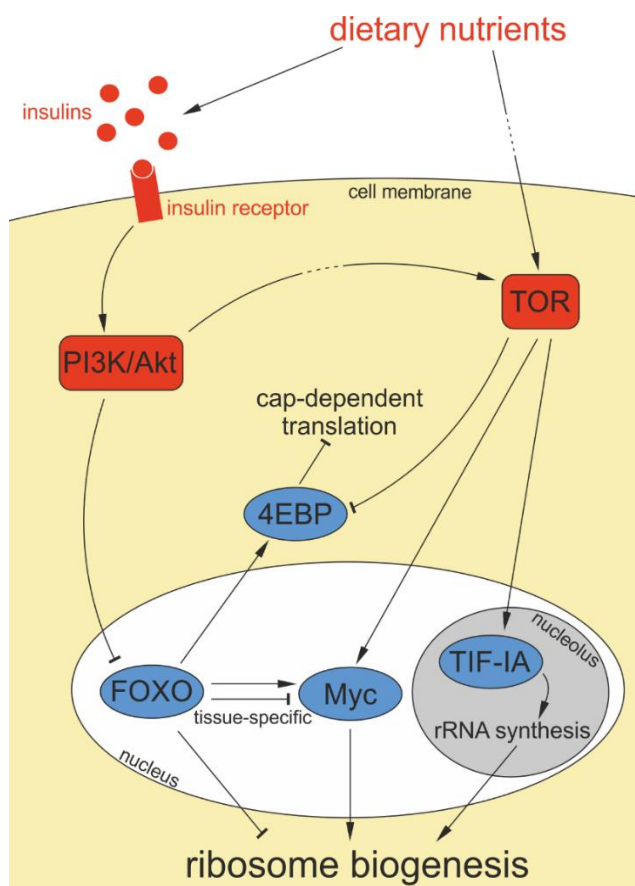
Figure 14: Simplified model of ribosome biogenesis regulation by the insulin/TOR pathway
Dietary nutrients activate the insulin/TOR pathway which regulates expression of FOXO, Myc and TIF-IA, which in turn regulate ribosome biogenesis. On a post-translational level, insulin/TOR also regulates 4EPB, which inhibits cap-dependent mRNA translation. Thus, insulin/TOR regulates growth in dependence of nutrient availability (figure adapted from Grewal (2009) with permission from Elsevier).

One way the TOR pathway regulates Myc expression is through S6 kinase (S6K). S6K is phosphorylated by TOR and then promotes expression of Myc (Parisi et al., 2011). However, S6K is also known to phosphorylate ribosomal protein S6 (RpS6) in *Drosophila (*Montagne et al., 1999). Furthermore, Ruvinsky et al. (2005) found a connection between RpS6 phosphorylation and the regulation of cell size in mice, while RpS6 missing its phospho-sites leads to an increased protein synthesis rate in mouse embryonic fibroblasts. In *Arabidopsis thaliana*, another role of phosphorylated RpS6 was suggested to be an involvement in rRNA synthesis (Kim et al., 2014; Son et al., 2015). In mammalian cells, a connection between TOR inhibition by rapamycin and RpS6 delocalization from the cytoplasm to the nucleus was found by Kazyken et al. (2014), even though they concluded that this effect is not caused by defective RpS6 phosphorylation. Given the high conservation of the TOR pathway and ribosome biogenesis among species, these findings may also be true in *Drosophila*.

In mammalian cells, insulin/TOR signaling was additionally shown to regulate growth via inhibition of cap-dependent mRNA translation mediated by 4EBP (Hay and Sonenberg, 2004; Figure 14). Mutations of 4EPB in *Drosophila* have minimal to no effects on growth when nutrient availability is sufficient (Miron et al., 2001). Under starving conditions, however, 4EBP mutants show a reduced life expectancy. Thus, 4EBP may be a "metabolic brake", reducing energy consumption by mRNA translation when nutrients are scarce (Teleman et al., 2005; Tettweiler et al., 2005).

As explained previously, Myc is a transcriptional regulator of *mbm*, which proposes a potential link between insulin/TOR signaling and Mbm expression for growth control in neuroblasts (see 3.2.; Hovhanyan et al., 2014). It was furthermore shown that ribosome biogenesis and RpS6 localization are affected negatively in *mbm* null mutants. However, whether these effects are linked to the TOR pathway remains elusive so far.

4. Aim of the thesis

In a previous work, it was shown that Mbm is involved in the regulation of neuroblast proliferation and the processing of ribosomal RNA (Hovhanyan et al., 2014). It was suggested that Mbm affects proliferation through a role in ribosome biosynthesis and that Mbm's zinc-finger motifs or its arginine/glycine rich region might be possible domains for rRNA binding. In a second study, flies carrying an Mbm construct with mutated zinc-fingers in the *mbm* null mutant (*mbm^{SH1819}; mbm^{ZnF}*) background were generated and first experiments were conducted (Cornelia Engert, Master Thesis, 2015).

The aim of this thesis was to identify a possible RNA binding domain in the arginine/glycine rich region of Mbm (the RGG-box) and to generate transgenic flies carrying an *mbm* construct with a deletion of the RGG-box in the *mbm^{SH1819}* background. With the help of the *mbm^{SH1819}; mbm^{ZnF}* and *mbm^{SH1819}; mbm^{dRGG}* mutant fly lines and in cell culture experiments, Mbm's molecular function in neuroblast proliferation and ribosome biogenesis should be further investigated. The following questions were addressed:

- Is Mbm^{dRGG} able to rescue the survivability and reduction in neuroblast size of the Mbm null mutant?

- Does Mbm rely on its RGG-box and zinc-finger motifs for its nucleolar localization?

- Does Mbm bind ribosomal RNA *in vitro* and are the RGG-box and zinc-finger motifs important rRNA-binding domains?

- RNA- and protein-binding functions of RGG-boxes were shown to be regulated by arginine methylation (see 3.3.1.). Is Mbm methylated within its RGG-box? Which protein arginine methyltransferases (in *Drosophila*: Darts) might be able to methylate Mbm's RGG-box?

- RpS6 is delocalized in *mbm* null mutant neuroblasts (Hovhanyan et al., 2014). Do the *mbm^{dRGG}* and *mbm^{ZnF}* mutations rescue RpS6 localization? Are protein synthesis rates affected in *mbm* null, *mbm^{dRGG}* and *mbm^{ZnF}* mutants?

5. Material

5.1. Fly stocks

Table 1: Fly lines used in this work

Stock label	Source
w1118	T. Raabe, Würzburg, Germany
mbm^{SH1819}/Cyo, Ubi-GFP	Oh et al., 2003
mbm^{SH1819}/Cyo, Ubi-GFP; pattB[mbm^{WT}]/TM6B, Tb	Hovhanyan et al., 2014
mbm^{SH1819}/Cyo, Ubi-GFP; pattB[mbm^{ZnF}]/TM6B, Tb	Cornelia Engert (AG Raabe)
mbm^{SH1819}/Cyo, Ubi-GFP; pattB[mbm$^{dRGG]}$/TM6B, Tb	produced for this work
mbm^{SH1819}/Cyo, Ubi-GFP; UAS-mRFP::RpS6/TM6B, Tb	Hovhanyan et al., 2014
Mz1060-Gal4	J. Urban, Mainz, Germany
UAS-mRFP::RpS6	Rosby et al., 2009

5.2. Enzymes

5.2.1. Polymerases

Table 2: Polymerases

Name	Manufacturer
Phusion® High-Fidelity DNA Polymerase	New England Biolabs
PowerUP^{TM} SYBR^{TM} Green Master Mix	Applied Biosystems
SP6 RNA Polymerase	Roche
T7 RNA Polymerase	Roche

5.2.2. Nucleases

Table 3: Nucleases

Name	Manufacturer
EcoRI-HF®	New England Biolabs
KpnI	New England Biolabs
SacI	New England Biolabs
SacII	New England Biolabs
XbaI	New England Biolabs
XhoI	New England Biolabs

5.2.3. Other enzymes

Table 4: Other enzymes

Name	Manufacturer
Arctic Phosphatase	New England Biolabs

5.3. Reagents

Table 5: Reagents

Name	Manufacturer
6x DNA loading dye	New England Biolabs
Acetic acid	Applichem
Agar Kobe I (Agar agar)	Carl Roth
Albumin Fraction V (Bovine serum albumin, BSA)	Applichem
Amido black	Applichem
β-mercaptoethanol	Applichem
Bromphenol blue	Applichem
Carbenicillin	Applichem
Cellfectin	Invitrogen
Chloroform	Applichem
Color Prestained Protein Standard Broad Range 11-245 kDa	New England Biolabs
cOmplete^{TM} EDTA-free Protease Inhibitor Cocktail	Roche
Coomassie Brillant Blue	Applichem
CutSmart® buffer	New England Biolabs
Cycloheximide	Sigma
Diethyl pyrocarbonate (DEPC)	Sigma
Dimethyl sulfoxide (DMSO; used in cell culture)	Applichem
Dimethyl sulfoxide (DMSO; used in PCR)	New England Biolabs
Dithiothreitol (DTT)	Carl Roth
D-Lysine	
D(+)-Saccharose Molecular Biology Grade	Applichem
Dulbecco's Phosphate Buffered Saline (PBS)	PAA
1 kb DNA Ladder	New England Biolabs
dNTPs (10 mM)	New England Biolabs
EDTA	Applichem
EGTA	Applichem
Fetal bovine serum (heat-inactivated for cell culture)	Biochrom AG
Glycerol	Applichem
Glycine	Applichem
Hygromycin B Gold	InvivoGen
Magnesium chloride hexahydrate (MgCl$_2$)	Carl Roth
Methanol	Applichem
Midori Green	Nippon Genetics
NEBuffer 4^{TM}	New England Biolabs
Nonfat dried milk powder	Applichem
NP-40	Applichem
Paraformaldehyde	Applichem
Pepstatin A	Roche
10x Phosphate buffered saline (PBS)	Fisher Scientific
Penicillin	PAA
peqGOLD Universal Agarose	peqLab

Name	Manufacturer
Phosphoric acid	Carl Roth
5x Phusion HF Buffer	New England Biolabs
Protein G Agarose	Roche
Puromycin	Sigma
RNase Inhibitor	Applied Biosystems
Rotiphorese® Gel 30 (37.5:1)	Carl Roth
Sodium chloride (NaCl)	Applichem
Sodium orthovanadate (Na_3VO_4)	Applichem
Sodium periodate ($NaIO_4$)	Sigma
Streptomycin	PAA
TEMED	Applichem
Tris Ultrapure	Applichem
Triton X-100	Carl Roth
TRIzol™	Invitrogen
Tryptone	Carl Roth
Tween® 20	Applichem
Vectashield Antifade Mounting Medium (H-1000)	Vector Laboratories
Yeast extract	Carl Roth

5.4. Kits

Table 6: Kits

Name	Manufacturer
DIG Northern Starter Kit	Roche
DIG Wash and Block Buffer Set	Roche
DNeasy Blood & Tissue Kit	Qiagen
High-Capacity cDNA Reverse Transciption Kit	Applied Biosystems
Nucleospin Gel and PCR Cleanup	Macherey-Nagel
QIAfilter Plasmid Midi Kit	Qiagen
QIAprep Spin Miniprep Kit	Qiagen
QuantiTect Reverse Transcription Kit	Qiagen
Total RNA Extraction Kit	Applied Biosystems

5.5. Cells

Table 7: Cells

Name	Manufacturer
Drosophila Schneider S2 cells	*Drosophila* Genomics Resource Center (DGRC)
E. coli DH5α	Invitrogen

5.6. Primers

Table 8: Primers

Primer name	Sequence (5'-3')
18S qPCR fwd	TAGACCGAGAGGTCCGGGTA
18S qPCR rev	CAAAGGGCAGGGACGTAATCAA
Akt qPCR fwd	GCGCGGTTACTGTTTCACCA
Akt qPCR rev	ATGTCACGGACGATTTCACG
Dart1-XhoI rev	TATCTACTCGAGGCGCATGCGGTATGTGTTCG
Dart5-XhoI rev	ATGCCGCTCGAGCAATCGCATGTTGTAACCTGTCC
cbp20 qPCR fwd	GTCTGATTCGGTGGACTGG
cbp20 qPCR rev	CAACGTTTGCCATAACCCC
EcoRI-Dart1 fwd	CAGACTGAATTCATGGCCAGCACAGACATTCC
KpnI-Dart5 fwd	GCATGTGGTACCATGAATTACTACGTCTGTCTGCACC
mbm fwd 33069	CGGCTCAACACGTGCGCCG
mbm r34258	TGGACAGTTTTTGAGACC
pAc5.1 Seq. fwd	CACTACCGTTTGAGTTCTTGTGC
pAc5.1 Seq. rev	TTAGAAGGCACAGTCGAGGCTG
Rp49 qPCR fwd	GCCCAAGATCGTGAAGAAGC
Rp49 qPCR rev	CGACGCACTCTGTTGTCG
RpL49 qPCR fwd	GCCCAGCATACAGGCCCAAG
RpL49 qPCR rev	AAGCGGCGACGCACTCTGTT
RpS6 qPCR fwd	ATGAAGCAGGGTGTCTTGACC
RpS6 qPCR rev	ACGGTAGCAGGAGTGTCC
SLIM mbm dRGG fwd short	CGTAACAACTCGTGGCAACC
SLIM mbm dRGG rev short	ATTATCCAGCTCCTGTTGGG
SLIM mbm dRGG fwd tailed	CATCAGCCAAACAAGCGTAACAACTCGTGGCAACC
SLIM mbm dRGG rev tailed	CTTGTTTGGCTGATGATTATCCAGCTCCTGTTGGG
SLIM T$\rightarrow$C Exon 1 F_S	AGAAGAAGGTTAACTCCTC
SLIM T$\rightarrow$C Exon 1 R_S	GCTCCGCTTTGACAAATTGC
SLIM T$\rightarrow$C Exon 1 F_T	CCAAATCTCCTAAAAAGAAGAAGGTTAACTCCTC
SLIM T$\rightarrow$C Exon 1 R_T	TTTTAGGAGATTTGGGCTCCGCTTTGACAAATTGC
SLIM T$\rightarrow$C Exon 2 F_S	TATCGGCCGCAGCCAGTCTAC
SLIM T$\rightarrow$C Exon 2 R_S	CTCGTTTCCGCTTCTGTTTGG
SLIM T$\rightarrow$C Exon 2 F_T	GCACCAAAGCCTCCGTATCGGCCGCAGCCAGTCTAC
SLIM T$\rightarrow$C Exon 2 R_T	CGGAGGCTTTGGTGCCTCGTTTCCGCTTCTGTTTGG
SLIM ZnF1 F_S	CGACAAGAAGGGCCACAC
SLIM ZnF1 R_S	TCCACGGTTTTACCCTTG
SLIM ZnF1 F_T	TGTGTATGGCATATGCGACAAGAAGGGCCACAC
SLIM ZnF1 R_T	CATATGCCATACACATCCACGGTTTTACCCTTG
SLIM ZnF2 F_S	TGCTCCGGTAGTTATCATGG
SLIM ZnF2 R_S	TCTGACACTGGAAGGAGGTG
SLIM ZnF2 F_T	TGATATATCGTAATTGCTCCGGTAGTTATCATGG
SLIM ZnF2 R_T	ATTACGATATCATCTGACACTGGAAGGAGGTG
Tub qPCR fwd	CGTCTGGACCACAAGTTCGA
Tub qPCR rev	CCTCCATACCCTCACCAACGT

5.7. Antibodies

5.7.1. Primary antibodies

Table 9: Primary antibodies

Antibody	Host species	Application	Dilution	Source	Cat. No.
anti-aDMA ASYM24	rabbit	WB	1:500	Merck	07-414
anti-aPKC	rabbit	IF	1:25	Santa Cruz Biotechnology	sc-216
anti-dNop5	rabbit	IF	1:800	G. Vorbrüggen, Göttingen, Germany	
anti-Fibrillarin 38F3	mouse	IF	1:100	Santa Cruz Biotechnology	sc-56676
anti-His$_6$ P5A11	mouse	WB	1:5000	DSHB	P5A11-c
anti-Mbm EP031195	rabbit	WB	1:166	Eurogentec	
anti-Mbm Syc-143	guinea pig	IF	1:100	Eurogentec	
anti-Miranda 81-0	mouse	IF	1:20	Fumio Matsuzaki, Kobe, Japan	
anti-myc 9E10	mouse	WB, IP	1:5,000 (WB)	Santa Cruz Biotechnology	sc-40
anti-sDMA SYM11	rabbit	WB	1:500	Merck	07-413
anti-Puromycin 12D10	mouse	WB, IF	1:5,000	Merck	MABE343
anti-RFP	rabbit	IF	1:100	Abcam	ab62341
anti-RpS6 54D2	mouse	IF	1:25	Cell Signaling Technology	2317

5.7.2. Secondary antibodies

Table 10: Secondary antibodies

Antibody	Conjugate	Host species	Application	Dilution	Source
anti-guinea pig	Alexa488	goat	IF	1:200	Dianova
anti-guinea pig	Cy3	goat	IF	1:200	Dianova
anti-mouse	Cy3	goat	IF	1:200	Dianova
anti-mouse	Cy5	donkey	IF	1:200	Dianova
anti-mouse	Alexa488	goat	IF	1:200	Dianova
anti-mouse	HRP	sheep	WB	1:10,000	GE Healthcare
anti-rabbit	Alexa 488	goat	IF	1:200	Molecular Probes
anti-rabbit	Cy3	goat	IF	1:100	Dianova
anti-rabbit	Cy5	goat	IF	1:200	Dianova
anti-rabbit	HRP	donkey	WB	1:10,000	GE Healthcare

5.8. Buffers and solutions

Amido black staining solution

1 % (w/v) amido black

10 % (v/v) acetic acid

90 % (v/v) ethanol

Apple juice agar

8.75 g agar agar

500 ml H_2O

→ solubilize by cooking

12.5 g D(+)-saccharose

125 ml apple juice

→ solubilize under stirring at 60 °C

→ mix both solutions

Bradford reagent

0.1 % (w/v) Coomassie Brilliant Blue

4.5 % (v/v) ethanol

8.5 % (v/v) phosphoric acid (H_3PO_4)

2x D-Buffer

20 mM Tris pH 8.0

20 mM $MgCl_2$ hexahydrate

5 mM dithiothreitol (DTT)

DEPC-H_2O

0.1 % (v/v) diethyl pyrocarbonate (DEPC) in H_2O

stirred for at least 1h, then autoclaved

Dot blot destaining solution

10 % (v/v) acetic acid

90% (v/v) ethanol

H-Buffer

50 mM Tris pH 9.0

20 mM EDTA pH 8.0

300 mM NaCl

IP lysis buffer

25 mM Tris pH 7.5

150 mM NaCl

2 mM EGTA (ethylene glycol-bis(β-aminoethyl ether)-N,N,N',N'-tetraacetic acid)

2 mM EDTA

10 % (v/v) glycerol

0.5 % (v/v) NP-40

4x Laemmli buffer

260 mM Tris-HCl pH 6.8

8 % (w/v) sodium dodecyl sulfate (SDS)

40% (v/v) glycerol

0.01 % (w/v) bromophenol blue

4 % (v/v) β-mercaptoethanol

LB^{Carb}

LB medium supplemented with 100 µg/ml carbenicillin

LB medium

1% (w/v) tryptone

0.5% (w/v) yeast extract

1% (w/v) NaCl

LB Agar

1% (w/v) tryptone

0.5% (w/v) yeast extract

1% (w/v) sodium chloride

1.4% (w/v) agar agar

Native IP elution buffer

0.2 M glycine pH 2.6

Native IP wash buffer

10 mM Tris pH 7.4

1 mM EDTA

1 mM EGTA

150 mM NaCl

1% (v/v) Triton X-100

0.2 mM Na_3VO_4 (sodium orthovanadate)

PBT

0.3 % (v/v) Triton X-100 in 1x PBS

PLP

2.8 % paraformaldehyde

9.8 mM sodium periodate ($NaIO_4$)

73.5 mM D-lysine

15.8 mM monosodium phosphate (NaH_2PO_4)

13.6 mM disodium phosphate (Na_2HPO_4)

RNA-binding buffer

10 mM Tris pH 7.5

50 mM NaCl

1 mM $MgCl_2$

0.5 mM EDTA

4 % (v/v) glycerol

0.5 mM dithiothreitol (DTT)

in DEPC-H_2O

SDS-PAGE running buffer

25 mM Tris

200 mM glycine

0.1 % SDS

SDS-PAGE separating gel buffer

1.5 M Tris pH 8.8

0.4 % SDS

SDS-PAGE stacking gel buffer

0.5 M Tris pH 6.8

0.4 % SDS

50x TAE (tris-acetate-EDTA) buffer

2 M tris

1 M acetic acid

50 mM EDTA

Tankblot running buffer

25mM Tris

192 mM glycine

20 % (v/v) methanol

10x TBS (tris buffered saline)

100 mM tris pH 7.5

1.5 M NaCl

TBS-T

1x TBS

0.1 % Tween® 20

5.9. Machines, equipment and software

5.9.1. Machines

Table 11: Machines

Name	Manufacturer
7-2020 (vortexer)	neoLab
accu-jet Pro (pipette)	Brand
Analytic A200S (balance)	Sartorius
Arpege 40 (liquid nitrogen tank)	Air Liquide
BioPhotometer	Eppendorf
Centrifuge 5415 D	Eppendorf
Centrifuge 5415 R	Eppendorf
Centrifuge 5417 R	Eppendorf
ChemoCam Imager	Intas Science Imaging
Criterion Blotter	(Bio-Rad)
Easypet (pipette)	Eppendorf

Name	Manufacturer
E-BOX VX2 Gel Documentation System	peqLab
Electronicrührer Monotherm	Variomag
EPS600 (PSU)	Pharmacia Biotech
FLUOVIEW 1000 IX81	Olympus
Gel iX Imager	Intas Science Imaging
GNA 100 (electrophoresis chamber)	Pharmacia Biotech
Heraeus Multifuge X1R	Thermo Scientific
INB 400 (incubator)	Memmert
innova 4330 Refrigerated Incubator Shaker	New Brunswick Scientific
IPP 110 (incubator)	Memmert
KL 200 LED (binoculars)	Zeiss
LaminAir HB 2448 (sterile bench)	Heraeus Instruments
LD79 (rotator)	Labinco BV
Mastercycler® ep Gradient S	Eppendorf
Mastercycler® Gradient	Eppendorf
Mini-PROTEAN Tetra System	Bio-Rad
Mixing Block MB-102	BIOER
Multigel (SDS-PAGE chamber)	Biometra
Mz16F (fluorescence binoculars)	Leica
NanoDrop 2000c UV-Vis Spectrophotometer	Thermo Scientific
Orbital Shaker-Incubator ES-20	Grant-bio
Pipetman P20	Gilson
Pipetman P200	Gilson
Pipetus	Hirschmann Laborgeräte
Platefuge	Benchmark Scientific
PowerPac 200	Bio-Rad
Reference pipettes 10, 100 & 1000 µl	Eppendorf
RS-RT05 (rollator)	Phoenix Instruments
Seven Easy (pH-meter)	Mettler Toledo
Sonorex (sonicator)	Bandelin
SPO 61 (balance)	Scaltec
StepOne Plus Real Time PCR System	Applied Biosystems
Sub-Cell GT (electrophoresis chamber)	Bio-Rad
TCS SPE	Leica
Thermomixer comfort	Eppendorf
Typ 12801 (heating plate)	Medax
Unimax 2010 (shaker)	Heidolf
UVC500 UV Crosslinker	Hoefer
Vortex-Genie 2	Scientific Industries
WS-5 (shaker)	Edmund Bühler
WT-17 (nutator)	Biometra

5.9.2. Equipment

Table 12: Equipment

Name	Manufacturer
6 cm petri dishes	greiner bio-one
6-Well plates	Sarstedt
Cell culture flasks 25 ml	Sarsted
Cell culture flasks 75 ml	Sarsted
Cover slips	Marienfeld
Cryovials	nunc
Hybond® P Western blotting membrane, PVDF	Amersham
Neubauer improved cell counting chamber	Hausser Scientific
Protran BA 85 (0.45 µm nitrocellulose membrane)	GE Healthcare Life Sciences
Object slides	Marienfeld
X-ray film	Typon Röntgenfilm GMBH

5.9.3. Software

Table 13: Software

Name	Manufacturer/Source
Corel Draw X5	Corel
Corel Draw 2018	Corel
Fiji (ImageJ)	https://fiji.sc/; Schindelin et al., 2012
GENtle v.1.9.4	gentle.magnusmanske.de
MUSCLE	https://www.ebi.ac.uk/Tools/msa/muscle/; Chojnacki et al., 2017
NEBioCalculator^{TM}	https://nebiocalculator.neb.com/#!/ligation
Office 2010	Microsoft
Office 365	Microsoft
Origin 2018b 64Bit	OriginLabs Corporation
Primer-BLAST	https://www.ncbi.nlm.nih.gov/tools/primer-blast/
R v.3.0.1	www.r-project.org

6. Methods

6.1. General molecular biology methods

6.1.1. Extraction of genomic DNA (gDNA) from *Drosophila* S2R+ cells

Stably or transiently transfected S2R+ cell lines were grown to approximately 1×10^7 cells/ml. 2 ml of cell suspension were centrifuged at 1,200 x g for 5 min, the supernatant was discarded and the cell pellet was resuspended in 5 ml PBS (Dulbecco's Phosphate Buffered Saline, PAA). Following centrifugation at 1,200 x g for 5 min, the pellet was resuspended in 200 µl PBS. gDNA was extracted using the DNeasy Blood & Tissue Kit (Qiagen) according to the kit's "Animal Blood (Spin-Column Protocol)" starting at paragraph 1c with the addition of 20 µl proteinase K.

6.1.2. Polymerase chain reaction (PCR)

To amplify desired stretches of DNA, standard PCR was performed in an Eppendorf Mastercycler® ep Gradient S using Phusion® High Fidelity DNA Polymerase (New England Biolabs (NEB)). Primers were designed with GENtle v.1.9.4. (gentle.magnusmanske.de) and ordered from Thermo Scientific. The annealing temperature of the specific primer pair was determined using NEB's Tm calculator (https://tmcalculator.neb.com). See Table 14 and Table 15 for the composition and the cycle of a standard PCR, respectively.

Table 14: standard PCR components

Reagent	Volume (µl)	Final concentration
5x Phusion HF Buffer (NEB)	10	1x
10 mM dNTPs	1	0.2 mM
10 µM fwd primer	2.5	0.5 µM
10 µM rev primer	2.5	0.5 µM
DNA template	variable	variable
optional: DMSO (NEB)	2.5	5%
Phusion High Fidelity Polymerase (NEB)	0.5	1 U
H$_2$O	*ad* 50 µl	

Table 15: standard PCR cycle

Temperature	Time	Number of cycles
98 °C	30 s	1
98 °C	10 s	
variable	20 s	25-35
72 °C	30s / kb	
72 °C	10 min	1
4 °C	∞	

6.1.3. Agarose gel electrophoresis

Agarose gel electrophoresis was used to separate DNA fragments according their size. 1% (w/v) agarose gels in 1x TAE buffer were prepared and 2.5 µl of Midori Green (Nippon Genetics) were added. The DNA samples were mixed in a 1:6 ratio with 6x DNA loading dye and loaded onto the gel. 5 µl 1 kb DNA Ladder (NEB) were used for size reference. The electrophoresis was carried out by applying 80 to 120 V for 60 to 90 min. A Gel iX Imager (Intas Science Imaging) or an E-BOX VX2 Gel Documentation System (peqLab) was used to visualize DNA fragments using UV light.

6.1.4. Restriction digestion

To prepare DNA fragments and plasmids for cloning or to screen clones for successful insertion, a restriction digestion was performed (Table 16). Unless mentioned otherwise, digestions were carried out at 37 °C for 1 h.

Table 16: Standard restriction digestion

Reagent	Volume (µl)
10x restriction buffer (variable)	2.5
plasmid DNA (up to 1 µg)	variable
Restriction enzyme I	0.5
(Restriction enzyme II	0.5)
H$_2$O	*ad* 25 µl

6.1.5. Cloning

Cloning was performed to insert a DNA fragment amplified by PCR into vector DNA or to transfer DNA fragments between plasmids. Complementary overhangs on both the recipient plasmid as well as the insert DNA were generated by restriction digestion (see 6.1.4.). The linearized vector was dephosphorylated using Antarctic Phosphatase (NEB) to prevent recircularization (Table 17). Dephosphorylation was performed for 1 h at 37 °C. The reaction was stopped by incubation at 80 °C for 2 min.

Table 17: Composition of a dephosphorylation reaction

Reagent	Volume (µl)
linearized vector	variable (2 µg of DNA)
10x Antarctic Phosphatase Buffer (NEB)	3
Antarctic Phosphatase (NEB)	2
H$_2$O	*ad* 30 µl

The digested insert and vector were run through a 1% agarose gel (see 6.1.3.). The desired DNA fragments were extracted from the agarose gel slices using the Nucleospin Gel and PCR Cleanup kit (Macherey-Nagel) according to the kit's protocol. The DNA was eluted with 20 µl H_2O and the DNA concentration was measured using a BioPhotometer (Eppendorf).

The ligation was carried out with an insert:vector ratio of 5:1. The insert DNA mass to be used for 100 ng of vector DNA was calculated with the ligation module of NEBioCalculator[TM]. See Table 18 for the composition of a standard ligation reaction. Before the ligase was added, the ligation reaction was incubated at 45 °C for 5 min and briefly cooled down on ice. After the addition of the ligase, the reaction was carried out at 16 °C for 2 h. Following a further incubation step at RT for 10 min, 5 µl of the ligation reaction were used for transformation into *E. coli* DH5α (Invitrogen) (see 6.1.6.)

Table 18: Composition of a standard ligation reaction

Reagent	Volume (µl)
10x T4 DNA Ligase Buffer (NEB)	2
linearized vector	variable (100 ng of vector DNA)
insert DNA	variable (5:1 insert:vector ratio)
T4 DNA Ligase (NEB)	1
H_2O	*ad* 20 µl

6.1.6. Transformation

The amplification of plasmid DNA was achieved by transformation into *E. coli* DH5α cells (Invitrogen). 50 µl *E. coli* DH5α suspension stored at -80 °C was thawed on ice for 30 min. Plasmid DNA (variable amount) was added, the probe was mixed by flipping and incubated on ice for 20 min. The bacteria were heat-shocked at 42 °C for 60 s, briefly put back on ice and 300 µl LB medium containing 100 µg/ml carbenicillin (Applichem; henceforth called LB[Carb]) were added (note: all vectors used in this work carry a resistance gene for ampicillin, for which carbenicillin is a more stable analog). The sample was incubated in a thermoshaker at 37 °C for 1 h under shaking at 300 rpm before it was plated onto an LB-agar plate containing 100 µg/ml carbenicillin. Incubation occured at 37 °C overnight.

6.1.7. Miniprep

Plasmid DNA was extracted from liquid *E. coli* culture using the QIAprep Spin Miniprep Kit (Qiagen). A clone of previously transformed *E. coli* was picked carefully with a pipette tip, added to a test tube with 2 ml LB^{Carb} and incubated at 37 °C and 180 rpm for at least 5 h. The bacteria suspension was pelleted by centrifugation at 16,000 x g for 1 min. The supernatant was discarded and the plasmid DNA was extracted from the cell pellet according to the kit's „QIAprep spin" protocol. The DNA was eluted using 30 µl of H$_2$O.

6.1.8. Sequencing

Sequencing of plasmid DNA as well as purified PCR products was carried out by Eurofins Genomics (85560 Ebersberg, Germany) using their „TubeSeq Service". The DNA concentration of the sample was measured with a BioPhotometer (Eppendorf) or with a NanoDrop 2000c UV-Vis Spectrophotometer (Thermo Scientific). Sample preparation was done according to Eurofins' "TubeSeq Service Sample Submission Guide". The results were analyzed using GENtle v.1.9.4.

6.1.9. Midiprep

Plasmid DNA of a clone carrying the desired construct was amplified via midiprep using the QIAfilter Plasmid Midi Kit (Qiagen). 50 ml of LB^{Carb} were inoculated with the desired *E. coli* clone. Following overnight incubation at 37 °C and 180 rpm, the bacteria suspension was centrifuged for 15 min at 5,000 x g. The supernatant was discarded and the pellet was resuspended in 4 ml Buffer P1 (Qiagen). The midiprep was carried out according to the kit's protocol except for steps 11 and 12, when the centrifugation steps were performed at 5,000 x g and 4 °C for 60 min and 30 min, respectively. The plasmid DNA was redissolved in H$_2$O by vigorous shaking on a vortexer for at least 30 min.

6.1.10. RNA extraction

Total RNA was extracted from *Drosophila* larval brains using TRIzol^{TM} (Invitrogen). 15 brains were dissected and transferred into a 1.5 ml reaction tube on ice containing 10 µl 1x PBS (diluted from 10x PBS (Fisher Scientific) with DEPC-H$_2$O). 1 ml of TRIzol was added, the sample was sonicated 3x 30 s and put on ice for 30 s between each sonication. 200 µl

chloroform were added, the sample was mixed, incubated for 3 min and centrifuged at 12,000 x g for 15 min. The aqueous phase was carefully pipetted into a new 1.5 ml reaction tube. The RNA extraction was subsequently performed according to the TRIzol™ reagent's protocol. 20 µl DEPC-H$_2$O were used for the resuspension of the RNA. The yield was determined using a NanoDrop 2000c UV-Vis Spectrophotometer (Thermo Scientific).

6.1.11. Reverse transcription

RNA was reverse transcribed into cDNA using either the High-Capacity cDNA Reverse Transcription Kit (Applied Biosystems) or the QuantiTect Reverse Transcription Kit (Qiagen) following the respective protocol.

6.1.12. Quantitative real-time PCR (qPCR)

qPCR was performed to investigate the expression levels of certain genes of interest in *Drosophila* larval brains. Total RNA was extracted and reverse transcribed into cDNA as described in sections 6.1.10. and 6.1.11. Primers for qPCR were designed using GENtle v.1.9.4. and checked for unspecific binding sites, matching melting temperatures (58 ±1 °C) as well as the probability of primer dimer formation using Primer-BLAST. qPCRs were carried out in a StepOne Plus Real Time PCR System (Applied Biosystems) using PowerUP™ SYBR™ Green Master Mix (Applied Biosystems) according to the kit's protocol with an annealing temperature of 58 °C. The optimal concentrations of both the forward and reverse primers were determined running a qPCR with 1 ng of template cDNA and all possible combinations of 100 nM, 300 nM and 600 nM of both primers. The combination for which the qPCR yielded the earliest start of the exponential phase as well as a melting curve fitting the expected product was used for further qPCR runs. The primer efficiency was determined by a qPCR run with a 7-fold 1:5 serial dilution starting with 10 ng and all samples were run in dublicates. The C$_t$ values were plotted against the log-transformed dilutions of template cDNA and the slope of the regression line was used to calculate the primer efficiency:

$$effiency = (5^{\frac{-1}{slope\ of\ regression\ line}} - 1)$$

Additionally, the R^2 value of the regression line was verified to be over 0.98, so that the precision of the regression line could be trusted. All further experiments were run in

triplicates with 1 ng of template cDNA and the previously determined optimal primer concentration. The fold change in expression of a gene of interest in two different genotypes was calculated in comparison to a housekeeping gene using the ddC_t method (Livak and Schmittgen, 2001). Statistical analysis was done by a Mann-Whitney U test in Origin (in accordance with Goni et al, 2009).

6.2. General biochemistry methods

6.2.1. Immunoprecipitation (IP)

Proteins expressed in *Drosophila* S2R+ cells were isolated by immunoprecipitation (IP). To this end, 4 ml of cell suspension with a density of 5 to 10 x 10^6 cells/ml were centrifuged at 1,200 x g and 4 °C for 5 min, the supernatant was discarded. The pellet was washed by resuspension in 10 ml Dulbecco's PBS (ice-cold; PAA) and centrifugation at 1,200 x g for 5 min. The pellet was washed once more with 2 ml cold PBS and transferred into a 2 ml reaction tube. Following another centrifugation at 1,200 x g and 4 °C for 5 min, the supernatant was discarded and the pellet was resuspended in 100 µl IP lysis buffer supplemented with 1x cOmplete™ EDTA-free Protease Inhibitor Cocktail (Roche) and 0.7 µg/ml pepstatin A (Roche). Following incubation at 4 °C on a rotator for 40 min, the lysate was centrifuged at 1,200 x g and 4 °C for 5 min. The supernatant was transferred into a pre-cooled 1.5 ml reaction tube. 50 µl protein G agarose beads (Roche) were added and the sample was incubated on a rotator at 4 °C for 1 h. The beads were pelleted at 12,000 x g and 4 °C for 1 min and the supernatant was transferred into a new pre-cooled 1.5 ml reaction tube. Following the addition of the antibody (amount depending on the antibody used), the sample was incubated overnight on a rotator at 4 °C. 80 µl protein G agarose beads were added and the sample was put on a rotator at 4 °C for 3 h. The beads were then washed 3x with 1 ml IP lysis buffer (supplemented with the previously mentioned protease inhibitors) by centrifugation at 12,000 x g and 4 °C for 1 min and discarding the supernatant. Elution of the proteins was performed by adding 80 µl 2x Laemmli buffer and heating to 95 °C for 5 min. The protein G agarose beads were pelleted by centrifugation at 12,000 x g for 1 min, before the samples were loaded onto an SDS-PAGE gel (see 6.2.4.)

6.2.2. Native immunoprecipitation

Native immunoprecipitation was performed to isolate proteins in their native, non-denatured state to use them for down-stream experiments. Native IP was done according to standard IP with the following exceptions: 150 µl IP lysis buffer (with protease inhibitors) were used for lysis of the cells and the cell suspension was sonified for 5x 30 s in cold water and put on ice for 30 s between each sonification step before incubation at 4 °C for 40 min. 100 µl and 200 µl protein G agarose beads (Roche) were used for preclearing of the lysate and the immunoprecipitation, respectively. The washing steps were performed with 500 µl native IP washing buffer supplemented with 1x cOmplete^{TM} EDTA-free Protease Inhibitor Cocktail (Roche) and 0.7 µg/ml pepstatin A (Roche). Elution of the proteins was carried out by adding 200 µl native IP elution buffer, incubation on a rotator at 4 °C for 20 min and pelleting of the beads at 12,000 x g and 4 °C for 1 min. The supernatant was transferred into a pre-cooled 1.5 ml reaction tube and mixed with 200 µl 1 M Tris-HCl pH 8.0. The IP product was aliquoted, immediately shock-frozen in liquid nitrogen and stored at -80 °C.

6.2.3. Measurement of protein concentrations

6.2.3.1. Bradford Assay

The protein concentrations in cell or tissue lysates without Laemmli buffer were be measured by Bradford assay (Bradford, 1976). 120 µl of the lysate were mixed with 950 µl Bradford solution and the OD$_{600}$ was measured using a BioPhotometer (Eppendorf). Using known BSA concentrations, a standard curve was determined and used to calculate the protein concentrations of the samples.

6.2.3.2. Dot blot

To estimate the concentration of a protein sample mixed with Laemmli buffer, a dot blot was performed. First, a serial dilution of BSA with concentrations between 0.025 µg/µl and 1 µg/µl was prepared. 8 µl of each BSA dilution and 8 µl of each sample were mixed with 8 µl methanol (MeOH). Of each sample, 3 x 3 µl were pipetted onto a PVDF membrane (Amersham) and allowed to air-dry. The membrane was then stained for 3 min in amido black staining solution and washed 3 x 10 min in destaining solution. The protein concentration of the samples was subsequently estimated by comparison of their staining intensity with the intensity of the different BSA dilutions.

6.2.4. Sodium dodecyl sulfate polyacrylamide gel electrophoresis (SDS-PAGE)

Protein samples prepared for western or northwestern blot were subjected to SDS-PAGE to separate the proteins according to their molecular weight (after Laemmli, 1970). The gels were prepared with a 4 % stacking and a 9 % separating gel (Table 19). For subsequent northwestern blots, 5 % glycerol were added to the separating gel and only DEPC-H_2O was used for all buffers. The samples (mixed with Laemmli buffer) as well as 5 µl of Color Prestained Protein Standard Broad Range 11-245 kDa (NEB) were incubated at 95 °C for 5 min and briefly cooled down on ice before equal amounts of protein were loaded on the gel. The gel was run at 80 V until the probes had entered the separating gel and then at 150 to 200 V until the colored running front was nearly running out of the gel.

Table 19: Composition of SDS-PAGE gels

4 % stacking gel		9 % separating gel	
Reagent	**Volume**	**Reagent**	**Volume**
Stacking gel buffer	2.5 ml	Separating gel buffer	2.5 ml
Rotiphorese® Gel 30 (37.5:1)	1.3 ml	Rotiphorese® Gel 30 (37.5:1)	3.0 ml
H_2O	6.2 ml	H_2O	4.5 ml
TEMED	70 µl	TEMED	70 µl
10 % ammonium persulfate	14 µl	10 % ammonium persulfate	7 µl

6.2.5. Western blot (WB)

Using a Criterion^{TM} Blotter (Bio-Rad) tankblot system according to its manual, western blots were performed to transfer proteins from an SDS-PAGE gel to a nitrocellulose or a PVDF membrane for immunodetection of the protein(s) of interest. Following transfer at 80 V for 30 min, the membrane was blocked with 5 % (w/v) milk powder in TBS-T or 3 % (w/v) BSA in TBS-T for 1h at RT. Primary antibody incubation was done overnight in blocking solution in a 50 ml reaction tube on a rollator at 4 °C. Following washing with TBS-T 3x 15 minutes, incubation with the secondary, HRP-linked antibody diluted in TBS-T occurred for 1 h at RT. After additional washing steps with TBS-T for 3x 8 min at RT, detection of the blot was performed using ECL^{TM} Prime Western Blotting System (GE Healthcare) and a ChemoCam Imager (Intas Science Imaging) or an x-ray film (Typon Röntgenfilm GMBH).

6.2.6. Northwestern blot

Northwestern blots were performed to visualize RNA-protein hybrids separated by an SDS-PAGE. Transfer of the proteins to a PVDF membrane was carried out using a Criterion™ Blotter (Bio-Rad) tankblot system according to its manual. The tankblot running buffer was prepared with DEPC-H_2O. Following blotting, the membrane was baked on a heating plate at 80 °C for 1 h. Blocking and detection were performed using the DIG Wash and Block Buffer Set (Roche) according to its manual, however without the hybridization steps. Visualization was done with a ChemoCam Imager (Intas Science Imaging) or an x-ray film (Typon Röntgenfilm GMBH).

6.3. Maintaining of fly lines

Flies were kept in glass vials with a height of 9 cm and a diameter of 3 cm or in plastic vials with a height of 4.5 cm and a diameter of 9.5 cm. The nutrition medium consisted of 0.8% agar, 2.2% sugar beet molasses, 8.0% malt extract, 1.8% yeast, 1.0% soy flour, 8.0% corn flour and 0.3% hydrobenzoic acid. Fly vials were maintained in a climate chamber at 25 °C and a relative humidity of ~60% with a 12:12h light:dark (LD) cycle.

6.4. Generation of an *mbm^dRGG* mutant fly line

In previous works, fly lines carrying either a wild-type or a zinc-finger mutant genomic construct of *mbm* on the third chromosome and an *mbm* null mutation on the second chromosome have been generated (Hovhanyan et al., 2014; Cornelia Engert, Master Thesis, 2015). To this end, *mbm* was amplified from genomic DNA (gDNA) via PCR and cloned into the pUASTattB vector (Bischof et al., 2007). This pUASTattB-*mbm^WT* construct was modified via mutagenesis PCR to mutate Mbm's two zinc-finger domains, thereby generating pUASTattB-*mbm^ZnF*. Both constructs were injected into *Drosophila melanogaster* embryos by BestGene Inc (Chino Hills, CA 91709, U.S.A.). The pUASTattB transformation vector enables transgenesis into the genome at an attP site mediated by PhiC31 integrase. In the flies used for injection (BDSC #9750), this attP site is located at chromosomal position 65B2 on the 3rd chromosome (Anna Hovhanyan, PhD Thesis, 2014; Cornelia Engert, Master Thesis, 2015; BestGene Inc.). The injected fly lines were crossed into an *mbm* null mutant background (Cornelia Engert, Master Thesis, 2015).

In this work, a new fly line was generated which carries a genomic, RGG-box deleted construct of *mbm*. To this end, the existing pUASTattB-*mbm^WT^* constuct was mutated via SLIM-PCR (Chiu et al., 2004) to delete the RGG-box and sent to BestGene Inc. for injection. Several independent transgenic fly lines were obtained and crossed into the *mbm* null mutant background.

6.4.1. Site-directed, ligase-independent mutagenesis (SLIM) PCR

To delete Mbm's RGG-box from pUASTattB-*mbm^WT^*, SLIM-PCR (Chiu et al., 2004) was performed. The basic principle of a deletion via SLIM-PCR relies on the use of two primer pairs in a single PCR reaction. One primer pair flanks the sequence to be deleted, the other pair is identical to the first pair on the 3' end, but with 15 nucleotide long complementary overhangs on the 5' end. This PCR reaction linearizes the pUASTattB-*mbm^WT^* plasmid and deletes the RGG-box, leading to four different products either with no overhang, overhangs on both ends or with overhangs only on the 5' or on the 3' prime end (of the coding strand). The denaturation and re-hybridization of the mixture of PCR products leads to only two hybrids that feature complementary overhangs on both ends, thereby enabling recircularization and transformation into *E. coli*. The benefit of this method is that only the correct products are able to recircularize, leading to very few viable *E. coli* clones under antibiotic selection which mostly contain the correct plasmid. The following protocol was adapted from the original publication by Chiu et al. (2004).

SLIM-PCR was performed using the non-tailed primers flanking *mbm*'s RGG-box (primers "SLIM mbm dRGG fwd short" and "rev short") and the tailed primers ("SLIM mbm dRGG fwd tailed" and "rev tailed", Table 8) in a single reaction. Thereby, pUASTattB-*mbm^WT^* was linearized and amplified without the RGG-box, resulting in pUASTattB-*mbm^dRGG^* (see Table 20 and Table 21 for the SLIM PCR protocol). The annealing temperature was determined using NEB's Tm calculator (https://tmcalculator.neb.com), only considering the non-tailed primers.

Table 20: SLIM-PCR components

Reagent	Volume (µl)	Final concentration
5x Phusion HF Buffer (NEB)	10	1x
10 mM dNTPs	1	0.2 mM
10 µM Primer Mix	1	0.2 µM
DNA template (200 pg/µl)	1	1 ng
DMSO (NEB)	2.5	5%
Phusion High Fidelity Polymerase (NEB)	0.5	1 U
H_2O	*ad* 50 µl	

Table 21: SLIM-PCR cycle

Temperature	Time	Number of cycles
98 °C	1 min	1
98 °C	10 s	
61 °C	20 s	30
72 °C	6 min	
72 °C	10 min	1
4 °C	∞	

To eliminate the template DNA from the mixture, the PCR product was digested with DpnI. 5 µl 2x D-Buffer, 0.5 µl DpnI (NEB) and 4.5 µl H_2O were added to the PCR product to a final volume of 60 µl. The mixture was incubated at 37 °C for 2 h. 25 µl of the digested sample were mixed with 25 µl H-Buffer, denatured at 99 °C for 3 min and hybridized in two cycles of 65 °C for 5 min and 30 °C for 15 min. 5 µl of the hybridization product were used for transformation into *E. coli* DH5α (Invitrogen) (see 6.1.6.). Following miniprep (see 6.1.7.), the success of the SLIM was verified by sequencing with the primers „mbm fwd 33069" (Table 8) as described earlier (see 6.1.8.). A correct clone was amplified by transformation into *E. coli* and isolated by midiprep (see 6.1.9.).

6.4.2. Injection into fly embryos by BestGene Inc.

The midiprep product of the desired construct pUASTattB-*mbm^{dRGG}* was sent to BestGene Inc. (Chino Hills, CA, U.S.A.) for injection into *Drosophila melanogaster* embryos and PhiC31 mediated integration into the genome at the attP site at chromosomal position 65B2 on the 3rd chromosome (BDSC stock #9750).

6.4.3. Crossing into *mbm* null mutant background

The *P[mbm^{dRGG}]* fly lines received from BestGene Inc. were crossed over balancer chromosomes TM6B, Tb and then into the *mbm* null mutant background called *mbm^{SH1819}*. The final genotype was $+; \frac{P[mbm^{SH1819}]}{Cyo,\ Ubi-GFP}; \frac{P[mbm^{dRGG}]}{TM6B,\ Tb}$. These crossings were carried out by Prof. Dr. Thomas Raabe.

Homozygous larvae with the genotype +; P[*mbm^{SH1819}*]; P[*mbm^{dRGG}*] were used for experiments and are henceforth called *mbm^{SH1819}*; *mbm^{dRGG}*.

6.5. Survival Assay

To investigate the viability of the *mbm* null mutant (*mbm^{SH1819}*), dRGG mutant (*mbm^{SH1819}*; *mbm^{dRGG}*) and zinc-finger mutant (*mbm^{SH1819}*; *mbm^{ZnF}*) fly lines as well as the genomic rescue line (*mbm^{SH1819}*; *mbm^{WT}*), homozygous larvae were selected and their development monitored over the course of at least 14 days.

The fly stocks were transferred to apple juice agar plates for controlled egg deposition. To prepare these plates, 8.75 g agar agar were solubilized in 500 ml H_2O by boiling in a microwave oven. Seperately, 12.5 g D(+)-Saccharose were solubilized in 125 ml apple juice by heating to 60 °C and stirring with a magnetic stirrer. Both solutions were mixed and then poured into petri dishes with a diameter of 6 cm. Finally, a solution of approximately 500 mg baker's yeast in 5 ml H_2O was applied to the surface of the apple juice agar with a paintbrush and allowed to air-dry.

The flies were transferred onto the apple juice agar plates and kept in a climate chamber at 25 °C for 24 h. The flies were discarded and larvae homozygous for *mbm^{SH1819}*, *mbm^{SH1819}*; *mbm^{dRGG}*, *mbm^{SH1819}*; *mbm^{ZnF}* or *mbm^{SH1819}*; *mbm^{WT}* were selected and transferred to petri dishes containing fly nutrition medium (see 6.3). The next 14 days, the plates were kept at 25 °C and pupae as well as fully eclosed adult flies were counted.

w^{1118} was used as a wild-type (negative) control and the *mbm* null mutant *mbm^{SH1819}* as a positive control. The rescue line *mbm^{SH1819}*; *mbm^{WT}* was included to see whether the genomic *mbm* construct inserted into the 3rd chromosome at position 65B2 is generally able to revert the *mbm^{SH1819}* phenotype. Percentages of larvae that pupated and that finally reached adulthood, respectively, were determined in seven independent experiments. Statistical

analysis was done with Origin 2018b by usage of a Mann-Whitney-U test. Alpha error accumulation was adjusted by Bonferroni correction.

6.6. Immunostainings of larval brains

Immunostainings were performed to investigate the localization of specific proteins in larval brain neuroblasts of the different *mbm* mutant fly lines. To this end, L3 larvae were selected, brains were dissected in 1x PBS (Fisher Scientific) and transferred into fixation solution (PLP; see 5.8.). Following fixation for 25 min on ice, the brains were washed in 0.3 % Triton X-100 in PBS (PBT) at RT on a nutator for 10 min or until the brains of all other fly lines were ready to continue. All following steps were carried out on a nutator. Blocking was performed in 3% normal goat serum (NGS) in PBT at RT for 2h. The brains were incubated overnight in a solution of primary antibodies (Table 9) in 3 % NGS in PBT at 4 °C. After washing three times for 1 h in PBT at RT, the brains were subjected to a dilution of secondary antibodies (Table 10) in PBT in the dark, either for 3 h at RT or overnight at 4 °C. The final washing step was carried out overnight in PBT in the dark at 4 °C. The brains were then embedded on an object slide in a drop of Vectashield (Vector Laboratories) and covered with a cover slide which was fixated with nail polish.

Confocal laser-scanning microscopy (CLSM) was performed with an Olympus FLUOVIEW 1000 IX81 or a Leica TCS SPE using a 40x oil immersion objective with 3x digital zoom and a step size of 0.7 µm. The Z-stack generated by the microscope's software was opened in and modified with Fiji (ImageJ) (Schindelin et al., 2012).

6.6.1. Neuroblast (NB) cell size measurements

Neuroblast cell sizes were measured using CLSM image stacks of immunostained L3 larval brains and Fiji (Schindelin et al., 2012). The cell membranes of the neuroblasts could be determined by antibody-staining against NB specific markers aPKC and/or Miranda. Each neuroblast was measured using Fiji's free hand tool in the focal plane in which its area was the biggest. The NB areas in µm² of each genotype were averaged and then used for statistical analysis. Normal distribution was confirmed by a Kolmogorov-Smirnov test and significance was tested by a Student's t-test using Origin 2018b (OriginLabs). Alpha error accumulation was corrected by Bonferroni correction.

6.7. Generation of stable *mbm* overexpression *Drosophila* S2R+ cell lines

Several experiments required the expression of the *mbm* constructs mbm^{WT}, mbm^{dRGG}, mbm^{ZnF} as well as a double mutant $mbm^{dRGG, ZnF}$ in *Drosophila* Schneider S2R+ cells (*Drosophila* Genomics Resource Center, DGRC). In a previous work, an S2R+ cell line carrying the overexpression construct pAc5.1-*myc-mbm*^{WT} was generated (Roland Jeblick, Diploma Thesis, 2006). In the present work, the pAc5.1-*myc-mbm*^{WT} plasmid was newly generated from this cell line and subjected to SLIM to generate the dRGG, the ZnF as well as the dRGG, ZnF double mutant.

6.7.1. Cloning of pAc5.1-*myc-mbm*^{WT}

Total gDNA of the stable cell line carrying pAc5.1-*myc-mbm*^{WT} was extracted as described previously (see 6.1.1.). To amplify mbm^{WT} including the flanking restrictions sites EcoRI and XhoI, standard PCR was performed (see 6.1.2.) using 5 µl gDNA. pAc5.1 sequencing primers were used, annealing was performed at 68 °C and the PCR was run for 30 cycles. The success of the PCR was verified via agarose gel electrophoresis (see 5.1.3). For further amplification, 1 µl of PCR product was used in a second PCR otherwise carried out like the first one. This second PCR product was purified using the Nucleospin Gel and PCR Cleanup kit (Macherey-Nagel) according to the kit's protocol. The DNA was eluted with 20 µl H_2O. To clone mbm^{WT} into the pAc5.1-*myc* vector, 19 µl of purified PCR product and 2 µg of pAc5.1-*myc* vector were digested with EcoRI-HF® and XhoI (NEB) using NEB's CutSmart® buffer. Both reactions were upscaled to a total volume of 50 µl and otherwise carried out as described previously (see 6.1.4 through 6.1.6.). Miniprep (section 6.1.7.), control restriction digestion (6.1.4.), sequencing (6.1.8.) and midiprep (6.1.9.) were performed as described previously. For sequencing, pAc5.1 sequencing primers were used and the results were analyzed using GENtle v.1.9.4.

6.7.2. Mutagenesis of the RGG-box and/or the zinc-finger domains in pAc5.1-*myc-mbm* via SLIM

The deletion of the RGG-box in pAc5.1-*myc-mbm*^{WT} was performed exactly as described previously for pUASTattB-*mbm*^{WT} using the same primers for SLIM-PCR (see 6.4.1.). The SLIM product was amplified via transformation and miniprep (see 6.1.6. and 6.1.7.). Sequencing (see 6.1.8.) using the pAc5.1 sequencing primers as well as the *mbm*-specific

reverse primer "mbm r34258" revealed two undesired mutations (S→P) in pAc5.1-*myc-mbm*^{dRGG} in comparison to *mbm*'s gene sequence retrieved from flybase.org (CG11604) and to pUAST-*mbm*^{dRGG}. Both mutations were then also found in pAc5.1-*myc-mbm*^{WT} generated in this work as well as in the gDNA extracted from the stable pAc5.1-*myc-mbm*^{WT} S2 cell line which existed previously in our lab. Therefore, these unwanted mutations in both plasmids were corrected via two rounds of SLIM using the primers "SLIM T→C Exon 1 F$_S$", "SLIM T→C Exon 1 R$_S$", "SLIM T→C Exon 1 F$_T$" and "SLIM T→C Exon 1 F$_T$" in the first round and "SLIM T→C Exon 2 F$_S$", "SLIM T→C Exon 2 R$_S$", "SLIM T→C Exon 2 F$_T$" as well as "SLIM T→C Exon 2 F$_T$" in the second round (see Table 8).

Further SLIM-PCRs were performed to substitute the first amino acid in *mbm*'s two zink finger domains (C354Y and C371Y) in pAc5.1-*myc-mbm*^{WT} and pAc5.1-*myc-mbm*^{dRGG}. Primers used were "SLIM ZnF1 F$_S$", "SLIM ZnF1 R$_S$", "SLIM ZnF1 F$_T$" and "SLIM ZnF1 R$_T$" for C354Y and "SLIM ZnF2 F$_S$", "SLIM ZnF2 R$_S$", "SLIM ZnF2 F$_T$" as well as "SLIM ZnF2 R$_T$" for C371Y (see Table 8).

6.7.3. Stable transfection into *Drosophila* S2R+ cells

The plasmids pAc5.1-*myc-mbm*^{WT}, pAc5.1-*myc-mbm*^{dRGG}, pAc5.1-*myc-mbm*^{ZnF} and pAc5.1-*myc-mbm*^{dRGG,ZnF} were transfected into Schneider S2 cells. To this end, S2R+ cells were cultured at 25 °C in full medium (Schneider's *Drosophila* Medium (Biowest) supplemented with 10 % heat-inactivated fetal bovine serum (FBS; Biochrom AG) and 1 % penicillin/streptomycin (Invitrogen)) to a density of approximately 5 x 10^6 cells/ml. For each transfection, 1.8 x 10^6 cells were transferred into a well of a 6-well plate and the total volume per well was adjusted to 3 ml with full medium. The cells were grown overnight in 25 °C. The medium was aspirated and 2 ml of serum-free Schneider medium (SFM) was pipetted to each well. For each transfection, 100 µl of SFM were mixed with 8 µl Cellfectin (Invitrogen). In a second reaction tube, 3.6 µg of either pAc5.1-*myc-mbm*^{WT}, pAc5.1-*myc-mbm*^{dRGG}, pAc5.1-*myc-mbm*^{ZnF} or pAc5.1-*myc-mbm*^{dRGG,ZnF} as well as 0.8 µg pCoHygro (Invitrogen) were added to 100 µl SFM and mixed by vortexing. For each transfection, the tubes were mixed and incubated at RT for 30 min before 800 µl SFM were added. The SFM previously added to the cells was aspirated and the transfection mixtures were pipetted onto the cells. Following incubation at 25 °C for 5 h, the transfection medium was removed by aspiration and 3 ml full medium were added. The cells were grown at 25 °C for 3 days, then resuspended, pelleted at 1,200 x g for 5 min, resuspended in 5 ml fresh full medium and transferred into a 25 ml cell

culture flask. The cell cultures were split 1:5 with fresh full medium every three to four days. After two weeks, full medium added to the cell cultures was supplemented with 0.2 µg/µl Hygromycin B Gold (InvivoGen) for the selection of successfully transfected cells.

6.7.4. Long-term storage of S2R+ cells in liquid N_2

Aliquots of the stably transfected cell lines were stored in liquid nitrogen. The cell density was determined using a Neubauer improved cell counting chamber and the cells were pelleted at 1,200 x g for 5 min. The supernatant (conditioned medium) was transferred into a new tube and the cells were resuspended in 10 ml Dulbecco's PBS (Biowest). Following centrifugation at 1,200 x g for 5 min, the supernatant was discarded and the cell pellet was resuspended in freezing medium (40 % conditioned medium, 40 % fresh full medium, 10 % heat-inactivated FCS (Biochrom AG), 10 % DMSO (Applichem)). The amount of freezing medium was adjusted to a final cell density of 1.1 x 10^7 cells/ml. The cell suspension was split into 1 ml aliquots in cryovials. The cryovials were wrapped into paper towels, placed in a Styrofoam box and frozen at -80 °C. After a week, the cryovials were transferred into a liquid nitrogen tank.

To take frozen cells into culture, a cryovial was thawed at RT and the cell suspension was washed twice by centrifugation at 1,200 x g for 5 min, discarding the supernatant and resuspending in 10 ml Dulbecco's PBS. After the second washing step, the cells were resuspended in 5 ml full medium and transferred into a 25 ml cell culture flask. For the first two weeks, the medium was aspirated and the cells were resuspended in fresh full medium. Then, hygromycin B selection was started as described previously (see 6.7.3.).

6.8. RNA-binding assay

The RNA-binding assay was adapted from E-Shehawi & Elseehy (2013) as well as Cornelia Engert, Master Thesis (2015) and used to investigate the ability of different Mbm mutants to bind to ribosomal RNA (rRNA) probes. To this end, myc-tagged Mbm proteins with either wild-type amino acid sequence (myc-Mbm^{WT}), a deleted RGG-box (myc-Mbm^{dRGG}), mutated zinc-fingers (myc-Mbm^{ZnF}) or the double mutation (myc-Mbm^{dRGG,ZnF}) were expressed in *Drosophila* S2R+ cells and isolated via native immunoprecipitation (IP) as described earlier (see 6.2.2.). The protein concentrations of the IP products were estimated using a dot blot (see

6.2.3.2.). The digoxygenin-labeled rRNA probes needed for the assay were generated as described in section 6.8.1.

6.8.1. Generation of digoxygenin-labeled rRNA probes

In previous works, fragments of ribosomal DNA were amplified by PCR and cloned into pSTBlue-1 AccepTor™ vector (Novagen) for later *in-vitro* transcription into digoxygenin (DIG)-labeled rRNA probes (Prof. Dr. Thomas Raabe, AG Raabe; Cornelia Engert, Master Thesis, 2015).

In the present study, the generation of DIG-labeled RNA probes was performed using the DIG Northern Starter Kit (Roche). The rDNA sequences for the different probes had been cloned into pTSBlue-1 using the restriction enzymes KpnI and SacI (Prof. Dr. Thomas Raabe, AG Raabe; Cornelia Engert, Master Thesis, 2015). The plasmids were linearized using either KpnI or SacI and the rDNA was *in-vitro* transcribed using either T7 or SP6 RNA polymerase (Roche). The restriction enzyme and RNA polymerase were chosen depending of the orientation of the rDNA insert in pTSBlue-1 so that sense-DIG-rRNA probes were generated. The DIG-labeling *in-vitro* transcription was performed according to the DIG Nothern Starter Kit's manual. The labeling efficiency was also determined according to the kit's manual using a Biodyne B Transfer (positively charged nylon) Membrane, 0.45 µm (PALL). Cross-linking was performed with a Hoefer UVC500 UV crosslinker by applying 120,000 µJ/cm² with UV light at a wavelength of 254 nm.

6.8.2. RNA-binding assay

80 ng of immunoprecipitated protein (see 6.6.1. and 6.6.2.) were mixed with 1.5 µl RNase inhibitor (Applied Biosystems) and the total volume was adjusted to 18.5 µl with RNA-binding buffer. After incubation at RT for 5 min, 0.5 µl DIG-labeled rRNA probe (150 ng) were added to the sample and incubated at RT for 30 min. The bonds between rRNA molecules and proteins were stabilized by crosslinking on ice for 10 min using a UV closslinker (Hoefer UVC500). Unbound rRNA was digested by adding 1 µl RNase A (1 µg/µl) and incubation at 37 °C for 15 min. The reaction was stopped and the probes were prepared for SDS-PAGE by mixing with 20 µl 2x Laemmli buffer. SDS-PAGE was performed as described earlier (see 6.2.4.), but 5 % glycerol were added to the separating gel

and DEPC-H$_2$O was used to prepare all the solutions needed. Northwestern blot was carried out to visualize the rRNA-protein hybrids separated by SDS-PAGE (see 6.2.6.).

6.9. Demethylation assay

To investigate the methylation status of Mbm^{dRGG} in comparison to Mbm^{WT} expressed in S2R+ cells, demethylation assays were performed (adapted from Chen et al., 2004). Stable S2R+ cell lines expressing myc-Mbm^{WT} or myc-Mbm^{dRGG} as well as untransfected S2R+ cells were grown to a density of approximately 5 x 10^6 cells/ml. The cells were resuspended and 5 ml of each cell line were evenly split into two wells of a 6-well plate. To one well of each cell line, 500 µl full medium (see 6.7.3.) supplemented with 10 µM adenosine dialdehyde (AdOx) were added. Following incubation at 25 °C for 5 h, IP was performed using 5 µl mouse anti-myc 9E10 antibody (Santa Cruz Biotechnology) as described previously (see 6.2.1.). The IP products were subjected to SDS-PAGE (see 6.2.4.) followed by western blot (see 6.2.5.) using the primary antibodies anti-myc 9E10, anti-mbm95, anti-sDMA SYM11 (anti-symmetrical dimethylated arginines) and anti-aDMA ASYM24 (anti-asymmetrical dimethylated arginines; see Table 9).

6.10. Methylation assay

By methylation assay, it was attempted to investigate the ability of *Drosophila* arginine methyl transferases 1 and 5 (DART1 & DART5) to methylate Mbm's RGG-box. To this end, total RNA was extracted from *w1118* flies using a Total RNA Extraction Kit (Applied Biosystems). Ten female flies were homogenized in 400 µl lysis buffer (supplied by the kit) and RNA was extracted according to the kit's protocol. The RNA was reverse transcribed using a High-Capacity cDNA Reverse Transcription Kit (Applied Biosystems) following its protocol. Using the cDNA as a template, the genes *dart1* and *dart5* were amplified by PCR (see 6.1.2.) at an annealing temperature of 66 °C using the primers "EcoRI-Dart1 fwd" and "Dart1-XhoI rev" for *dart1* and "EcoRI-Dart5 fwd" and "Dart5-XhoI rev" for *dart5*. Thereby, an EcoRI restriction site was added at the 5' end and an XhoI restriction site was added at the 3' end of both genes. Both constructs were cloned into pMT/V5-His A, a CuSO$_4$-inducable transfection vector (Invitrogen), using EcoRI-HF and XhoI restriction enzymes (see 6.1.5.) and thereby fusing the genes to a His$_6$-tag. The newly generated plasmids were amplified, isolated and verified by sequencing as described earlier (see 6.1.6. through 6.1.9). 1 µg of

both plasmids was transiently transfected into the stable pAc5.1-*myc-mbm*[WT] and pAc5.1-*myc-mbm*[dRGG] S2R+ cell lines generated previously (see 6.7.). The transient transfection was carried out like the stable transfection (see 6.7.3.), but without cotransfection of pCoHygro. The transfected cells were grown in full medium for two days and then the expression of *his6-dart1* or *his6-dart5* was induced by adding 350 µM $CuSO_4$. Following 24 h of incubation, the cells were pelleted by centrifugation at 1,200 x g and 4 °C for 5 min, the pellet was resuspended in 10 ml cold Dulbecco's PBS (Biowest) and pelleted again at 1,200 x g and 4 °C for 5 min. The cells were lysed by resuspension in 60 µl 1x Laemmli and heating to 95 °C for 10 min. SDS-PAGE and western blot were performed as described earlier (see 6.6.4. and 6.6.5.), using the antibodies anti-myc 9E10, anti-His6 HIS.H8, SYM11 and ASYM24 (Table 9).

6.11. Puromycin assay

Puromycin is an aminoacyl-tRNA analog that can be incorporated into newly synthesized proteins, thereby terminating the translation (Nathans, 1964; Nakano and Hara, 1979; Hansen et al., 1994). It is therefore used in Puromycin assays to investigate protein synthesis rates in *Drosophila* larval tissues *ex vivo* (adapted from Schmidt et al., 2009, Deliu et al., 2017). 15 larvae were inverted in Schneider's *Drosophila* Medium (Biowest) supplemented with 10 % heat-inactivated FBS (Biochrom AG) by opening their posterior end with forceps and turning them inside-out. The inverted larvae were then transferred into 1.5 ml reaction tubes containing Schneider medium with 10% FBS and 10 µg/ml puromycin. A negative control was additionally supplemented with 100 µg/ml cycloheximide and incubation of all samples was carried out on a rotator at RT for 40 min. The inverted larvae were then transferred into ice-cold PBS, the brains were dissected and immediately transferred into 10 µl 2x Laemmli buffer. SDS-PAGE and western blot were performed (see 6.2.4. and 6.2.5.) and newly synthesized proteins with incorporated puromycin could be detected with anti-puromycin 12D10 antibody (Table 9).

6.11.1. Quantification of puromycin assays

The signal intensity of the western blots of four independent experiments was quantified with Fiji (ImageJ) using its gel analysis function. For each genotype or treatment, the total intensity of the whole lane on the blots was measured, normalized to the loading control (α-Tubulin)

and plotted relative to the intensity of puromycin-treated w^{1118} larval brains. Statistical analysis was done in R by a Wilcoxon-Rank-Sum (Mann-Whitney-U) test.

7. Results

7.1. Deletion of Mbm's RGG-box

For the generation of *mbm*^{dRGG} mutant flies as well as the expression of Mbm^{dRGG} in *Drosophila* S2R+ cells, *mbm* was cloned into the pUASTattB or pAc5.1-*myc* vector, respectively, and the RGG-box was deleted. Mbm's RGG-box was defined including one di-RGG and one di-RG motif in close proximity (Figure 15). The single RGG downstream of the di-RG motif was also included in the deletion.

Figure 15: Definition of Mbm's RGG-box
Mbm's RGG-box was defined including one di-RGG (red) and one di-RG motif (green). A single RGG (blue) in close proximity to the di-RG motif was also included in the deleted part.

Sequencing analysis showed the successful deletion of the RGG-box, spanning base pairs 247 – 342 of *mbm*'s coding sequence (Figure 16).

Figure 16: Sequencing results showing the RGG-deletion
The sequence coding for Mbm's RGG-box was deleted by SLIM-PCR and sequencing results were aligned with wild-type *mbm* (flybase.org) to verify the desired deletion. Shown here is an excerpt of the sequencing results including the deletion of base pairs 247 – 342 of *mbm*'s coding sequence. Stars indicate matching base pairs and dashes missing base pairs in *mbm*^{dRGG} in comparison to *mbm*.

7.2. Phenotypical characterization of *mbm*^{dRGG} mutant flies

7.2.1. Viability is decreased in flies expressing *mbm*^{dRGG} and *mbm*^{ZnF}

The ability of the *mbm*^{dRGG} and *mbm*^{ZnF} transgenes to rescue the lethality of *mbm*^{SH1819} was investigated. Two independent fly lines carrying the *mbm*^{ZnF} transgene and three independent fly lines carrying the *mbm*^{dRGG} transgene crossed into the *mbm*^{SH1819} background were tested

in survival assays (see 6.4.3. and 6.5; Figure 17). While the wild-type line w^{1118} showed 85.1 ±10.1 % of larvae reaching pupal stage and 81.1 ±8.5 % of larvae reaching adulthood, the viability of *mbm* null mutant larvae is significantly decreased with 44.3 ±16.6 % (p = 0.012) reaching the pupal stage and 0 % reaching adulthood (p = 0.007). *mbm^{SH1819}; mbm^{WT}* rescues the ability to reach the pupal stage (86.8 ±10.7 %), but significantly fewer larvae (45.1 ±15.1 %; p = 0.014) reach the adult stage. Thus, viability in *mbm^{SH1819}; mbm^{WT}* is not fully rescued. In the two zinc-finger mutant lines *mbm^{SH1819}; mbm^{ZnF}* 2-1M and 2-3M, few larvae reach the pupal stage (10.8 ±11.9 %; p = 0.012 and 21.1 ±9.9 %; p = 0.012, respectively) and only some pupated larvae finally reach adulthood (3.4 ±5.9 %, p = 0.014 and 2.3 ±6.1 %, p = 0.007, respectively). Interestingly, pupation rates in the zinc-finger mutants are also significantly decreased compared to *mbm^{SH1819}* (p = 0.014 for *mbm^{ZnF}* 2-1M and p = 0.03 for *mbm^{ZnF}* 2-3M; see red asterisks in Figure 17). The deletion of Mbm's RGG-box has a less severe effect on pupation rates in all three independent *mbm^{dRGG}* mutant lines, but in the dRGG mutant lines M1 and M4 they are still significantly lower compared to w^{1118} (M1: 58.0 ±14.5 %, p = 0.048; M3: 65.2 ±12.9 %, p = 0.078; M4: 51.1 ±17.2 %, p = 0.018). However, only few escapers reach adulthood (M1: 2.0 ±4.9 %, p = 0.021; M3: 0.6 ±1.5 %, p = 0.007; M4: 0.6 ±1.5 %, p = 0.007).

For all further experiments, only *mbm^{SH1819}; mbm^{ZnF}* 2-1M and *mbm^{SH1819}; mbm^{dRGG}* M1 were used, then simply referred to as *mbm^{SH1819}; mbm^{ZnF}* and *mbm^{SH1819}; mbm^{dRGG}*, respectively.
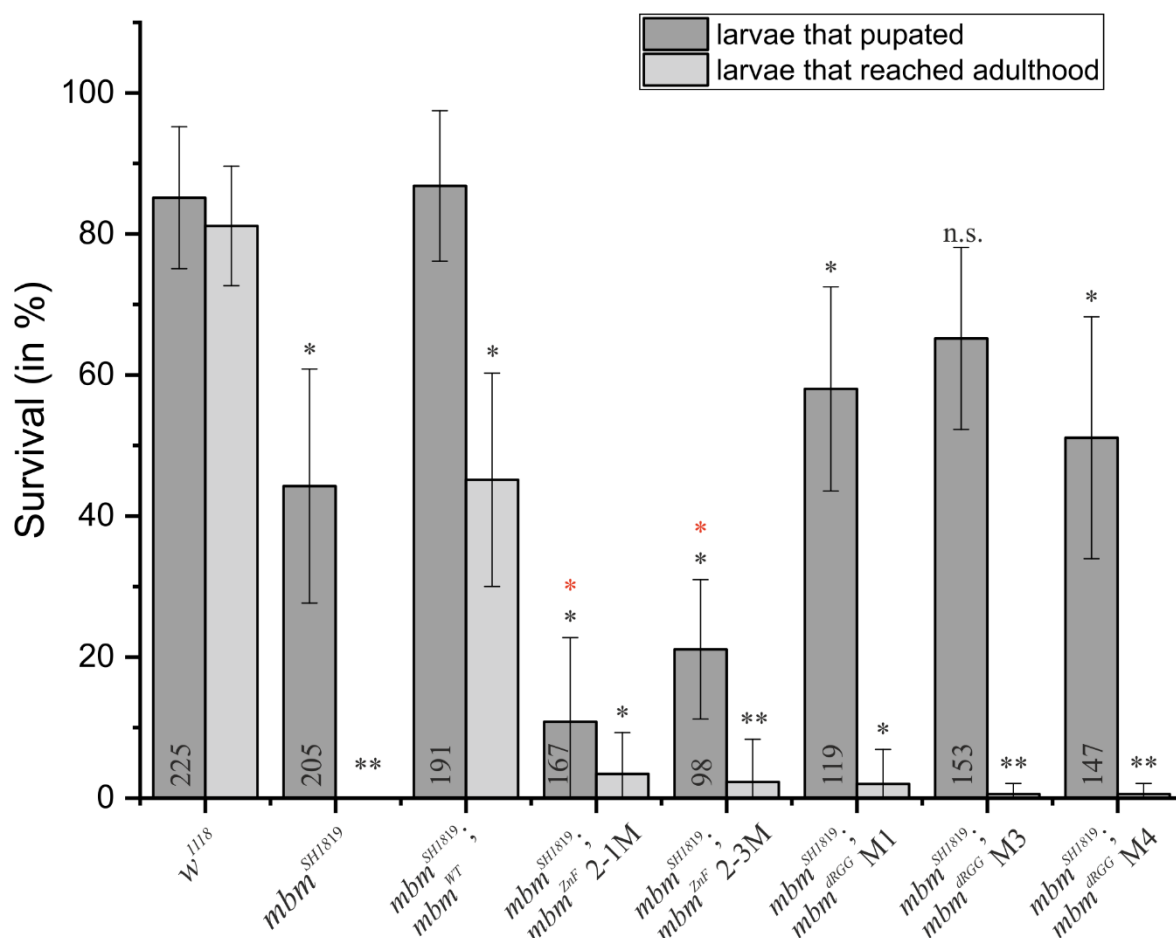
Figure 17: Results of the viability assays
The development of the larvae was monitored for two weeks after larval hatching. Seven independent experiments were performed and survival rates were averaged. The percentage of larvae that pupated (dark grey bars) and larvae that finally reached adulthood (light grey bars) is shown here. The numbers in the dark grey bars indicate the overall number of larvae used per genotype. The black asterisks indicate significant difference in comparison to w^{1118}, red asterisks indicate significance compared to mbm^{SH1819} (* p < 0.05, ** p < 0.01, n.s. = not significant).

7.2.2. Mbm is delocalized in dRGG and ZnF mutant larval neuroblasts

In wild-type larval neuroblasts, Mbm is localized to the nucleolus. To investigate possible effects on Mbm localization caused by the mbm^{dRGG} and mbm^{ZnF} mutations, larval brains were dissected and immunostained with antibodies against Mbm, neuroblast markers Miranda (Mir) and aPKC as well as the nucleolar marker dNop5 (Figure 18). In w^{1118} and the rescue line mbm^{SH1819}; mbm^{WT}, Mbm is localized to the nucleolus while it is completely absent in the null mutant mbm^{SH1819} as it was reported previously (Hovhanyan et al., 2014). The rescue line shows that genomic mbm constructs inserted in position 65B2 in the 3rd chromosome are generally able to be expressed and localized correctly. In mbm^{SH1819}; mbm^{dRGG}, in which Mbm is expressed without its RGG-box, Mbm is also present in the nucleolus, but partially delocalized to the nucleus. In contrast, in the zinc-finger mutant mbm^{SH1819}; mbm^{ZnF}, Mbm is

completely delocalized to the cytoplasm. The aPKC staining was barely visible in contrast to the very strong staining of dNop5 on the same channel, but neuroblasts could still be determined by staining of Miranda.
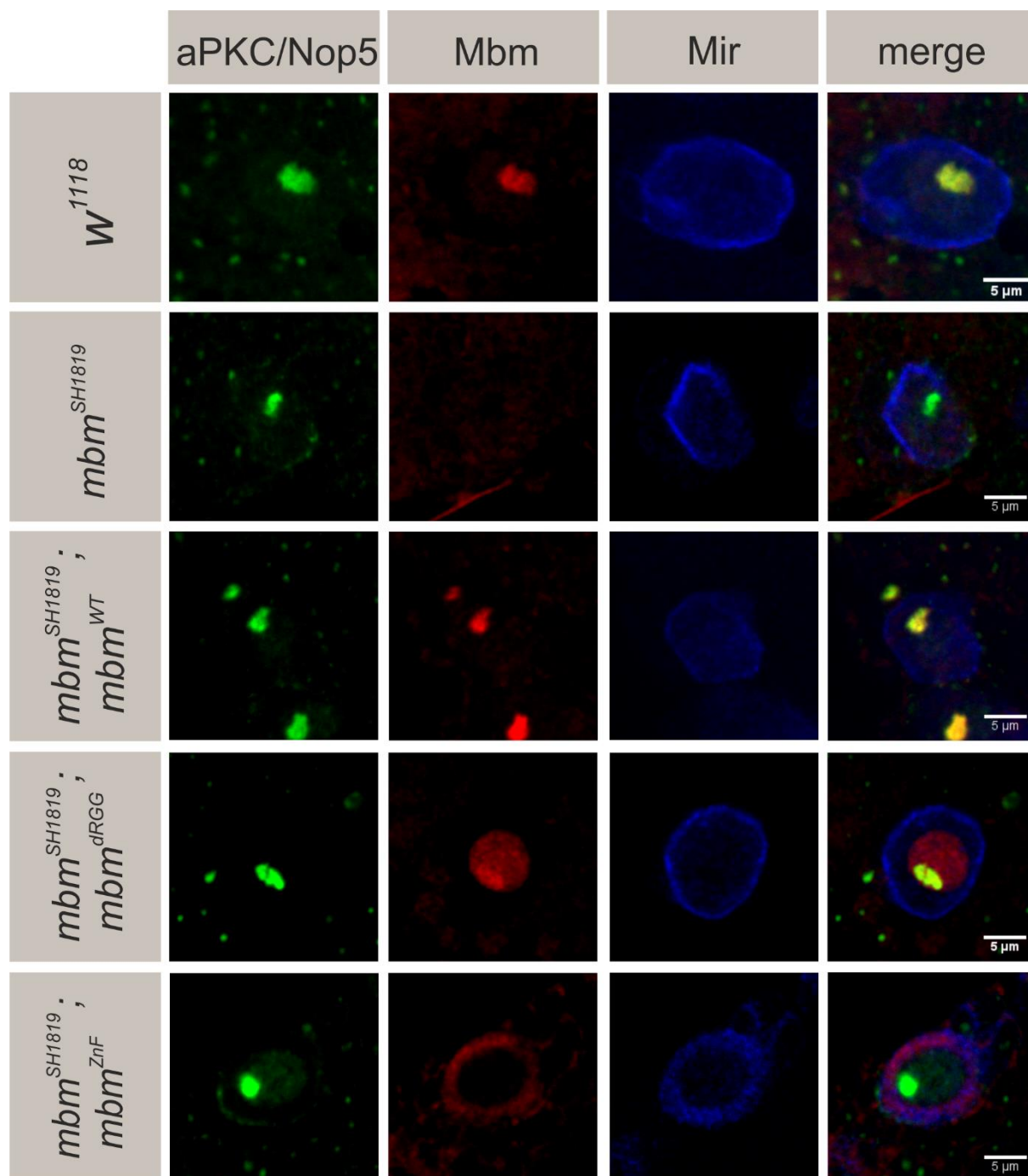
Figure 18: Mbm is delocalized in dRGG and ZnF mutant neuroblasts
Interphase neuroblasts were stained for neuroblast marker aPKC and nucleolar marker dNop5 (green), Mbm (red) as well as neuroblast marker Miranda (Mir, blue). Representative images are shown here. Mbm is located in the nucleus in *w1118* and the rescue line *mbm^{SH1819}; mbm^{WT}*, while it is absent in the null mutant *mbm^{SH1819}*, partially delocalized to the nucleus in the RGG-mutant *mbm^{SH1819}; mbm^{dRGG}* and fully delocalized to the cytoplasm in the zinc-finger mutant *mbm^{SH1819}; mbm^{ZnF}*. The aPKC staining is barely visible in contrast to the strong staining of dNop5.

7.2.3. Neuroblast cell size is significantly decreased in dRGG mutants

Since it was reported previously that neuroblasts are significantly smaller in the *mbm* null mutant *mbm^{SH1819}* (Hovhanyan et al., 2014), NB cell sizes in *mbm^{dRGG}* and *mbm^{ZnF}* mutant larval brains were measured (see 6.6.1.). Neuroblasts were measured regardless of their cell cycle state. NBs in the *mbm* null mutant were significantly smaller (94.2 ±26.2 µm²; p = 0.0012; n = 203) compared to *w^{1118}* (104.2 ±26.4 µm²; n = 169). Similarly, the dRGG mutant *mbm^{SH1819}; mbm^{dRGG}* showed significantly smaller NB sizes (97.5 ±22.4 µm²; p = 0.032; n = 205). NB sizes in *mbm^{SH1819}; mbm^{ZnF}* were found to not be significantly different to the wild-type (105.4 ±18.4 µm²; p = 2.44; n = 212) which is consistent with the findings in an earlier work (Cornelia Engert, Master Thesis, 2015). The neuroblasts in the rescue line are also not significantly different to *w^{1118}* (102.0 ±29.7 µm²; p = 1.88; n = 157; Figure 19).
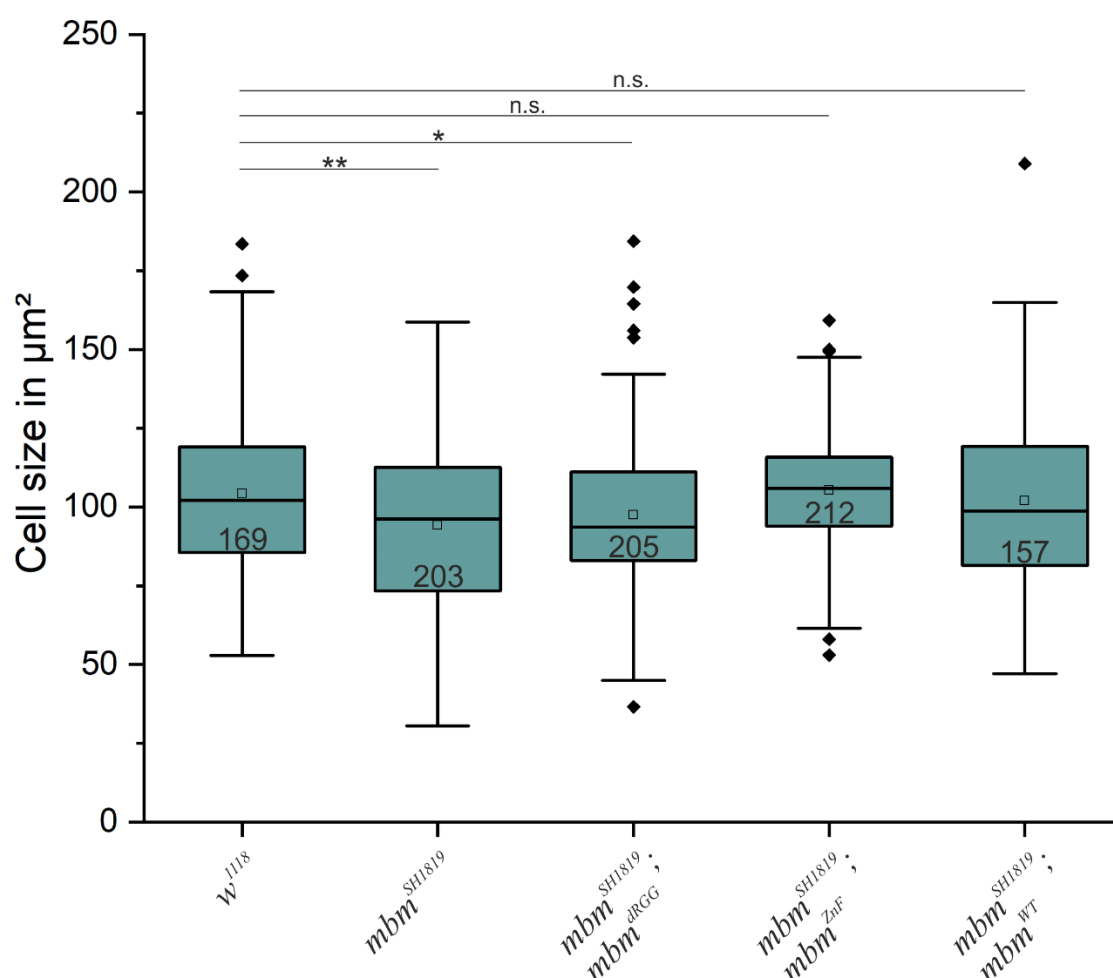
Figure 19: Neuroblast size is significantly decreased in *mbm^{dRGG}* mutants
Neuroblasts in *mbm^{SH1819}* are significantly smaller (p = 0.0012) compared to *w^{1118}* (as reported in Hovhanyan et al., 2014). Similarly, significantly smaller NBs were found in *mbm^{dRGG}* mutants (p = 0.032). Neuroblast size in the zinc-finger mutant *mbm^{SH1819}; mbm^{ZnF}* and in the rescue line *mbm^{SH1819}; mbm^{WT}* are not significantly different to *w^{1118}* (p = 2.44 and p = 1.41, respectively). (* = p < 0.05; ** = p < 0.01; n.s. = not significant).

Additionally, total brain size was observed to be visibly reduced in mbm^{SH1819} and mbm^{SH1819}; mbm^{ZnF} 3rd instar larvae, but no measurements were carried out. In mbm^{SH1819}; mbm^{dRGG} larvae, however, total brain size does not seem to be reduced.

7.3. The role of Mbm's RGG-box in ribosome biogenesis

7.3.1. Mbm[dRGG] shows decreased binding of ribosomal RNA

In an earlier work it was suggested that Mbm plays a role in ribosome biogenesis, since it could be shown that Mbm influences the processing of ribosomal RNA (rRNA) (Hovhanyan et al., 2014). This finding raises the question which protein domain of Mbm is capable of binding rRNA, enabling an interaction between the protein and the RNA. Two likely candidates are Mbm's RGG-box as well as its zinc-finger domains. In order to shed light into these domains' rRNA-binding capabilities, RNA-binding assays were performed using myc-tagged Mbm constructs with either wild-type Mbm sequence (myc-Mbm[WT]), a deleted RGG-box (myc-Mbm[dRGG]), mutated zinc-fingers (myc-Mbm[ZnF]) or a double mutant (myc-Mbm[dRGG,ZnF]) expressed in *Drosophila* S2R+ cells. The rRNA probes used in this experiment are depicted in (Figure 20).
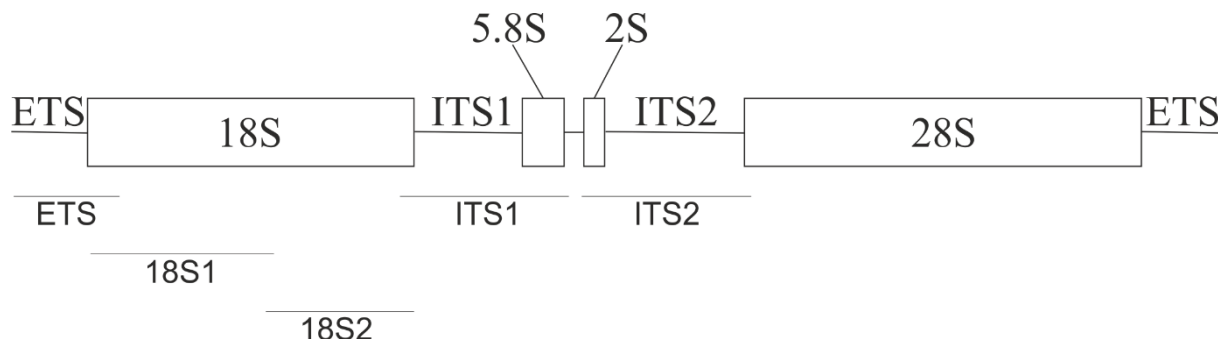
Figure 20: Structure of the rDNA and locations of the rRNA probes.
The rDNA of *Drosophila melanogaster* contains the genes for the 18S, 5.8S, 2S and 28S rRNAs (boxes) that are part of the ribosomal subunits. Upstream of the 18S DNA lies an external transcribed spacer (ETS), the internal transcribed spacer 1 (ITS1) is located in between 18S and 5.8S rDNA and the internal transcribed spacer 2 (ITS2) lies in between 2S and 28S rDNA. Below the rDNA strand, the fragments are shown which were *in-vitro* transcribed into rRNA probes including their designation used in this work (figure adapted from Cornelia Engert, Master Thesis, 2015).

In the binding assay, all rRNA probes show weaker binding to myc-Mbm[dRGG] compared to myc-Mbm[WT], which is mostly evident in the case of ITS1. Surprisingly, ETS, ITS1 and ITS2 show stronger binding to the zinc-finger mutant myc-Mbm[ZnF] compared to the wild-type construct and this effect is increased even further in the double mutant myc-Mbm[dRGG,ZnF] (Figure 21A). The loading control (Figure 21C) shows that all myc-Mbm constructs were approximately evenly applied and that differences in Figure 21A are not caused by uneven

loading. myc-Mbm was expected to run at approximately 100 kDa, however, additional protein bands are visible at ~200 and ~300 kDa, which cannot be explained by truncated protein. Thus, a control blot of myc-Mbm^{WT} bound to ITS1 was detected with anti-Mbm EP031195 antibody to see whether these bands are caused by the binding of two or three Mbm proteins to one rRNA molecule. Probing northwestern blots with anti-Mbm proved difficult, but weak bands are visible at ~200 and ~300 kDa, indicating Mbm dimers and trimers (see Figure 21B). In contrast, in the loading control with the same amounts of protein samples but without rRNA probes, these two upper bands do not appear (Figure 21C).
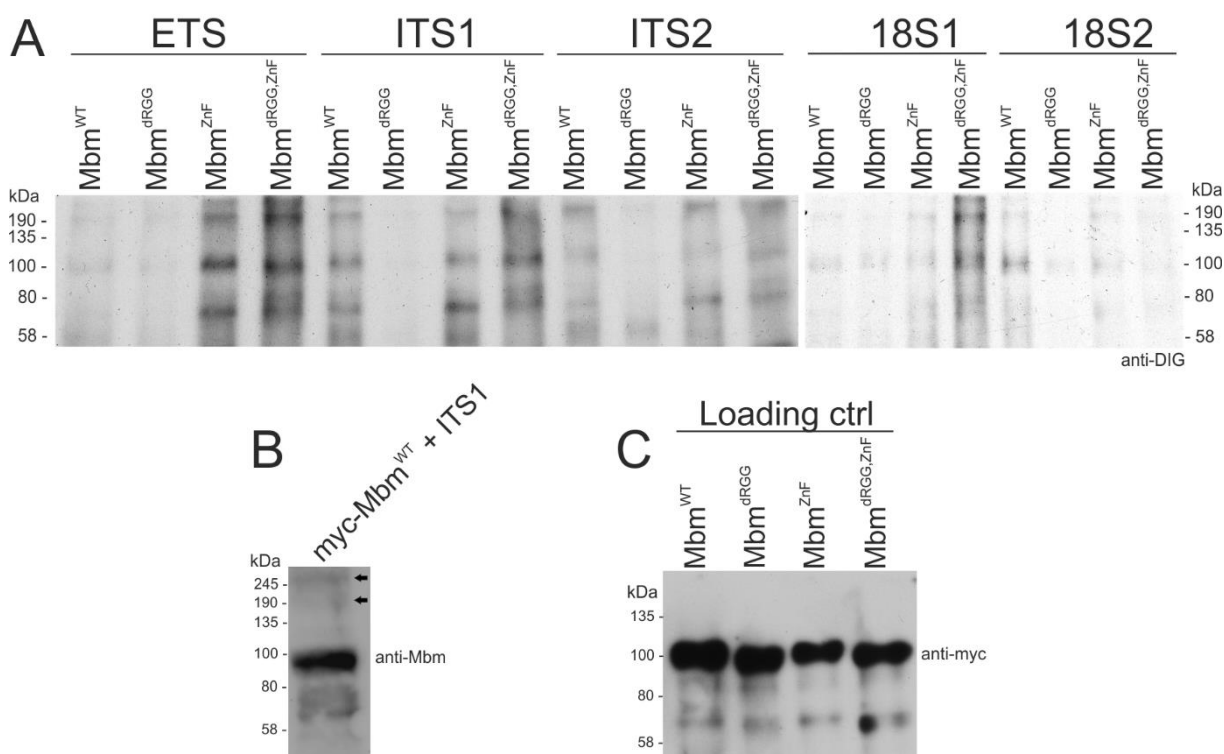
Figure 21: rRNA-binding is decreased in myc-Mbm^{dRGG}, increased in myc-Mbm^{ZnF} and the double mutant
myc-Mbm constructs were expressed in S2R+ cells and purified by IP for RNA-binding assays with DIG-labelled rRNA probes. **A** All rRNA probes show weaker binding to myc-Mbm^{dRGG} in comparison to myc-Mbm^{WT} with the biggest difference found in the case of ITS1. myc-Mbm^{ZnF} shows stronger binding of the rRNA probes, while the double mutant myc-Mbm^{dRGG,ZnF} appears to have the strongest binding affinity to all rRNA probes except 18S2. **B** The bands at ~200 and ~300 kDa seem to be dimers and trimers of Mbm verified by detection with anti-Mbm (indicated by arrows). **C** The same volume of each protein sample used for the binding assay was used as a loading control (without rRNA probes), showing that all samples were approximately evenly applied.

7.3.1.1. Investigation of the methylation status of Mbm's RGG-box

Since the methylation status of RG/RGG domains is important for their RNA-binding capabilities (Blackwell et al., 2010), it was investigated whether Mbm is methylated within its RGG-box. To this end, myc-Mbm^{WT} and myc-Mbm^{dRGG} constructs were expressed in

Drosophila S2R+ cells and purified by immunoprecipitation using anti-myc 9E10 antibodies. Western blots were performed using antibodies against symmetrically and asymmetrically dimethylated arginines (SYM11 and ASYM24 antibodies, respectively). As a negative control, cells were treated with AdOx, a methylation inhibitor. No asymmetric dimethylation could be observed. However, Mbm^{WT} was found to be symmetrically dimethylated, while no methylation occurred in Mbm^{dRGG} (Figure 22). Thus, Mbm seems to be symmetrically dimethylated within its RGG-box in S2R+ cells. Unfortunately, these results could not be replicated and can therefore only be seen as a hint.
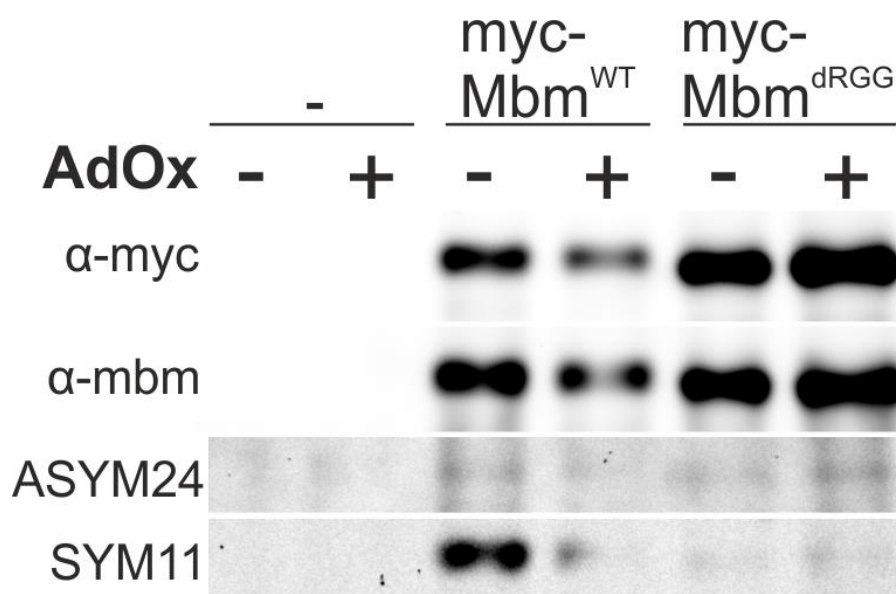
Figure 22: Mbm might be methylated within its RGG-box
Immunoprecipitated myc-Mbm^{WT} expressed in S2R+ cells shows symmetric dimethylation (SYM11) which is reduced upon AdOx treatment. No asymmetric dimethylation (ASYM24) was observed in myc-Mbm^{WT}. In myc-Mbm^{dRGG}, neither symmetric nor asymmetric dimethylation was found. Untransfected S2R+ cells were used as a control for specificity of the IP. Unfortunately, these results could not be replicated.

7.3.1.2 Investigation of Mbm methylation mediated by Dart1 and Dart5

The methylation status of Mbm's RGG-box might be important for its RNA-binding capabilities. Darts1 and Dart5 were assumed to be the most promising candidates for the regulation of protein-RNA binding by asymmetric or symmetric methylation of RGG-boxes, respectively (see 3.3.1.). Therefore, forced methylation of myc-Mbm by overexpression of Dart1 and Dart5 was attempted in *Drosophila* S2R+ cells. Total cell lysates were used for western blots and symmetric or asymmetric dimethylation was detected by SYM11 or ASYM24 antibodies, respectively (Figure 23). Successful expression of the myc-Mbm constructs and His$_6$-Dart1 or Hi$_6$-Dart5 was ensured by detection with anti-myc 9E10 or anti-His$_6$ HIS.H8 antibodies, respectively (see 6.10.). No symmetric dimethylation of myc-Mbm^{WT}

or myc-Mbm^{dRGG} was found. By detection with ASYM24, several bands can be seen at the approximate size of myc-Mbm, but they were also found in the cell lysate of untransfected S2R+ cells, showing unspecific detection. Based on these results, it seems that myc-Mbm cannot be methylated by His$_6$-Dart1 or His$_6$-Dart5 in *Drosophila* S2R+ cells.
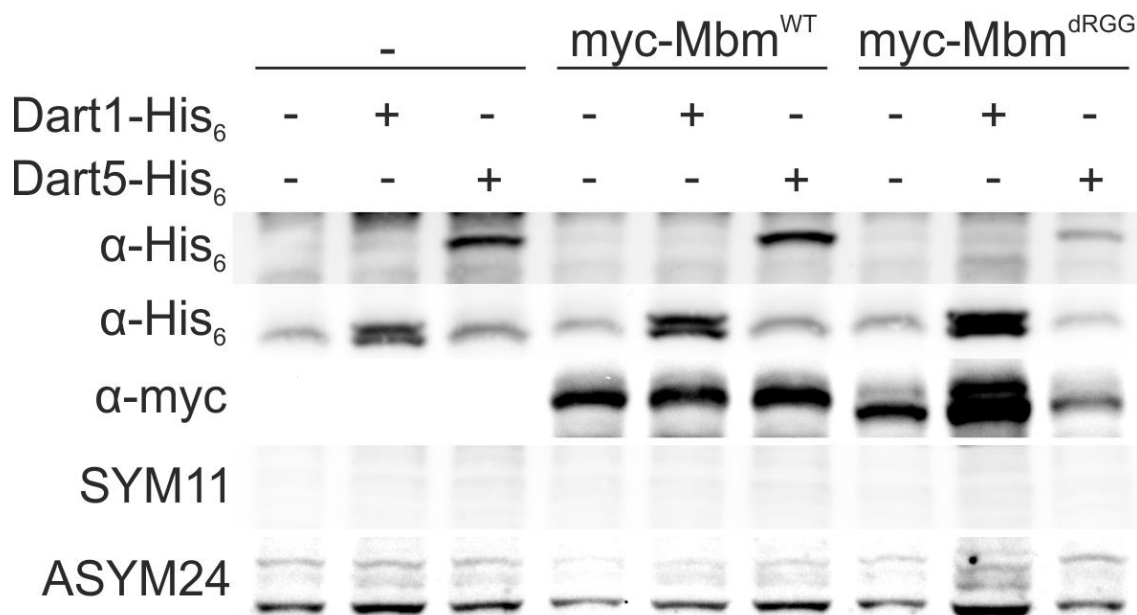

Figure 23: Mbm is not methylated in *Drosophila* S2R+ cells upon Dart1 or Dart5 overexpression
myc-Mbm^{WT} and myc-Mbm^{dRGG} were co-expressed with His$_6$-Dart1 or His$_6$-Dart5 in *Drosophila* S2R+ cells. Total cell lysates were used for western blots. Detection with anti-His$_6$ HIS.H8 antibodies ensured the expression of His$_6$-Dart1 (~46 kDa) or His$_6$-Dart5 (~75 kDa). Expression of myc-Mbm constructs was ensured by detection with anti-myc 9E10 antibodies. Detection with SYM11 antibodies revealed no symmetric methylation of both myc-Mbm constructs. ASYM24 antibodies detected several unspecific bands at the approximate size of myc-Mbm which are also present in cell lysate of unstransfected S2R+ cells. Thus, no asymmetric methylation occured in both myc-Mbm constructs.

7.3.2. Ribosomal protein RpS6 is partially delocalized in Mbm null, dRGG and ZnF mutant neuroblasts

The findings that *mbm^{dRGG}* and *mbm^{ZnF}* mutations influence Mbm's rRNA-binding capabilities, raised the question whether ribosome biogenesis is affected in these mutant fly lines. This might be reflected in failure of ribosomal subunit transport. In an earlier work, a localization defect of RFP-tagged RpS6, a small ribosomal subunit protein, was found in neuroblasts of the *mbm* null mutant *mbm^{SH1819}* (Hovhanyan et al., 2014). Localization of the large ribosomal subunit protein RpL11, in contrast, was not affected. Thus, the influence of *mbm^{dRGG}* and *mbm^{ZnF}* mutations on RpS6 localization in L3 larval neuroblasts was investigated by immunostainings with anti-RpS6 54D2 antibodies (Figure 24). In *w1118,* RpS6 is localized in the cytoplasm and the nucleolus, while in the *mbm^{SH1819}* RpS6 staining could only be observed in the cytoplasm. In the rescue line *mbm^{SH1819}; mbm^{WT}*, this phenotype

is reverted to a wild-type-like state. *mbm^{SH1819}; mbm^{dRGG}* and *mbm^{SH1819}; mbm^{ZnF}*, however, do not show nucleolar RpS6 staining.
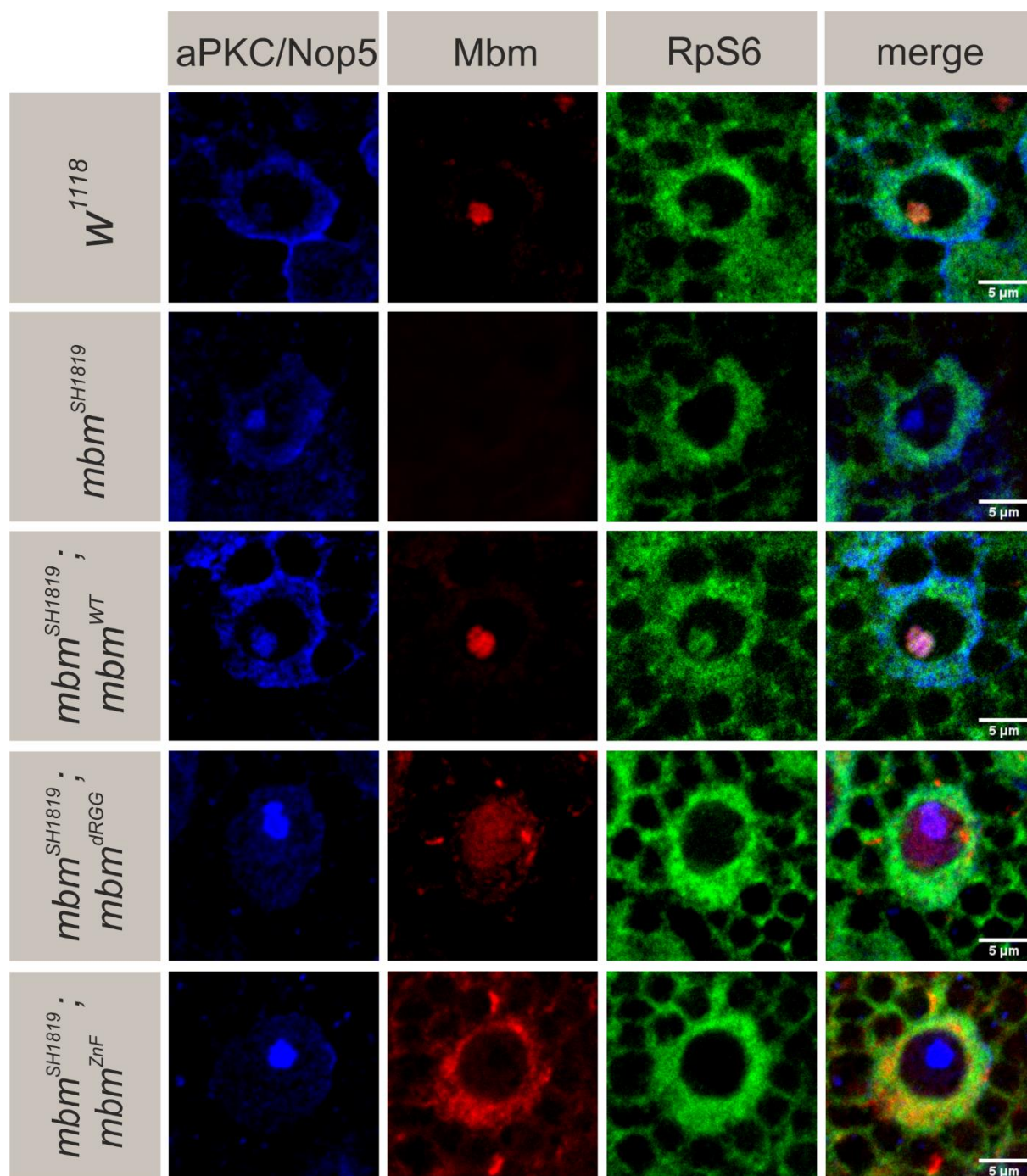
Figure 24: RpS6 is partially delocalized in *mbm* null, dRGG and ZnF mutant neuroblasts
In *w^{1118}* and *mbm^{SH1819}; mbm^{WT}* (rescue) neuroblasts, anti-RpS6 staining (green) was found in the cytoplasm and the nucleolus whereas in the Mbm (red) mutant fly lines *mbm^{SH1819}*, *mbm^{SH1819}; mbm^{dRGG}* and *mbm^{SH1819}; mbm^{ZnF}* RpS6-staining could only be observed in the cytoplasm. aPKC and dNop5 (blue) were used as a neuroblast or nucleolar marker, respectively.

These results contradict the findings from Hovhanyan et al. (2014), where RFP-RpS6 was found to be localized only in the cytoplasm in the wild-type background and mostly in the

nucleolus in the *mbm* null mutant background. Therefore, it was attempted to replicate their approach. *UAS-mRFP::RpS6* was expressed in a wild-type and an *mbm* null mutant background by the neuroblast-specific driver *Mz1060-Gal4*. Since autofluorescence of RFP::RpS6 was insufficient, immunostainings with anti-RFP and anti-RpS6 antibodies were performed. Staining against RpS6 showed nucleolar and cytoplasmic localization in the wild-type background, but only cytoplasmic localization in the *mbm* null mutant background (Figure 25 A). These results are consistent with those shown in Figure 24. The anti-RFP antibody, however, does only exhibit cytoplasmic staining in both the wild-type and *mbm* null mutant background (Figure 25 B). Yet, mRFP-RpS6 might not reflect the behavior of the endogenous RpS6 protein.
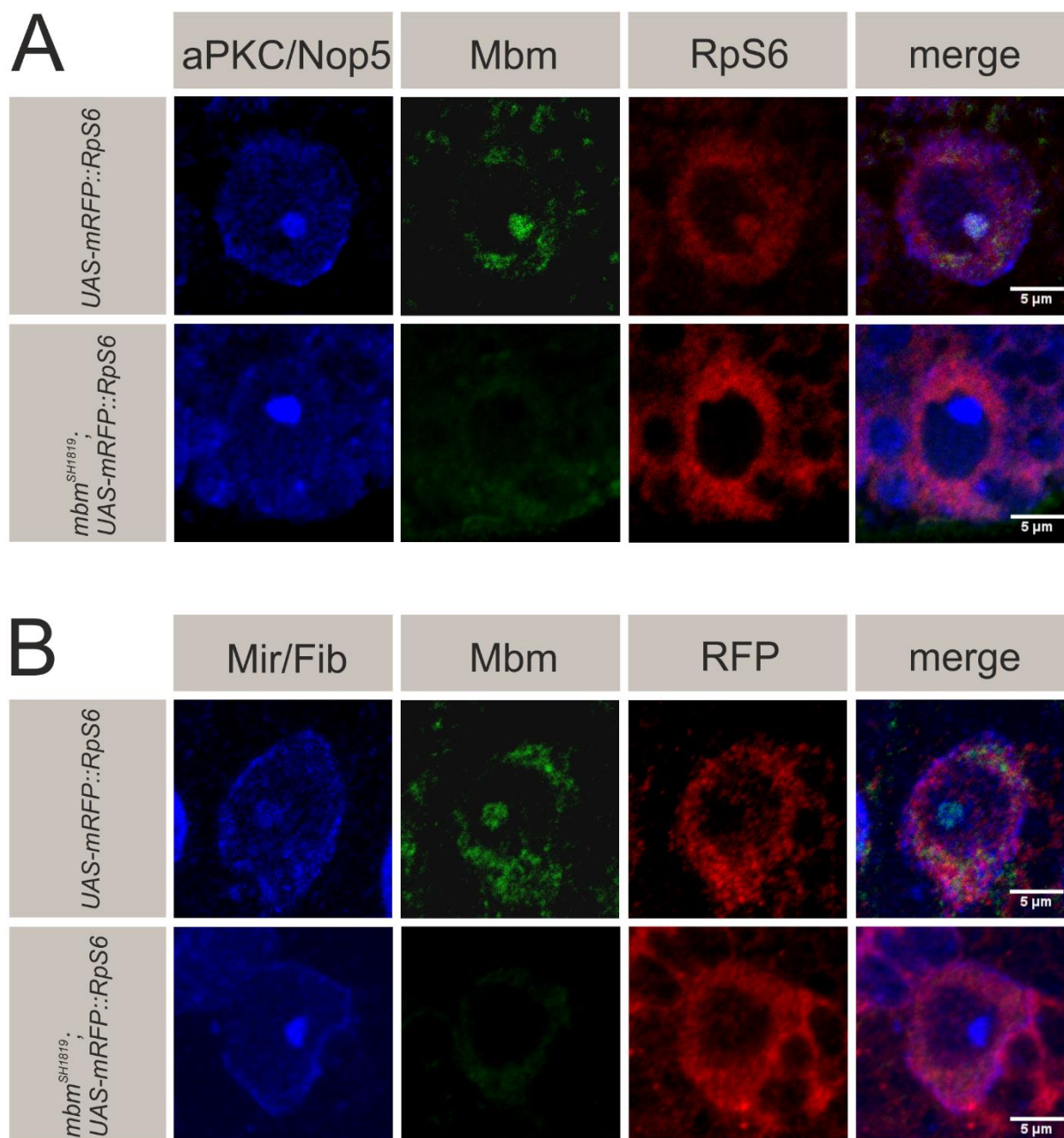
Figure 25: mRFP::RpS6 is not translocated to the nucleolus
A Upon neuroblast specific overexpression of *UAS-mRFP::RpS6* by *Mz1060-Gal4*, RpS6 staining (red) showed nucleolar and cytoplasmic localization in the wild-type background and only cytoplasmic localization in the *mbm* null mutant background (Mbm in green; results consistent with Figure 24). aPKC was used as a neuroblast and dNop5 as a nucleolar marker (blue). **B** Anti-RFP staining (red) revealed only cytoplasmic localization in both the wild-type and the *mbm* null mutant background (Mbm in green). Miranda (Mir) was used as a neuroblast and fibrillarin (Fib) as a nucleolar marker (blue).

7.3.3. Protein synthesis is increased in *mbm^SH1819^; mbm^dRGG^* mutant larval brains

The findings that rRNA processing is affected in *mbm* null mutants (Hovhanyan et al., 2014) and that the small ribosomal subunit protein RpS6 is partially delocalized in *mbm* null, dRGG and ZnF mutant neuroblasts raised the question whether ribosome function is also affected. To elucidate ribosome function in these mutants, protein synthesis rates in larval brains were

investigated by puromycin labeling (Deliu et al., 2017; see 6.11.). Inverted L3 larvae were incubated with puromycin in Schneider medium, brains were dissected, lysed and subjected to Western blots using anti-Puromycin 12D10 antibodies (Figure 26). In w^{1118}, anti-Puromycin detection is mildly increased in puromycin-treated compared to untreated larval brains. Co-incubation with cycloheximide, a protein synthesis inhibitor, abolishes puromycin incorporation, verifying puromycin labeling as a read-out for protein synthesis rates. In larval brains of the *mbm* null mutant mbm^{SH1819}, protein synthesis rates appear to be similar compared to the wild-type line w^{1118}. In the rescue line mbm^{SH1819}; mbm^{WT} and the zinc-finger mutant mbm^{SH1819}; mbm^{ZnF}, however, protein synthesis rates are slightly increased and in the dRGG mutant mbm^{SH1819}; mbm^{dRGG}, protein synthesis rates seem to be strongly increased compared to the wild-type.
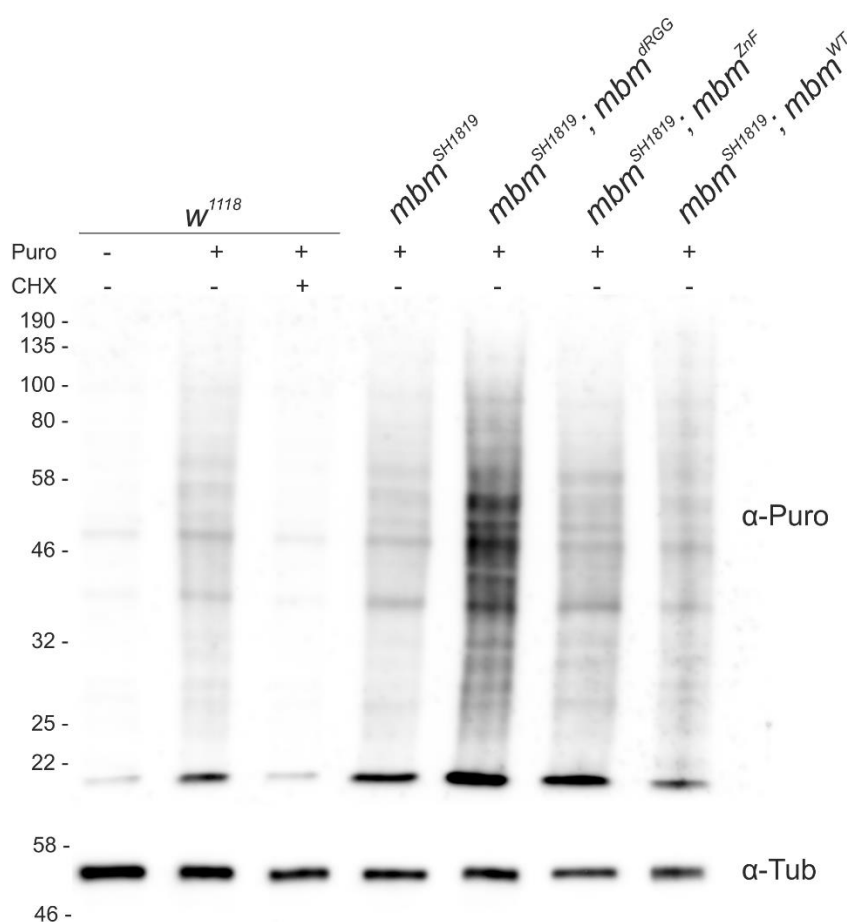
Figure 26: Protein synthesis rate is increased in *mbm^dRGG* mutant larval brains
Inverted 3rd instar larvae were treated with puromycin (Puro), thereby labeling newly synthesized proteins and allowing detection with anti-Puro antibodies. Western blots revealed an increase in protein synthesis in mbm^{SH1819}; mbm^{dRGG} mutants. Detection with anti-Tubulin was used as a loading control.

The signal intensity of the Western blots of four independent experiments was quantified with Fiji (see 6.11.1.). Each genotype or treatment was compared to puromycin-treated w^{1118} larval brains (Figure 27). Upon co-incubation with cycloheximide (CHX), the relative intensity (0.31 ±0.16) is nearly back to untreated levels (0.15 ±0.15), verifying puromycin labeling as a

valid measure for protein synthesis rates. In the *mbm* null mutant line mbm^{SH1819}, the protein synthesis rate is nearly at the same level as in w^{1118} (1.23 ±0.53). In the zinc-finger mutant mbm^{SH1819}; mbm^{ZnF}, the protein synthesis rate seems to be roughly doubled (2.26 ±1.24). Surprisingly, in the mbm^{SH1819}; mbm^{dRGG} mutant fly line, protein synthesis rates are on average almost four times higher than in w^{1118} (3.75 ±1.62; p = 0.021). The rescue line mbm^{SH1819}; mbm^{WT} also shows approximately doubled protein synthesis rates (2.04 ±0.29).
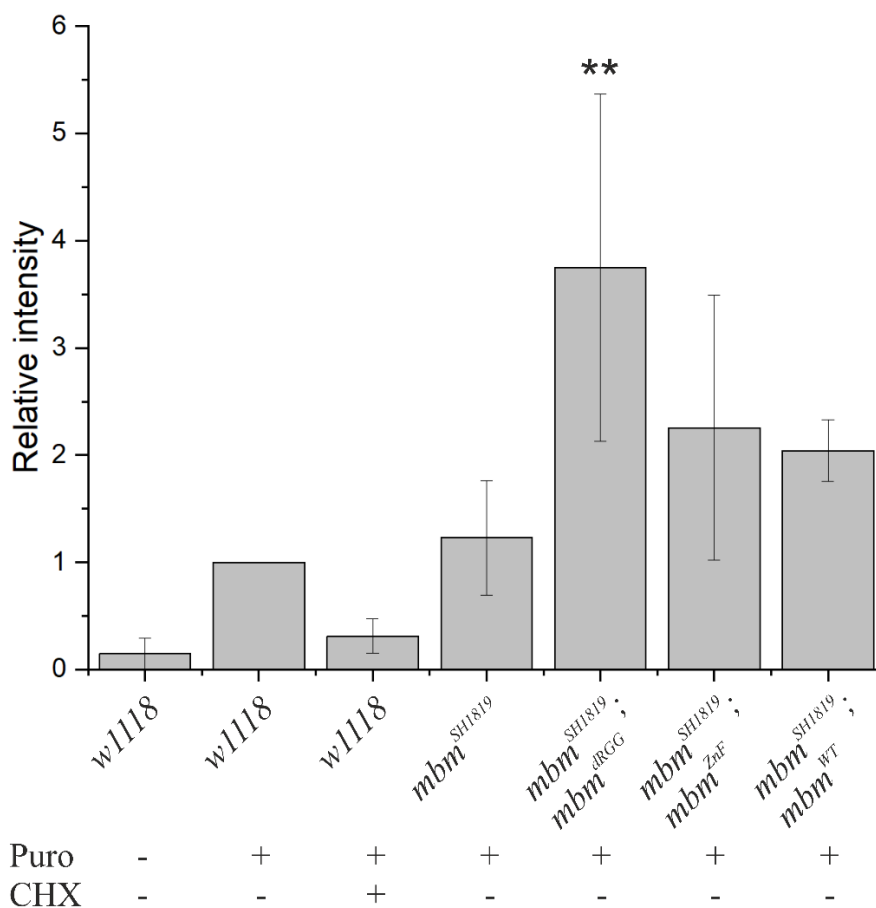
Figure 27: Quantification of puromycin labeling western blots
Signal intensity on western blots of four independent puromycin labeling experiments was measured and plotted relative to the intensity of puromycin-treated w^{1118} 3rd instar larval brains. Protein synthesis rates are significantly increased in mbm^{dRGG} mutant larval brains (p = 0.021).

7.4. Influence of mbm^{dRGG} on the TOR pathway

Hovhanyan et al. (2014) proposed a possible role of Mbm in the TOR pathway. In the present work, the puromycin assays (see 7.3.3.) showed increased protein synthesis rates in mbm^{dRGG} mutant larval brains which might be caused by changes in TOR signaling. To investigate whether expression of genes involved in TOR signaling is increased in mbm^{dRGG} mutant larval brains, qPCRs for *tor*, *akt* and *s6k* were performed. *rp49* was used as the housekeeping gene. No significant differences in expression levels of *tor, akt* and *s6k* could be found in any of the

mbm mutant flies compared to w^{1118}. However, only three biological replicates could be tested so far. *tor* expression in *mbm*^{dRGG} larval brains is close to a significant increase (3.58 ±1.4 fold expression; p = 0.06) and it might also be slightly increased in *mbm*^{ZnF} mutants (2.27 ±0.82) while there is nearly no change in *mbm*^{SH1819} mutants (1.06 ±0.11 fold expression). In the rescue line *mbm*^{WT}, mean *tor* expression levels are nearly unchanged, but vary quite a bit between biological replicates (1.21 ±0.63; Figure 28A). In the case of *akt* expression levels, high variability in biological replicates but no significant differences were found between w^{1118} and the *mbm* mutant larval brains (Figure 28B). *s6k* expression levels also show no significant differences, but a high variability between the three samples, especially for *mbm*^{dRGG} (4.2 ±4.2 fold expression; Figure 28C).
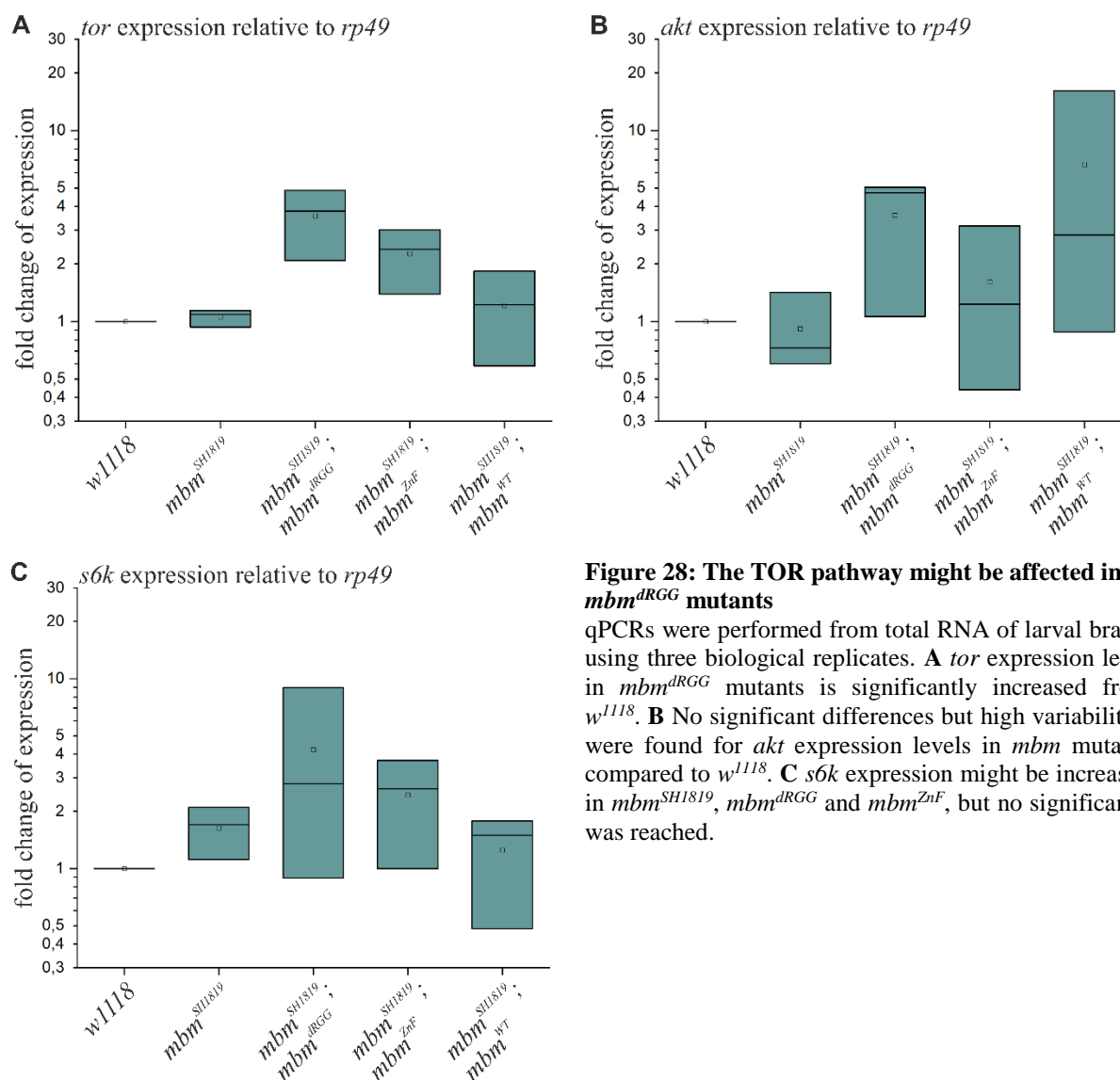
Figure 28: The TOR pathway might be affected in *mbm*^{dRGG} mutants

qPCRs were performed from total RNA of larval brains using three biological replicates. **A** *tor* expression level in *mbm*^{dRGG} mutants is significantly increased from w^{1118}. **B** No significant differences but high variabilities were found for *akt* expression levels in *mbm* mutants compared to w^{1118}. **C** *s6k* expression might be increased in *mbm*^{SH1819}, *mbm*^{dRGG} and *mbm*^{ZnF}, but no significance was reached.

8. Discussion

In earlier studies, functions of Mbm in brain development and neuroblast proliferation in *Drosophila* were investigated using the hypomorphic mutation *mbm¹* and the null mutation *mbm^{SH1819}* (Raabe et al., 2004; Hovhanyan et al., 2014). Mbm was identified as a nucleolar protein involved in neuroblast proliferation. In *mbm* null mutants, smaller NB sizes and fewer NB progeny cells were found as well as an effect on rRNA processing and the localization of ribosomal protein RpS6. Furthermore, Mbm was shown to be a transcriptional target of Myc and it might therefore be regulated by the insulin/TOR pathway. These results led to the suggestion that Mbm might be implicated in ribosome biogenesis, thereby regulating NB proliferation (Hovhanyan et al., 2014). Mbm's exact functions, however, remained unclear. Mbm features an RGG-box (N-terminal) and two zinc-finger domains (C-terminal; see Figure 9 and Figure 15) which are candidates for possible rRNA binding domains. Flies expressing a genomic *mbm* construct with mutated zinc-fingers (*mbm^{ZnF}*) were generated and investigated in an earlier study (Cornelia Engert, Master Thesis, 2015). Preliminary analyses performed on these mutant larval brains showed no effects on NB size and no binding of C-terminal Mbm constructs (expressed in *E. coli*) to rRNA probes *in vitro*, suggesting that the zinc-finger domains are not important for a possible role in ribosome biogenesis. The N-terminal half of Mbm, however, was shown to bind to rRNA probes, meaning that the RGG-box might be involved.

In the present study, the function of Mbm's RGG-box was investigated in *in vivo* and *in vitro* experiments. Additionally, the zinc-finger mutant was included in most experiments to further elucidate this domain's functions.

8.1. The RGG-box and zinc-fingers are important for Mbm's functions

The effect of the deletion of Mbm's RGG-box was first tested *in vivo* by survival assays (Figure 17). As it was reported previously (Hovhanyan et al., 2014), the *mbm* null mutant *mbm^{SH1819}* showed decreased survival until and lethality during pupal stage. While approximately 60 % of the *mbm^{dRGG}* mutant larvae of all three independent lines pupated, which is a significant decrease in the transgenic lines *mbm^{dRGG}* M1 and *mbm^{dRGG}* M4 compared to *w^{1118}* (~85 % pupation rate), only very few adult flies eclosed. This suggests that Mbm function does indeed rely on its RGG-box during larval stage, but even more during pupal stage. However, it cannot be excluded that the less severe effect of the *mbm^{dRGG}*

mutation on larval viability is caused by a maternal effect. Only 35% of maternal mRNAs were reported to be degraded during the maternal-to-zygotic transition in the embryo (Tadros and Lipshitz, 2009; Cui et al., 2016), thus one could speculate that some maternal mRNAs persist into the larval stages. On the other hand, reduced survival of the rescue line mbm^{SH1819}; mbm^{WT} until adulthood implies that full rescue of the mbm^{SH1819} phenotype by genomic mbm constructs inserted into the 3rd chromosome in position 65B2 is not possible. The reason for this is unclear, but it could be due to insufficient expression levels or the expression pattern of the genomic mbm constructs. In the future, this should be investigated by qPCR analysis or by Western blotting. Nonetheless, this might enhance the effects of mbm^{dRGG} and mbm^{ZnF} mutations during pupal stage. Mbm's role during pupal stage, however, remains elusive. So far, Mbm was only shown to have functions in neuroblasts (Hovhanyan et al., 2014; personal communication: Thomas Raabe), which build up the adult CNS throughout embryonic and larval stages and then disappear during pupal stage (see 3.1.; reviewed in Harding and White, 2018). In the present study, it was furthermore observed that mbm^{SH1819}; mbm^{dRGG} flies often seem to develop normally in the pupae and then die shortly before or even during eclosion. Thus, Mbm might play a role in locomotor control during eclosion, but it is also possible that deficits in brain development caused by the mbm^{dRGG} mutation impedes the ability to eclose. Apart from these observations, this study mainly focuses on Mbm's functions during larval stage.

In the case of pupation rates, there seems to be a slight improvement in the three mbm^{dRGG} mutant lines (M1: ~58 %; M3: ~65 %; M4: ~51 %) compared to the null mutant mbm^{SH1819} (~44 %). This suggests at least a partial ability of Mbm^{dRGG} to rescue the mbm^{SH1819} phenotype. Thus, Mbm might retain some of its functions even without its RGG-box, but the impact of the mutation during larval stages is still severe.

Additionally, two zinc-finger mutant lines (mbm^{SH1819}; mbm^{ZnF} 2-1M and 2-3M) were included in the rescue experiments. Surprisingly, survival rates during larval stages were significantly decreased even compared to the mbm null mutant. Thus, the mbm^{ZnF} mutation has a worse effect than Mbm not being present at all. A highly speculative explanation for this could be that the two amino acid substitutions in Mbm^{ZnF} lead to a misfolding of the protein, thereby facilitating or blocking interaction of another motif with DNA, RNA or other proteins. This is supported by the results of the rRNA-binding assays (Figure 21) showing that myc-Mbm^{ZnF} and the double mutant myc-Mbm^{dRGG,ZnF} exhibit stronger binding to rRNA probes than myc-Mbm^{WT} and myc-Mbm^{dRGG}. Mbm^{ZnF} might therefore interfere with rRNA

processing or possibly with the translation of certain mRNAs (discussed in more detail in 8.2.1.).

Moreover, both Mbm^{dRGG} and Mbm^{ZnF} were found to be mislocalized in 3rd instar larval neuroblasts (Figure 18). Mbm was previously reported to be a nucleolar protein (Hovhanyan et al., 2014), but while this is the case for w^{1118} and mbm^{SH1819}; mbm^{WT} larval NBs, in mbm^{dRGG} mutants Mbm is partially delocalized to the nucleus. In mbm^{ZnF} mutants, on the other hand, Mbm is fully delocalized to the cytoplasm. Thus, both motifs seem to be important for correct localization of Mbm. For RGG-boxes, roles in protein translocation have been reported previously. For example, vertebrate nucleolin was shown to depend on its RGG-box for nucleolar localization (Ginisty et al., 1999; Pellar and DiMario, 2003) and human hnRNP A2 is partially delocalized from the nucleus to the cytoplasm when its RGG-box is deleted (Nichols et al., 2000). For zinc-finger motifs the situation is less clear. Localization defects in zinc-finger mutants were reported for mammalian EEA1 which contains a FYVE type zinc-finger (Stenmark et al., 1996) and for mammalian JAZ which contains a C_2H_2 zinc-finger (Yang et al., 1999). For C_2HC type zinc-fingers like in Mbm, however, no reports regarding zinc-finger dependent protein localization were found. Furthermore, it can't be excluded that the mislocalization of Mbm^{dRGG} and Mbm^{ZnF} is only caused by conformational changes of the protein induced by the mutations, thereby blocking other protein domains or making them accessible. In an earlier study, Mbm localization to the nucleolus was shown to depend on phosphorylation of its acidic clusters AC-1 and AC-2 by the kinase CK2α (Hovhanyan et al., 2014). Upon knock-down of CK2α or mutation of the phosphorylation sites, Mbm was partially delocalized to the cytoplasm. Possibly, defects in protein folding of Mbm^{ZnF} and Mbm^{dRGG} might impede the interaction with CK2α and might therefore be a factor in the mislocalization. However, other factors have to be involved, since even the mutation of Mbm's phosphorylation sites AC-1 and AC-2 did not lead to a full delocalization to the cytoplasm in contrast to the zinc-finger mutation. One could try to solve this problem by generating and investigating different RGG and zinc-finger mutants. For example, instead of deleting the whole RGG-box, one could substitute the arginines in the RG/RGG motifs with another amino acid. In the Mbm^{ZnF} mutants, which were generated in an earlier work (Cornelia Engert, Master Thesis, 2015), the first cysteine of both zinc-finger motifs was substituted with tyrosine. However, the aromatic side chain of tyrosine is hydrophobic and bigger compared to the one of cysteine, which might induce defects in protein folding. Possibly, a smaller amino acid like glycine might be a better choice. In the

case that the sulfide residue of cysteine is important for Mbm's structure through disulfide bridges, however, methionine might be the right substitute.

Altogether, it can be concluded that both the dRGG and zinc-finger mutations have different, but severe effects on Mbm localization and function. Future experiments could include ChIP-seq, RNA-seq or co-immunoprecipitation followed by mass spectrometry to find possible binding targets of Mbm. Furthermore, one should investigate flies carrying the mbm^{dRGG} or mbm^{ZnF} mutation in the wild-type background to see whether there are dominant negative effects.

8.2. Mbm is involved in ribosome biogenesis in neuroblasts

Previously, it was suggested that Mbm affects neuroblast proliferation through a role in ribosome biogenesis (Hovhanyan et al., 2014). Thereby, Mbm might be involved in the regulation of protein synthesis and since it is transcriptionally regulated by Myc, it might be a downstream target of insulin/TOR signaling. The present study provides further insight into these proposed roles of Mbm and the importance of its RGG-box therein.

At first, NB cell size was investigated since it is known to be decreased in mbm null mutants (Hovhanyan et al., 2014). It could be shown that NB cell size is also significantly decreased in mbm^{dRGG} mutants while cell size is rescued in the $mbm^{SH1819}; mbm^{WT}$ line (Figure 19). Thus, re-growth of NBs in mbm^{dRGG} mutants seems to be affected similarly as in mbm null mutants providing further hints for the importance of Mbm's RGG-box. In mbm^{ZnF} mutants, in contrast, NB size was found not to be affected, which is consistent with the findings of an earlier work (Cornelia Engert, Master Thesis, 2015).

8.2.1. Mbm's RGG-box is important for rRNA binding *in vitro*

To investigate a possible role of Mbm in ribosome biogenesis by regulation of rRNA processing, rRNA binding assays were performed (Figure 21). This connection was already drawn by Hovhanyan et al. (2014) with Northern blots showing an additional intermediate rRNA processing product in mbm^{SH1819} mutants. In the present study, it could be shown that Mbm does indeed bind to several rRNA probes *in vitro*, with the highest binding affinity to ITS1. The RGG deleted construct Mbm^{dRGG}, in contrast, showed weaker binding to the rRNA probes than wild-type Mbm. These results provide further evidence that Mbm is involved in

ribosome biogenesis via a role in rRNA processing and that this function might be dependent of the RGG-box. However, no other reports of proteins depending on their RGG-box specificly for rRNA binding were found. Nucleolin, for example, contains an RGG-box, but its binding to rRNA is mediated by other RNA binding domains (Ghisolfi-Nieto et al., 1996; Serin et al., 1996; Bouvet et al., 1998). It can therefore not be excluded that the results of this *in vitro* assay are caused by unspecific binding and that Mbm is involved in rRNA processing by interaction with another protein *in vivo*. However, the facts that NB sizes are reduced in both the *mbm*[SH1819] and the *mbm*[SH1819]*; mbm*[dRGG] larvae (Figure 19) and that rRNA processing is affected in *mbm*[SH1819] together with the results of the binding assays suggest a role for Mbm's RGG-box in rRNA processing.

Interestingly, the binding affinity of Mbm[ZnF] is increased compared to Mbm[WT] and for the double mutant Mbm[dRGG,ZnF] it is increased even further. So far, there is no explanation for this other than possible conformational changes of the protein induced by the mutations leading to unknown RNA binding motifs to become accessible. If there was an unspecific binding of rRNA in the *mbm*[SH1819]*; mbm*[ZnF] mutant larval NBs, this might explain the reduced survival rate of larvae even compared to the null mutant *mbm*[SH1819] (Figure 17). However, in larval NBs Mbm[ZnF] is delocalized to the cytoplasm (Figure 18) and thus should not be able to directly influence rRNA processing. On the other hand, it might be possible that Mbm[ZnF] binds to rRNA in the nucleolus, but does not disassociate again and gets transported to the cytoplasm together with the rRNA. However, this would probably impede ribosome assembly while protein synthesis rates seem to be even slightly higher in *mbm*[ZnF] mutant larval brains (Figure 26). Furthermore, if Mbm[ZnF] bound rRNA in the nucleolus, one would expect at least a weak nucleolar signal in the immunostainings, but Mbm[ZnF] appears to be fully delocalized to the cytoplasm. On the other hand, it is also possible that Mbm[ZnF] does not only exhibit a higher binding affinity specific to rRNA molecules, but also to mRNAs. Mbm[ZnF] might therefore interfere with the translation of certain mRNAs, which could also be an explanation for the strong effect of the zinc-finger mutation on viability. One possibility to test this hypothesis might be an RNA-ChIP followed by RT-PCR and sequencing. Since the target sequence for the sequencing primers is unknown, one might be able to make use of the poly T tail of the cDNA or try to use short random primer sequences.

In future experiments, one should try to perform Northern blots again to investigate intermediate products of rRNA processing in *mbm*[dRGG] and *mbm*[ZnF] mutants. In the present study, Northern blots were attempted, but no distinct bands showing rRNA processing

intermediates could be observed. Thus, further optimization of the protocol would be necessary in order to be successful.

8.2.2. Mbm is essential for the correct localization of RpS6

Hovhanyan et al. (2014) could furthermore show a defect in RpS6 localization in mbm^{SH1819} mutant larval NBs, which is another hint to Mbm's implication in ribosome biogenesis. This was also investigated in the present study, but while mislocalized RpS6 was found in all three *mbm* mutant lines, the phenotype was the exact opposite of what was reported by Hovhanyan et al. (2014). However, the experiments were conducted in a different way: they overexpressed an mRFP::RpS6 construct specifically in neuroblasts in wild-type and mbm^{SH1819} background and took images of the autofluorescence of mRFP. In the present study, an anti-RpS6 antibody was used for the staining of endogenous RpS6. While Hovhanyan et al. (2014) could show cytoplasmic localization of mRFP::RpS6 in the wild-type background and mostly nucleolar localization in the mbm^{SH1819} background, in this study RpS6 was found cytoplasmic as well as nucleolar in the wild-type and in the rescue line and only cytoplasmic in mbm^{SH1819}, mbm^{SH1819}; mbm^{dRGG} and mbm^{SH1819}; mbm^{ZnF} mutant larval NBs (Figure 24). Since ribosomal proteins are synthesized in the cytoplasm and then transported into the nucleolus where they are assembled into the pre-ribosomal particles (Schlosser et al., 2003; Bohnsack and Bohnsack, 2019), it would make sense to find RpS6 in the cytoplasm and in the nucleolus in the wild-type. In this case, RpS6 translocation into the nucleolus seems to be defective in NBs of all three *mbm* mutant lines. In the approach of Hovhanyan et al. (2014), localization and assembly into ribosomes may have been disturbed by the mRFP-tag, leading to different results. Under this assumption, however, it is interesting that the *mbm* null mutation still has an influence on the localization of mRFP::RpS6. To shed light into this, it was attempted to replicate the approach of Hovhanyan et al. (2014) (Figure 25). However, autofluorescence of mRFP::RpS6 was not sufficient, thus staining with anti-RFP was tested. mRFP::RpS6 was only found in the cytoplasm in the wild-type as well as the mbm^{SH1819} background while staining with anti-RpS6 revealed the same phenotype as before. Whether these different results compared to Hovhanyan et al. (2014) were caused by faulty overexpression of mRFP::RpS6 or by unspecific binding of the anti-RFP antibody remains elusive. The relatively weak anti-RpS6 staining (Figure 25 A), however, could imply that only endogenous RpS6 is expressed or that the RpS6 antibody does not detect mRFP::RpS6. In the meantime, however, the experiment was repeated using an anti-mCherry antibody instead of

anti-RFP, revealing ambiguous results with some NBs confirming the findings of Hovhanyan et al. (2014) and others showing RpS6 localization as found in the present study (personal communication: Thomas Raabe). Whether these conflicting results are caused either by improper translocation of mRFP::RpS6 or by unspecific binding of the antibodies that were used, remains elusive.

Even though these two experimental approaches regarding the localization of RpS6 in *mbm* null mutant neuroblasts yielded different results, both of them hint to a role of Mbm in RpS6 translocation. Interestingly, *mbm*^{dRGG} and *mbm*^{ZnF} mutations seem to influence RpS6 translocation in the same way as the *mbm* null mutation, hinting to a loss of function in both these mutant lines. This is easier to explain for *mbm*^{dRGG}, as the RGG-box might be needed for the binding of RpS6 or for the interaction with another protein implicated in RpS6 translocation. Why the same effect is seen in *mbm*^{ZnF} mutants remains elusive. In both mutants, protein folding of Mbm might be defective, thereby leading to a (partial) loss of function.

It is important to note, however, that ribosome biogenesis cannot be completely disrupted since this would be fatal for the cells. In the fully assembled ribosome, RpS6 is located at the interface between the small and large ribosomal subunit and it is suggested to be implicated in mRNA and tRNA binding (Nygard and Nika, 1982; Nygard and Nilsson, 1990). Even the heterozygous deletion of *rps6* leads to a Minute phenotype which includes prolonged development, reduced fertility, low viability and short, thin bristles caused by insufficient protein synthesis rates (Lambertsson, 1998; Marygold et al., 2007). Thus, RpS6 still has to be assembled into ribosomes in the *mbm* mutants, albeit at possibly lower rates.

An alternative method to investigate RpS6 localization in NBs of the different Mbm mutant lines might be the isolation of the NBs by cell sorting followed by cell fractionation and Western blot analysis using the anti-RpS6 antibody. Thereby, one might be able to determine the relative RpS6 levels between the nucleolus and the cytoplasm.

8.2.3. Protein synthesis is increased in *mbm*^{SH1819}; *mbm*^{dRGG} mutant larval brains

If ribosome biogenesis was impeded in *mbm* mutant larval neuroblasts, one would expect a change in protein synthesis rates. Therefore, protein synthesis was investigated by puromycin labeling of nascent proteins and subsequent Western blotting (Figure 26 and Figure 27). In *mbm*^{SH1819}, the protein synthesis rate is at approximately the same level as in *w*^{1118}, suggesting

that the effect on rRNA processing shown by Hovhanyan et al. (2014) as well as the disturbed RpS6 localization do not influence ribosome activity. In the mbm^{SH1819}; mbm^{ZnF} and mbm^{SH1819}; mbm^{WT} transgenic lines, protein synthesis seems to be roughly doubled, providing another hint that some phenotypes may be induced by rescue with genomic *mbm* constructs inserted in the 3rd chromosome in position 65B2. However, protein synthesis in mbm^{SH1819}; mbm^{dRGG} larval brains is even further and significantly increased. Thus, there have to be additional effects of the mbm^{dRGG} mutation besides the RpS6 delocalization that potentially influence ribosome activity. Interestingly, it was shown in mouse embryonic fibroblasts, that mutation of RpS6's phosphorylation sites does not impede its function in the ribosome, but even increases protein synthesis rates while the cells are significantly reduced in size (Ruvinsky et al., 2005). They also found a small increase in elongation rate, but not to a degree that would explain the increase in protein synthesis. The exact mechanism remains unknown, but these results suggest a negative regulatory effect of RpS6 phosphorylation on protein synthesis (Biever et al., 2015). This raises the question whether RpS6 phosphorylation might be reduced in mbm^{dRGG} mutants. RpS6 is phosphorylated by S6K which in turn is activated by the TOR signaling pathway (Montagne et al., 1999; Parisi et al., 2011). Could it be possible that Mbm plays a role in TOR signaling? On the other hand, it is puzzling, that protein synthesis is not increased in *mbm* null mutant larval brains. Therefore, there might be unspecific interactions with proteins, DNA or RNA caused by the RGG deletion. Possibly, these interactions can only happen upon nuclear localization of Mbm^{dRGG} in contrast to cytoplasmic localization of Mbm^{ZnF}, nucleolar localization of wild-type Mbm or its absence in *mbm* null mutants.

It is important to note, however, that this approach to investigate protein synthesis does not reflect the situation specific for neuroblasts but for the larval brain as a whole. Since NBs are very large compared to other cells in the brain, it was assumed that changes in protein synthesis induced by *mbm* mutations might be detectable in whole larval brains. A better approach might be the isolation of neuroblasts from the different *mbm* mutant larval brains by cell sorting. Nonetheless, differences between w^{1118} and the mbm^{dRGG}, mbm^{ZnF} and mbm^{WT} mutant lines were found. However, the experiment should be conducted several times more to improve the possibility of statistical analysis.

8.2.4. TOR expression might be increased in *mbm^SH1819; mbm^dRGG* mutant larval brains

Fueled by the results that protein synthesis rates are increased in *mbm^dRGG* mutant larval brains and since ribosome biogenesis and thereby protein synthesis is regulated by the insulin/TOR pathway (Grewal et al., 2007; Hall et al., 2007), the expression levels of *tor*, *akt* and *s6k* genes was investigated by qPCRs (Figure 28). Unfortunately, only three biological replicates could be examined. For *akt*, which is a downstream target in insulin signaling and which indirectly activates TOR (reviewed in Grewal, 2009), the results in the three biological replicates were highly variable and hardly allow to draw any conclusion. In the case of *tor*, however, expression might be increased in *mbm^SH1819; mbm^dRGG* and possibly also in *mbm^SH1819; mbm^ZnF* mutant larval brains, while there is no increase in *mbm^SH1819* mutants. The *tor* expression levels roughly fit the protein synthesis rates in the different genotypes shown in Figure 27. These results further suggest that protein synthesis is indeed increased in *mbm^dRGG* mutants even though RpS6 is delocalized and the NB cell size is significantly decreased. However, since neither protein synthesis nor *tor* expression levels are changed in the *mbm* null mutant, the role of the RGG-box remains elusive. Possibly, Mbm's RGG-box plays a regulatory role in ribosome biogenesis, which in the wild-type is only induced in certain situations. For example, 4EBP, which is another component of the insulin/TOR pathway, acts as metabolic brake only during low nutrient availability (Teleman et al., 2005; Tettweiler et al., 2005). Therefore, in certain situations Mbm might act as a promoter of TOR signaling mediated by its RGG-box. Since Myc is a downstream target of TOR and Mbm in turn is transcriptionally regulated by Myc (Hovhanyan et al., 2014), this might even be a positive feedback loop.

As explained earlier, a decrease in cell size but an increase in protein synthesis rates was found in mouse embryonic fibroblasts expressing RpS6 with mutated phosphorylation sites (Ruvinsky et al., 2005). This leads to the question whether RpS6 phosphorylation is decreased in *mbm^dRGG* mutant larval brains, which might be caused by a decrease in *s6k* expression or activity. However, *s6k* expression seems to be even increased in *mbm^SH1819; mbm^dRGG* larval brains (Figure 28 C). Since only three biological replicates were examined and the variability between the samples was high, no significant difference was found. Generally, all qPCRs should be repeated several times more to increase the chances of finding significant differences and to shed more light into the situation. Furthermore, one should try to investigate the expression of genes of the TOR pathway on the protein level by Western blotting. There are also commercially available phospho-RpS6 antibodies which could be used to examine RpS6 phosphorylation levels in the *mbm* mutant lines.

8.3. Mbm might be methylated within its RGG-box

In earlier studies, arginine methylation in RGG/RG motifs was shown to either promote or inhibit protein-protein as well as protein-RNA interactions (Cote and Richard, 2005; Yu et al., 2004; Blackwell et al., 2010; Wei et al., 2014). Since Mbm binds to rRNA probes through its RGG-box *in vitro* (Figure 21), it was attempted to investigate the methylation status of Mbm overexpressed in *Drosophila* S2R+ cells. The first experiment (Figure 22) showed symmetric dimethylation in myc-Mbm^{WT}, but no methylation in myc-Mbm^{dRGG}. According to these results, Mbm is symmetrically dimethylated within its RGG-box. Unfortunately, several attempts to replicate these results were not successful, showing no methylation at all. Many different experimental conditions were tested to no avail. It is puzzling, why these first results appeared so distinct while all further experiments exhibited no methylation. Possibly, arginine methylation in S2R+ cells depends on a certain condition, which was met by chance in the first experiment.

Another attempt to elucidate the methylation status of Mbm was done by overexpression of His$_6$-tagged Dart1 or Dart5 additionally to myc-Mbm^{WT} or myc-Mbm^{dRGG}. Dart1 and Dart5 are the most promising candidates for asymmetric and symmetric dimethylation of RGG/RG motifs in *Drosophila* (see 3.3.1.). In the case of successful forced methylation in the S2R+ cells, it was furthermore planned to immunoprecipitate the myc-Mbm^{WT} and myc-Mbm^{dRGG} proteins to conduct RNA-binding assays with methylated and unmethylated Mbm. However, neither symmetric nor asymmetric methylation of myc-Mbm^{WT} and myc-Mbm^{dRGG} could be observed (Figure 23). Whether this is due to the experimental conditions or to Dart1 and Dart5 simply not being able to methylate Mbm, is unknown. It is also possible that the myc- and His$_6$-tags interfere with the interaction of the proteins. The SYM11 and ASYM24 antibodies are widely used to detect arginine methylation and are also known to work well in *Drosophila* (e.g. Kirino et al., 2009). If one would repeat the experiment maybe also including other Darts, however, one should think about a positive control that could indicate whether the antibodies work properly. Alternatively, one could try to perform *in vitro* methylation of Mbm with radioactive labeling using [^{3}H]AdoMet as a methyl group donor (as described e.g. in Nichols et al., 2000). Another possibility would be to investigate the methylation status of Mbm by mass spectrometry. However, Mbm's RGG-box might be methylated by other arginine methyltransferases than those used in this study or maybe its function does not rely on arginine methylation at all.

8.4. Mbm as a neuroblast-specific ribosome biogenesis factor

Mbm was previously shown to affect RpS6 localization in neuroblasts as well as rRNA processing and it was shown to be a transcriptional target of Myc, which suggests an involvement of Mbm in the regulation of ribosome biogenesis (Hovhanyan et al., 2014). Even though ribosome biogenesis is thought to be a highly conserved process, species- and even cell-type specific ribosome biogenesis factors (RBFs) as well as isoforms of ribosomal proteins (RPs) or post-translationally modified RPs were found (reviewed in Brombin et al., 2015). Since no role of Mbm outside of neuroblasts is known so far, Mbm is suggested to be a neuroblast-specific ribosome biogenesis factor (RBF) in *Drosophila*. Specifically in stem cells, RBFs are believed to be important for the regulation of differentiation as well as for the determination of stem cell identity and stem cell survival (Hayashi et al., 2014; Zhang et al., 2014; Xue and Barna, 2012; Brombin et al., 2015).

In the present study, it was attempted to elucidate the molecular basis of Mbm's functions by investigation of its zinc-finger motifs and especially its RGG-box. Some of the results are ambiguous, but the effects of the Mbm^{ZnF} and Mbm^{dRGG} mutations on rRNA binding *in vitro* and on RpS6 localization *in vivo* provide further evidence for Mbm's suggested role as an RBF. Furthermore, protein synthesis rates are increased in *mbm^{dRGG}* mutants even though NB size is significantly reduced. As discussed previously, this seems contradictory, but a similar effect was found in mouse embryonic fibroblasts upon mutation of RpS6's phosphorylation sites (Ruvinsky et al., 2005). Therefore, RpS6 phosphorylation levels in the *mbm^{SH1819}*, *mbm^{dRGG}* and *mbm^{ZnF}* mutants as well as the wild-type should be investigated by Western blot analysis or immunofluorescence using phospho-RpS6-specific antibodies. If Mbm was involved in RpS6 phosphorylation, this would be another role for Mbm as a ribosome biogenesis factor.

Diseases that are caused by mutations in RBFs, RPs or components of the rRNA transcription machinery are called ribosomopathies. In *Drosophila*, a well known ribosomopathy would be the Minute syndrome which is caused by over 60 mutations of RPs (Mills and Green, 2017). As discussed previously (see 8.2.2.), even the heterozygous deletion of *rps6* leads to a Minute phenotype including prolonged development, reduced fertility, low viability and short, thin bristles caused by insufficient protein synthesis rates (Lambertsson, 1998; Marygold et al., 2007). This underscores the importance of RpS6 and of Mbm as a regulator of RpS6 localization and possibly RpS6 phosphorylation. Many tissue specific ribosomopathies are caused by a decrease in protein synthesis rates, which induces upregulation of tumor

suppressor p53 and thereby cell cycle arrest and apoptosis (Mills and Green, 2017; Bohnsack and Bohnsack, 2019). In the *mbm* null mutant *mbm^{SH1819}*, in contrast, protein synthesis rates seem to be unchanged and in the *mbm^{dRGG}* mutant they are significantly increased. Furthermore, NBs in these mutants are significantly smaller compared to the wild-type, but they do not disappear until late larval stages. Therefore, an involvement of p53 in the ribosomopathies caused by the *mbm* mutations is unlikely. However, in fast-proliferating cell types, tissue specific ribosomopathies may also be caused by a reduction of ribosomes and thereby a decreased translation rate of specific mRNAs (Bohnsack and Bohnsack, 2019; Khajuria et al., 2018). While protein synthesis in the *mbm* mutants is not decreased, it could be possible that alterations of ribosomal proteins cause the ribosomes to favor certain mRNAs, thereby leading to insufficient expression of some genes. For example, human ribosomes that contain RpS25 and RpL10 were shown to prefer certain mRNAs involved in cell cycle and development (Shi et al., 2017; Bohnsack and Bohnsack, 2019). Thus, possible posttranslational alterations of RpS6 that might be directly or indirectly mediated by Mbm could be important for the the translation of a certain subset of mRNAs.

So far, the exact causes of the ribosomopathies in the *mbm^{SH1819}*, *mbm^{dRGG}* and *mbm^{ZnF}* mutants remain unclear, but several results suggest Mbm to be a ribosomal biogenesis factor in *Drosophila* neuroblasts.

8.5. Outlook

In summary, further evidence was found that Mbm is involved in regulation of ribosome biogenesis and NB proliferation. Possibly, some of Mbm's functions rely on its RGG-box. For example, the RGG-box is essential for the binding of rRNA probes *in vitro* and it might also play a role in regulation of the TOR pathway in neuroblasts. However, expression and activity levels of genes implicated in the TOR pathway should be further investigated by qPCR and Western blot analysis. To see whether rRNA processing is affected in *mbm^{dRGG}* mutants, Northern blots should be performed. Furthermore, one should investigate via Edu-pulse labeling whether NB progeny number is decreased in *mbm^{dRGG}* mutants. The zinc-finger motifs, on the other hand, do not seem to be important for rRNA binding, but the results are puzzling. Since the negative effects in the *mbm^{ZnF}* mutants might be due to faulty protein folding and unspecific interactions with other proteins, RNA or DNA, one could try to generate new mutants and chose another amino acid substitute for the first cysteine of both

zinc-finger motifs. Moreover, it should be investigated in further experiments whether the anti-RpS6 antibody specificly detects RpS6 in *Drosophila*, for example by RNAi knockdown of RpS6, which should reduce staining intensity. Furthermore, ribosomal proteins are known to fulfill roles outside of ribosomes (reviewed in Zhou et al., 2015). For example, phosphorylated RpS6 was shown to inhibit p53-induced tumor suppression in mice (Khalaileh et al., 2013). Therefore, it should be investigated whether the phenotypes in the *mbm* mutant lines are caused by ribosome-independent roles of RpS6, possibly in dependence of its phosphorylation status. Moreover, one could further examine Mbm's acidic clusters 1, 2 and/or 3 to show, for example, whether phosphorylation of Mbm is important for the correct localization of RpS6. Furthermore, future experiments could also include investigations to see whether type II NB lineages form properly in the different *mbm* mutants or whether the correct neurons are born in their specific time-frame during the temporal series even though NB proliferation is negatively affected.

9. Bibliography

Anna Hovhanyan, PhD Thesis, Universität Würzburg, 2014

Almeida, M. S. and S. J. Bray (2005). "Regulation of post-embryonic neuroblasts by Drosophila Grainyhead." Mech Dev **122**(12): 1282-1293.

Alvarez, J. A. and F. J. Diaz-Benjumea (2018). "Origin and specification of type II neuroblasts in the Drosophila embryo." Development **145**(7).

Aso, Y., K. Grubel, S. Busch, A. B. Friedrich, I. Siwanowicz and H. Tanimoto (2009). "The mushroom body of adult Drosophila characterized by GAL4 drivers." J Neurogenet **23**(1-2): 156-172.

Badertscher, L., T. Wild, C. Montellese, L. T. Alexander, L. Bammert, M. Sarazova, M. Stebler, G. Csucs, T. U. Mayer, N. Zamboni, I. Zemp, P. Horvath and U. Kutay (2015). "Genome-wide RNAi Screening Identifies Protein Modules Required for 40S Subunit Synthesis in Human Cells." Cell Rep **13**(12): 2879-2891.

Baumgardt, M., D. Karlsson, B. Y. Salmani, C. Bivik, R. B. MacDonald, E. Gunnar and S. Thor (2014). "Global programmed switch in neural daughter cell proliferation mode triggered by a temporal gene cascade." Dev Cell **30**(2): 192-208.

Baumgardt, M., D. Karlsson, J. Terriente, F. J. Diaz-Benjumea and S. Thor (2009). "Neuronal subtype specification within a lineage by opposing temporal feed-forward loops." Cell **139**(5): 969-982.

Bayraktar, O. A., J. Q. Boone, M. L. Drummond and C. Q. Doe (2010). "Drosophila type II neuroblast lineages keep Prospero levels low to generate large clones that contribute to the adult brain central complex." Neural Dev **5**: 26.

Bedford, M. T. (2007). "Arginine methylation at a glance." J Cell Sci **120**(Pt 24): 4243-4246.

Bedford, M. T. and S. G. Clarke (2009). "Protein arginine methylation in mammals: who, what, and why." Mol Cell **33**(1): 1-13.

Bedford, M. T. and S. Richard (2005). "Arginine methylation an emerging regulator of protein function." Mol Cell **18**(3): 263-272.

Bello, B., H. Reichert and F. Hirth (2006). "The brain tumor gene negatively regulates neural progenitor cell proliferation in the larval central brain of Drosophila." Development **133**(14): 2639-2648.

Bello, B. C., N. Izergina, E. Caussinus and H. Reichert (2008). "Amplification of neural stem cell proliferation by intermediate progenitor cells in Drosophila brain development." Neural Dev **3**: 5.

Berdnik, D., T. Torok, M. Gonzalez-Gaitan and J. A. Knoblich (2002). "The endocytic protein alpha-Adaptin is required for numb-mediated asymmetric cell division in Drosophila." Dev Cell **3**(2): 221-231.

BestGene Inc., https://www.thebestgene.com/PhiC31InfoPage.do (21.02.2019)

Betschinger, J., F. Eisenhaber and J. A. Knoblich (2005). "Phosphorylation-induced autoinhibition regulates the cytoskeletal protein Lethal (2) giant larvae." Curr Biol **15**(3): 276-282.

Betschinger, J. and J. A. Knoblich (2004). "Dare to be different: asymmetric cell division in Drosophila, C. elegans and vertebrates." Curr Biol **14**(16): R674-685.

Betschinger, J., K. Mechtler and J. A. Knoblich (2003). "The Par complex directs asymmetric cell division by phosphorylating the cytoskeletal protein Lgl." Nature **422**(6929): 326-330.

Betschinger, J., K. Mechtler and J. A. Knoblich (2006). "Asymmetric segregation of the tumor suppressor brat regulates self-renewal in Drosophila neural stem cells." Cell **124**(6): 1241-1253.

Biever, A., E. Valjent and E. Puighermanal (2015). "Ribosomal Protein S6 Phosphorylation in the Nervous System: From Regulation to Function." Front Mol Neurosci **8**: 75.

Bischof, J & Maeda, Robert & Hediger Niessen, Monika & Karch, Francois & Basler, Konrad. (2007). Cloning and transformation vector pUASTattB, complete sequence.

Blackwell, E., X. Zhang and S. Ceman (2010). "Arginines of the RGG box regulate FMRP association with polyribosomes and mRNA." Hum Mol Genet **19**(7): 1314-1323.

Bohnsack, K. E. and M. T. Bohnsack (2019). "Uncovering the assembly pathway of human ribosomes and its emerging links to disease." EMBO J **38**(13): e100278.

Boisvert, F. M., S. van Koningsbruggen, J. Navascues and A. I. Lamond (2007). "The multifunctional nucleolus." Nat Rev Mol Cell Biol **8**(7): 574-585.

Boria, I., E. Garelli, H. T. Gazda, A. Aspesi, P. Quarello, E. Pavesi, D. Ferrante, J. J. Meerpohl, M. Kartal, L. Da Costa, A. Proust, T. Leblanc, M. Simansour, N. Dahl, A. S. Frojmark, D. Pospisilova, R. Cmejla, A. H. Beggs, M. R. Sheen, M. Landowski, C. M. Buros, C. M. Clinton, L. J. Dobson, A. Vlachos, E. Atsidaftos, J. M. Lipton, S. R. Ellis, U. Ramenghi and I. Dianzani (2010). "The ribosomal basis of Diamond-Blackfan Anemia: mutation and database update." Hum Mutat **31**(12): 1269-1279.

Boulanger, M. C., T. B. Miranda, S. Clarke, M. Di Fruscio, B. Suter, P. Lasko and S. Richard (2004). "Characterization of the Drosophila protein arginine methyltransferases DART1 and DART4." Biochem J **379**(Pt 2): 283-289.

Bouvet, P., J. J. Diaz, K. Kindbeiter, J. J. Madjar and F. Amalric (1998). "Nucleolin interacts with several ribosomal proteins through its RGG domain." J Biol Chem **273**(30): 19025-19029.

Bowman, S. K., R. A. Neumuller, M. Novatchkova, Q. Du and J. A. Knoblich (2006). "The Drosophila NuMA Homolog Mud regulates spindle orientation in asymmetric cell division." Dev Cell **10**(6): 731-742.

Bowman, S. K., V. Rolland, J. Betschinger, K. A. Kinsey, G. Emery and J. A. Knoblich (2008). "The tumor suppressors Brat and Numb regulate transit-amplifying neuroblast lineages in Drosophila." Dev Cell **14**(4): 535-546.

Bradford, M. M. (1976). "A rapid and sensitive method for the quantitation of microgram quantities of protein utilizing the principle of protein-dye binding." Anal Biochem **72**: 248-254.

Branscombe, T. L., A. Frankel, J. H. Lee, J. R. Cook, Z. Yang, S. Pestka and S. Clarke (2001). "PRMT5 (Janus kinase-binding protein 1) catalyzes the formation of symmetric dimethylarginine residues in proteins." J Biol Chem **276**(35): 32971-32976.

Brombin, A., J. S. Joly and F. Jamen (2015). "New tricks for an old dog: ribosome biogenesis contributes to stem cell homeostasis." Curr Opin Genet Dev **34**: 61-70.

Burgering, B. M. (2008). "A brief introduction to FOXOlogy." Oncogene **27**(16): 2258-2262.

Campos-Ortega J., Hartenstein V.; Springer, Heidelberg, Germany: 1997. The embryonic development of Drosophila melanogaster.

Cenci, C. and A. P. Gould (2005). "Drosophila Grainyhead specifies late programmes of neural proliferation by regulating the mitotic activity and Hox-dependent apoptosis of neuroblasts." Development **132**(17): 3835-3845.

Ceron, J., F. J. Tejedor and F. Moya (2006). "A primary cell culture of Drosophila postembryonic larval neuroblasts to study cell cycle and asymmetric division." Eur J Cell Biol **85**(6): 567-575.

Chell, J. M. and A. H. Brand (2010). "Nutrition-responsive glia control exit of neural stem cells from quiescence." Cell **143**(7): 1161-1173.

Chen, D. H., K. T. Wu, C. J. Hung, M. Hsieh and C. Li (2004). "Effects of adenosine dialdehyde treatment on in vitro and in vivo stable protein methylation in HeLa cells." J Biochem **136**(3): 371-376.

Chiu, J., P. E. March, R. Lee and D. Tillett (2004). "Site-directed, Ligase-Independent Mutagenesis (SLIM): a single-tube methodology approaching 100% efficiency in 4 h." Nucleic Acids Res **32**(21): e174.

Chojnacki, S., A. Cowley, J. Lee, A. Foix and R. Lopez (2017). "Programmatic access to bioinformatics tools from EMBL-EBI update: 2017." Nucleic Acids Res **45**(W1): W550-W553.

Choksi, S. P., T. D. Southall, T. Bossing, K. Edoff, E. de Wit, B. E. Fischer, B. van Steensel, G. Micklem and A. H. Brand (2006). "Prospero acts as a binary switch between self-renewal and differentiation in Drosophila neural stem cells." Dev Cell **11**(6): 775-789.

Cognigni, P., J. Felsenberg and S. Waddell (2018). "Do the right thing: neural network mechanisms of memory formation, expression and update in Drosophila." Curr Opin Neurobiol **49**: 51-58.

Colombani, J., S. Raisin, S. Pantalacci, T. Radimerski, J. Montagne and P. Leopold (2003). "A nutrient sensor mechanism controls Drosophila growth." Cell **114**(6): 739-749.

Cook, J. R., J. H. Lee, Z. H. Yang, C. D. Krause, N. Herth, R. Hoffmann and S. Pestka (2006). "FBXO11/PRMT9, a new protein arginine methyltransferase, symmetrically dimethylates arginine residues." Biochem Biophys Res Commun **342**(2): 472-481.

Cornelia Engert, Master Thesis, Universität Würzburg, 2015

Cote, J. and S. Richard (2005). "Tudor domains bind symmetrical dimethylated arginines." J Biol Chem **280**(31): 28476-28483.

Crittenden, J. R., E. M. Skoulakis, K. A. Han, D. Kalderon and R. L. Davis (1998). "Tripartite mushroom body architecture revealed by antigenic markers." Learn Mem **5**(1-2): 38-51.

Cubas, P., J. F. de Celis, S. Campuzano and J. Modolell (1991). "Proneural clusters of achaete-scute expression and the generation of sensory organs in the Drosophila imaginal wing disc." Genes Dev **5**(6): 996-1008.

Cui, J., Y. W. Lai, C. V. Sartain, R. M. Zuckerman and M. F. Wolfner (2016). "The Drosophila prage Gene, Required for Maternal Transcript Destabilization in Embryos, Encodes a Predicted RNA Exonuclease." G3 (Bethesda) **6**(6): 1687-1693.

Datta, S. (1995). "Control of proliferation activation in quiescent neuroblasts of the Drosophila central nervous system." Development **121**(4): 1173-1182.

Datta, S. (1999). "Activation of neuroblast proliferation in explant culture of the Drosophila larval CNS." Brain Res **818**(1): 77-83.

de Belle, J. S. and M. Heisenberg (1996). "Expression of Drosophila mushroom body mutations in alternative genetic backgrounds: a case study of the mushroom body miniature gene (mbm)." Proc Natl Acad Sci U S A **93**(18): 9875-9880.

De Virgilio, C. and R. Loewith (2006). "The TOR signalling network from yeast to man." Int J Biochem Cell Biol **38**(9): 1476-1481.

Deliu, L. P., A. Ghosh and S. S. Grewal (2017). "Investigation of protein synthesis in Drosophila larvae using puromycin labelling." Biol Open **6**(8): 1229-1234.

Dewey, E. B., D. T. Taylor and C. A. Johnston (2016). "Rolling in the mud: Hippo controls oriented cell division." Cell Cycle **15**(5): 607-608.

Doe, C. Q. (1992). "Molecular markers for identified neuroblasts and ganglion mother cells in the Drosophila central nervous system." Development **116**(4): 855-863.

Doe, C. Q. (2017). "Temporal Patterning in the Drosophila CNS." Annu Rev Cell Dev Biol **33**: 219-240.

Ebens, A. J., H. Garren, B. N. Cheyette and S. L. Zipursky (1993). "The Drosophila anachronism locus: a glycoprotein secreted by glia inhibits neuroblast proliferation." Cell **74**(1): 15-27.

Egger, B., J. Q. Boone, N. R. Stevens, A. H. Brand and C. Q. Doe (2007). "Regulation of spindle orientation and neural stem cell fate in the Drosophila optic lobe." Neural Dev **2**: 1.

Egger, B., J. M. Chell and A. H. Brand (2008). "Insights into neural stem cell biology from flies." Philos Trans R Soc Lond B Biol Sci **363**(1489): 39-56.

El-Shehawi, Ahmed & Elseehy Mona, M. (2013). Optimization of chemiluminescent detection of mitochondrial RNA-protein interaction by nonradioactive mobility shift. African Journal of Biotechnology. 12. 1915-1920. 10.5897/AJB11.3254.

Farley-Barnes, K. I., K. L. McCann, L. M. Ogawa, J. Merkel, Y. V. Surovtseva and S. J. Baserga (2018). "Diverse Regulators of Human Ribosome Biogenesis Discovered by Changes in Nucleolar Number." Cell Rep **22**(7): 1923-1934.

Ferveur, J. F., K. F. Stortkuhl, R. F. Stocker and R. J. Greenspan (1995). "Genetic feminization of brain structures and changed sexual orientation in male Drosophila." Science **267**(5199): 902-905.

Filhol, O. and C. Cochet (2009). "Protein kinase CK2 in health and disease: Cellular functions of protein kinase CK2: a dynamic affair." Cell Mol Life Sci **66**(11-12): 1830-1839.

Foe, V. E. (1989). "Mitotic domains reveal early commitment of cells in Drosophila embryos." Development **107**(1): 1-22.

Friesen, W. J., S. Massenet, S. Paushkin, A. Wyce and G. Dreyfuss (2001). "SMN, the product of the spinal muscular atrophy gene, binds preferentially to dimethylarginine-containing protein targets." Mol Cell **7**(5): 1111-1117.

Gallant, P. (2013). "Myc function in Drosophila." Cold Spring Harb Perspect Med **3**(10): a014324.

Gallaud, E., T. Pham and C. Cabernard (2017). "Drosophila melanogaster Neuroblasts: A Model for Asymmetric Stem Cell Divisions." Results Probl Cell Differ **61**: 183-210.

Gary, J. D. and S. Clarke (1998). "RNA and protein interactions modulated by protein arginine methylation." Prog Nucleic Acid Res Mol Biol **61**: 65-131.

Ghisolfi-Nieto, L., G. Joseph, F. Puvion-Dutilleul, F. Amalric and P. Bouvet (1996). "Nucleolin is a sequence-specific RNA-binding protein: characterization of targets on pre-ribosomal RNA." J Mol Biol **260**(1): 34-53.

Giannakou, M. E. and L. Partridge (2007). "Role of insulin-like signalling in Drosophila lifespan." Trends Biochem Sci **32**(4): 180-188.

Ginisty, H., H. Sicard, B. Roger and P. Bouvet (1999). "Structure and functions of nucleolin." J Cell Sci **112 (Pt 6)**: 761-772.

Goni, R., P. García, S. Foissac (2009). The qPCR data statistical analysis. Integromics White Paper: Integromics SL., pp. 1-9

Gonsalvez, G. B., K. Praveen, A. J. Hicks, L. Tian and A. G. Matera (2008). "Sm protein methylation is dispensable for snRNP assembly in Drosophila melanogaster." RNA **14**(5): 878-887.

Gonzalez, F., S. Romani, P. Cubas, J. Modolell and S. Campuzano (1989). "Molecular analysis of the asense gene, a member of the achaete-scute complex of Drosophila melanogaster, and its novel role in optic lobe development." EMBO J **8**(12): 3553-3562.

Green, P., A. Y. Hartenstein and V. Hartenstein (1993). "The embryonic development of the Drosophila visual system." Cell Tissue Res **273**(3): 583-598.

Grewal, S. S. (2009). "Insulin/TOR signaling in growth and homeostasis: a view from the fly world." Int J Biochem Cell Biol **41**(5): 1006-1010.

Grewal, S. S., J. R. Evans and B. A. Edgar (2007). "Drosophila TIF-IA is required for ribosome synthesis and cell growth and is regulated by the TOR pathway." J Cell Biol **179**(6): 1105-1113.

Grewal, S. S., L. Li, A. Orian, R. N. Eisenman and B. A. Edgar (2005). "Myc-dependent regulation of ribosomal RNA synthesis during Drosophila development." Nat Cell Biol **7**(3): 295-302.

Grosskortenhaus, R., K. J. Robinson and C. Q. Doe (2006). "Pdm and Castor specify late-born motor neuron identity in the NB7-1 lineage." Genes Dev **20**(18): 2618-2627.

Hakes, A. E., L. Otsuki and A. H. Brand (2018). "A newly discovered neural stem cell population is generated by the optic lobe neuroepithelium during embryogenesis in Drosophila melanogaster." Development **145**(18).

Hall, D. J., S. S. Grewal, A. F. de la Cruz and B. A. Edgar (2007). "Rheb-TOR signaling promotes protein synthesis, but not glucose or amino acid import, in Drosophila." BMC Biol **5**: 10.

Hall, P. A. and F. M. Watt (1989). "Stem cells: the generation and maintenance of cellular diversity." Development **106**(4): 619-633.

Hansen, W. J., V. R. Lingappa and W. J. Welch (1994). "Complex environment of nascent polypeptide chains." J Biol Chem **269**(43): 26610-26613.

Harada, N., T. Takagi, Y. Nakano, R. Yamaji and H. Inui (2015). "Protein arginine methyltransferase 10 is required for androgen-dependent proliferation of LNCaP prostate cancer cells." Biosci Biotechnol Biochem **79**(9): 1430-1437.

Harding, K. and K. White (2018). "Drosophila as a Model for Developmental Biology: Stem Cell-Fate Decisions in the Developing Nervous System." J Dev Biol **6**(4).

Hartenstein, V., E. Rudloff and J. A. Campos-Ortega (1987). "The pattern of proliferation of the neuroblasts in the wild-type embryo of Drosophila melanogaster." Roux Arch Dev Biol **196**(8): 473-485.

Hay, N. and N. Sonenberg (2004). "Upstream and downstream of mTOR." Genes Dev **18**(16): 1926-1945.

Hayashi, Y., T. Kuroda, H. Kishimoto, C. Wang, A. Iwama and K. Kimura (2014). "Downregulation of rRNA transcription triggers cell differentiation." PLoS One **9**(5): e98586.

He, F., A. James, H. Raje, H. Ghaffari and P. DiMario (2015). "Deletion of Drosophila Nopp140 induces subcellular ribosomopathies." Chromosoma **124**(2): 191-208.

Heisenberg, M. (2003). "Mushroom body memoir: from maps to models." Nat Rev Neurosci **4**(4): 266-275.

Heisenberg, M., A. Borst, S. Wagner and D. Byers (1985). "Drosophila mushroom body mutants are deficient in olfactory learning." J Neurogenet **2**(1): 1-30.

Henras, A. K., C. Plisson-Chastang, M. F. O'Donohue, A. Chakraborty and P. E. Gleizes (2015). "An overview of pre-ribosomal RNA processing in eukaryotes." Wiley Interdiscip Rev RNA **6**(2): 225-242.

Hirata, J., H. Nakagoshi, Y. Nabeshima and F. Matsuzaki (1995). "Asymmetric segregation of the homeodomain protein Prospero during Drosophila development." Nature **377**(6550): 627-630.

Homem, C. C. and J. A. Knoblich (2012). "Drosophila neuroblasts: a model for stem cell biology." Development **139**(23): 4297-4310.

Hovhanyan, A., E. K. Herter, J. Pfannstiel, P. Gallant and T. Raabe (2014). "Drosophila mbm is a nucleolar myc and casein kinase 2 target required for ribosome biogenesis and cell growth of central brain neuroblasts." Mol Cell Biol **34**(10): 1878-1891.

Ito, K. and Y. Hotta (1992). "Proliferation pattern of postembryonic neuroblasts in the brain of Drosophila melanogaster." Dev Biol **149**(1): 134-148.

Ito, K., K. Suzuki, P. Estes, M. Ramaswami, D. Yamamoto and N. J. Strausfeld (1998). "The organization of extrinsic neurons and their implications in the functional roles of the mushroom bodies in Drosophila melanogaster Meigen." Learn Mem **5**(1-2): 52-77.

Izergina, N., J. Balmer, B. Bello and H. Reichert (2009). "Postembryonic development of transit amplifying neuroblast lineages in the Drosophila brain." Neural Dev **4**: 44.

Jahan, S. and J. R. Davie (2015). "Protein arginine methyltransferases (PRMTs): role in chromatin organization." Adv Biol Regul **57**: 173-184.

Jefferis, G. S., E. C. Marin, R. J. Watts and L. Luo (2002). "Development of neuronal connectivity in Drosophila antennal lobes and mushroom bodies." Curr Opin Neurobiol **12**(1): 80-86.

Jimenez, F. and J. A. Campos-Ortega (1990). "Defective neuroblast commitment in mutants of the achaete-scute complex and adjacent genes of D. melanogaster." Neuron **5**(1): 81-89.

Kambadur, R., K. Koizumi, C. Stivers, J. Nagle, S. J. Poole and W. F. Odenwald (1998). "Regulation of POU genes by castor and hunchback establishes layered compartments in the Drosophila CNS." Genes Dev **12**(2): 246-260.

Kanai, M. I., M. J. Kim, T. Akiyama, M. Takemura, K. Wharton, M. B. O'Connor and H. Nakato (2018). "Regulation of neuroblast proliferation by surface glia in the Drosophila larval brain." Sci Rep **8**(1): 3730.

Karcavich, R. and C. Q. Doe (2005). "Drosophila neuroblast 7-3 cell lineage: a model system for studying programmed cell death, Notch/Numb signaling, and sequential specification of ganglion mother cell identity." J Comp Neurol **481**(3): 240-251.

Kazyken, D., Y. Kaz, V. Kiyan, A. A. Zhylkibayev, C. H. Chen, N. K. Agarwal and D. Sarbassov dos (2014). "The nuclear import of ribosomal proteins is regulated by mTOR." Oncotarget **5**(20): 9577-9593.

Khajuria, R. K., M. Munschauer, J. C. Ulirsch, C. Fiorini, L. S. Ludwig, S. K. McFarland, N. J. Abdulhay, H. Specht, H. Keshishian, D. R. Mani, M. Jovanovic, S. R. Ellis, C. P. Fulco, J. M. Engreitz, S. Schutz, J. Lian, K. W. Gripp, O. K. Weinberg, G. S. Pinkus, L. Gehrke, A. Regev, E. S. Lander, H. T. Gazda, W. Y. Lee, V. G. Panse, S. A. Carr and V. G. Sankaran (2018). "Ribosome Levels Selectively Regulate Translation and Lineage Commitment in Human Hematopoiesis." Cell **173**(1): 90-103 e119.

Khalaileh, A., A. Dreazen, A. Khatib, R. Apel, A. Swisa, N. Kidess-Bassir, A. Maitra, O. Meyuhas, Y. Dor and G. Zamir (2013). "Phosphorylation of ribosomal protein S6 attenuates DNA damage and tumor suppression during development of pancreatic cancer." Cancer Res **73**(6): 1811-1820.

Kiledjian, M. and G. Dreyfuss (1992). "Primary structure and binding activity of the hnRNP U protein: binding RNA through RGG box." EMBO J **11**(7): 2655-2664.

Kim, Y. K., S. Kim, Y. J. Shin, Y. S. Hur, W. Y. Kim, M. S. Lee, C. I. Cheon and D. P. Verma (2014). "Ribosomal protein S6, a target of rapamycin, is involved in the regulation of rRNA genes by possible epigenetic changes in Arabidopsis." J Biol Chem **289**(7): 3901-3912.

Kirino, Y., N. Kim, M. de Planell-Saguer, E. Khandros, S. Chiorean, P. S. Klein, I. Rigoutsos, T. A. Jongens and Z. Mourelatos (2009). "Arginine methylation of Piwi proteins catalysed by dPRMT5 is required for Ago3 and Aub stability." Nat Cell Biol **11**(5): 652-658.

Klinge, S., F. Voigts-Hoffmann, M. Leibundgut and N. Ban (2012). "Atomic structures of the eukaryotic ribosome." Trends Biochem Sci **37**(5): 189-198.

Klinge, S. and J. L. Woolford, Jr. (2019). "Ribosome assembly coming into focus." Nat Rev Mol Cell Biol **20**(2): 116-131.

Knibiehler, B., C. Mirre and R. Rosset (1982). "Nucleolar organizer structure and activity in a nucleolus without fibrillar centres: the nucleolus in an established Drosophila cell line." J Cell Sci **57**: 351-364.

Knoblich, J. A. (2008). "Mechanisms of asymmetric stem cell division." Cell **132**(4): 583-597.

Kohler R.E., Lords of the Fly: Drosophila Genetics and the Experimental Life. University of Chicago Press; Chicago, IL, USA: 1994. p. xv.321p

Krause, C. D., Z. H. Yang, Y. S. Kim, J. H. Lee, J. R. Cook and S. Pestka (2007). "Protein arginine methyltransferases: evolution and assessment of their pharmacological and therapeutic potential." Pharmacol Ther **113**(1): 50-87.

Kusakawa, T., T. Shimakami, S. Kaneko, K. Yoshioka and S. Murakami (2007). "Functional interaction of hepatitis C Virus NS5B with Nucleolin GAR domain." J Biochem **141**(6): 917-927.

Laemmli, U. K. (1970). "Cleavage of structural proteins during the assembly of the head of bacteriophage T4." Nature **227**(5259): 680-685.

Lai, S. L. and C. Q. Doe (2014). "Transient nuclear Prospero induces neural progenitor quiescence." Elife **3**.

Lambertsson, A. (1998). "The minute genes in Drosophila and their molecular functions." Adv Genet **38**: 69-134.

Le Borgne, R., A. Bardin and F. Schweisguth (2005). "The roles of receptor and ligand endocytosis in regulating Notch signaling." Development **132**(8): 1751-1762.

Le Bouteiller, M., C. Souilhol, S. Beck-Cormier, A. Stedman, O. Burlen-Defranoux, S. Vandormael-Pournin, F. Bernex, A. Cumano and M. Cohen-Tannoudji (2013). "Notchless-dependent ribosome synthesis is required for the maintenance of adult hematopoietic stem cells." J Exp Med **210**(11): 2351-2369.

Lee, C. Y., R. O. Andersen, C. Cabernard, L. Manning, K. D. Tran, M. J. Lanskey, A. Bashirullah and C. Q. Doe (2006a). "Drosophila Aurora-A kinase inhibits neuroblast self-renewal by regulating aPKC/Numb cortical polarity and spindle orientation." Genes Dev **20**(24): 3464-3474.

Lee, C. Y., B. D. Wilkinson, S. E. Siegrist, R. P. Wharton and C. Q. Doe (2006b). "Brat is a Miranda cargo protein that promotes neuronal differentiation and inhibits neuroblast self-renewal." Dev Cell **10**(4): 441-449.

Lee, J. H., J. R. Cook, Z. H. Yang, O. Mirochnitchenko, S. I. Gunderson, A. M. Felix, N. Herth, R. Hoffmann and S. Pestka (2005). "PRMT7, a new protein arginine methyltransferase that synthesizes symmetric dimethylarginine." J Biol Chem **280**(5): 3656-3664.

Lee, T., A. Lee and L. Luo (1999). "Development of the Drosophila mushroom bodies: sequential generation of three distinct types of neurons from a neuroblast." Development **126**(18): 4065-4076.

Li, L., B. A. Edgar and S. S. Grewal (2010). "Nutritional control of gene expression in Drosophila larvae via TOR, Myc and a novel cis-regulatory element." BMC Cell Biol **11**: 7.

Li, X., Y. Xie and S. Zhu (2016). "Notch maintains Drosophila type II neuroblasts by suppressing expression of the Fez transcription factor Earmuff." Development **143**(14): 2511-2521.

Lischwe, M. A., R. G. Cook, Y. S. Ahn, L. C. Yeoman and H. Busch (1985). "Clustering of glycine and NG,NG-dimethylarginine in nucleolar protein C23." Biochemistry **24**(22): 6025-6028.

Livak, K. J. and T. D. Schmittgen (2001). "Analysis of relative gene expression data using real-time quantitative PCR and the 2(-Delta Delta C(T)) Method." Methods **25**(4): 402-408.

Long, E. O. and I. B. Dawid (1980). "Alternative pathways in the processing of ribosomal RNA precursor in Drosophila melanogaster." J Mol Biol **138**(4): 873-878.

Louvet, E., H. R. Junera, I. Berthuy and D. Hernandez-Verdun (2006). "Compartmentation of the nucleolar processing proteins in the granular component is a CK2-driven process." Mol Biol Cell **17**(6): 2537-2546.

Martin-Bermudo, M. D., C. Martinez, A. Rodriguez and F. Jimenez (1991). "Distribution and function of the lethal of scute gene product during early neurogenesis in Drosophila." Development **113**(2): 445-454.

Marygold, S. J., J. Roote, G. Reuter, A. Lambertsson, M. Ashburner, G. H. Millburn, P. M. Harrison, Z. Yu, N. Kenmochi, T. C. Kaufman, S. J. Leevers and K. R. Cook (2007). "The ribosomal protein genes and Minute loci of Drosophila melanogaster." Genome Biol **8**(10): R216.

Maurange, C., L. Cheng and A. P. Gould (2008). "Temporal transcription factors and their targets schedule the end of neural proliferation in Drosophila." Cell **133**(5): 891-902.

McBride, A. E. and P. A. Silver (2001). "State of the arg: protein methylation at arginine comes of age." Cell **106**(1): 5-8.

Mills, E. W. and R. Green (2017). "Ribosomopathies: There's strength in numbers." Science **358**(6363).

Miron, M., J. Verdu, P. E. Lachance, M. J. Birnbaum, P. F. Lasko and N. Sonenberg (2001). "The translational inhibitor 4E-BP is an effector of PI(3)K/Akt signalling and cell growth in Drosophila." Nat Cell Biol **3**(6): 596-601.

Montagne, J., M. J. Stewart, H. Stocker, E. Hafen, S. C. Kozma and G. Thomas (1999). "Drosophila S6 kinase: a regulator of cell size." Science **285**(5436): 2126-2129.

Mora, N., C. Oliva, M. Fiers, R. Ejsmont, A. Soldano, T. T. Zhang, J. Yan, A. Claeys, N. De Geest and B. A. Hassan (2018). "A Temporal Transcriptional Switch Governs Stem Cell Division, Neuronal Numbers, and Maintenance of Differentiation." Dev Cell **45**(1): 53-66 e55.

Morrison, S. J., N. M. Shah and D. J. Anderson (1997). "Regulatory mechanisms in stem cell biology." Cell **88**(3): 287-298.

Nakano, K. and H. Hara (1979). "Measurement of the protein-synthetic activity in vivo of various tissues in rats by using [3H]Puromycin." Biochem J **184**(3): 663-668.

Nathans, D. (1964). "Puromycin Inhibition of Protein Synthesis: Incorporation of Puromycin into Peptide Chains." Proc Natl Acad Sci U S A **51**: 585-592.

Negi, S. S. and M. O. Olson (2006). "Effects of interphase and mitotic phosphorylation on the mobility and location of nucleolar protein B23." J Cell Sci **119**(Pt 17): 3676-3685.

Nichols, R. C., X. W. Wang, J. Tang, B. J. Hamilton, F. A. High, H. R. Herschman and W. F. Rigby (2000). "The RGG domain in hnRNP A2 affects subcellular localization." Exp Cell Res **256**(2): 522-532.

Nygard, O. and H. Nika (1982). "Identification by RNA-protein cross-linking of ribosomal proteins located at the interface between the small and the large subunits of mammalian ribosomes." EMBO J **1**(3): 357-362.

Nygard, O. and L. Nilsson (1990). "Translational dynamics. Interactions between the translational factors, tRNA and ribosomes during eukaryotic protein synthesis." Eur J Biochem **191**(1): 1-17.

O'Dell, K. M., J. D. Armstrong, M. Y. Yang and K. Kaiser (1995). "Functional dissection of the Drosophila mushroom bodies by selective feminization of genetically defined subcompartments." Neuron **15**(1): 55-61.

Oh, S. W., T. Kingsley, H. H. Shin, Z. Zheng, H. W. Chen, X. Chen, H. Wang, P. Ruan, M. Moody and S. X. Hou (2003). "A P-element insertion screen identified mutations in 455 novel essential genes in Drosophila." Genetics **163**(1): 195-201.

Ohshiro, T., T. Yagami, C. Zhang and F. Matsuzaki (2000). "Role of cortical tumour-suppressor proteins in asymmetric division of Drosophila neuroblast." Nature **408**(6812): 593-596.

Oldham, S. and E. Hafen (2003). "Insulin/IGF and target of rapamycin signaling: a TOR de force in growth control." Trends Cell Biol **13**(2): 79-85.

Otsuki, L. and A. H. Brand (2018). "Cell cycle heterogeneity directs the timing of neural stem cell activation from quiescence." Science **360**(6384): 99-102.

Parisi, F., S. Riccardo, M. Daniel, M. Saqcena, N. Kundu, A. Pession, D. Grifoni, H. Stocker, E. Tabak and P. Bellosta (2011). "Drosophila insulin and target of rapamycin (TOR) pathways regulate GSK3 beta activity to control Myc stability and determine Myc expression in vivo." BMC Biol **9**: 65.

Pavlakis, G. N., B. R. Jordan, R. M. Wurst and J. N. Vournakis (1979). "Sequence and secondary structure of Drosophila melanogaster 5.8S and 2S rRNAs and of the processing site between them." Nucleic Acids Res **7**(8): 2213-2238.

Pellar, G. J. and P. J. DiMario (2003). "Deletion and site-specific mutagenesis of nucleolin's carboxy GAR domain." Chromosoma **111**(7): 461-469.

Peng, C. Y., L. Manning, R. Albertson and C. Q. Doe (2000). "The tumour-suppressor genes lgl and dlg regulate basal protein targeting in Drosophila neuroblasts." Nature **408**(6812): 596-600.

Peterson, C., G. E. Carney, B. J. Taylor and K. White (2002). "reaper is required for neuroblast apoptosis during Drosophila development." Development **129**(6): 1467-1476.

Plant, P. J., J. P. Fawcett, D. C. Lin, A. D. Holdorf, K. Binns, S. Kulkarni and T. Pawson (2003). "A polarity complex of mPar-6 and atypical PKC binds, phosphorylates and regulates mammalian Lgl." Nat Cell Biol **5**(4): 301-308.

Potten, C. S. and M. Loeffler (1990). "Stem cells: attributes, cycles, spirals, pitfalls and uncertainties. Lessons for and from the crypt." Development **110**(4): 1001-1020.

Prokop, A. and G. M. Technau (1991). "The origin of postembryonic neuroblasts in the ventral nerve cord of Drosophila melanogaster." Development **111**(1): 79-88.

Raabe, T., S. Clemens-Richter, T. Twardzik, A. Ebert, G. Gramlich and M. Heisenberg (2004). "Identification of mushroom body miniature, a zinc-finger protein implicated in brain development of Drosophila." Proc Natl Acad Sci U S A **101**(39): 14276-14281.

Rebollo, E., P. Sampaio, J. Januschke, S. Llamazares, H. Varmark and C. Gonzalez (2007). "Functionally unequal centrosomes drive spindle orientation in asymmetrically dividing Drosophila neural stem cells." Dev Cell **12**(3): 467-474.

Reichardt, I., F. Bonnay, V. Steinmann, I. Loedige, T. R. Burkard, G. Meister and J. A. Knoblich (2018). "The tumor suppressor Brat controls neuronal stem cell lineages by inhibiting Deadpan and Zelda." EMBO Rep **19**(1): 102-117.

Reichert, H. (2011). "Drosophila neural stem cells: cell cycle control of self-renewal, differentiation, and termination in brain development." Results Probl Cell Differ **53**: 529-546.

Rosby, R., Z. Cui, E. Rogers, M. A. deLivron, V. L. Robinson and P. J. DiMario (2009). "Knockdown of the Drosophila GTPase nucleostemin 1 impairs large ribosomal subunit biogenesis, cell growth, and midgut precursor cell maintenance." Mol Biol Cell **20**(20): 4424-4434.

Ruvinsky, I., N. Sharon, T. Lerer, H. Cohen, M. Stolovich-Rain, T. Nir, Y. Dor, P. Zisman and O. Meyuhas (2005). "Ribosomal protein S6 phosphorylation is a determinant of cell size and glucose homeostasis." Genes Dev **19**(18): 2199-2211.

Schindelin, J., I. Arganda-Carreras, E. Frise, V. Kaynig, M. Longair, T. Pietzsch, S. Preibisch, C. Rueden, S. Saalfeld, B. Schmid, J. Y. Tinevez, D. J. White, V. Hartenstein, K. Eliceiri, P. Tomancak and A. Cardona (2012). "Fiji: an open-source platform for biological-image analysis." Nat Methods **9**(7): 676-682.

Schlosser, I., M. Holzel, M. Murnseer, H. Burtscher, U. H. Weidle and D. Eick (2003). "A role for c-Myc in the regulation of ribosomal RNA processing." Nucleic Acids Res **31**(21): 6148-6156.

Schmidt, E. K., G. Clavarino, M. Ceppi and P. Pierre (2009). "SUnSET, a nonradioactive method to monitor protein synthesis." Nat Methods **6**(4): 275-277.

Schober, M., M. Schaefer and J. A. Knoblich (1999). "Bazooka recruits Inscuteable to orient asymmetric cell divisions in Drosophila neuroblasts." Nature **402**(6761): 548-551.

Schweisguth, F. (2004). "Regulation of notch signaling activity." Curr Biol **14**(3): R129-138.

Selenko, P., R. Sprangers, G. Stier, D. Buhler, U. Fischer and M. Sattler (2001). "SMN tudor domain structure and its interaction with the Sm proteins." Nat Struct Biol **8**(1): 27-31.

Serin, G., G. Joseph, C. Faucher, L. Ghisolfi, G. Bouche, F. Amalric and P. Bouvet (1996). "Localization of nucleolin binding sites on human and mouse pre-ribosomal RNA." Biochimie **78**(6): 530-538.

Shi, Z., K. Fujii, K. M. Kovary, N. R. Genuth, H. L. Rost, M. N. Teruel and M. Barna (2017). "Heterogeneous Ribosomes Preferentially Translate Distinct Subpools of mRNAs Genome-wide." Mol Cell **67**(1): 71-83 e77.

Siegrist, S. E. and C. Q. Doe (2005). "Microtubule-induced Pins/Galphai cortical polarity in Drosophila neuroblasts." Cell **123**(7): 1323-1335.

Siegrist, S. E. and C. Q. Doe (2006). "Extrinsic cues orient the cell division axis in Drosophila embryonic neuroblasts." Development **133**(3): 529-536.

Siegrist, S. E., N. S. Haque, C. H. Chen, B. A. Hay and I. K. Hariharan (2010). "Inactivation of both Foxo and reaper promotes long-term adult neurogenesis in Drosophila." Curr Biol **20**(7): 643-648.

Skeath, J. B. and S. B. Carroll (1991). "Regulation of achaete-scute gene expression and sensory organ pattern formation in the Drosophila wing." Genes Dev **5**(6): 984-995.

Skeath, J. B. and S. B. Carroll (1992). "Regulation of proneural gene expression and cell fate during neuroblast segregation in the Drosophila embryo." Development **114**(4): 939-946.

Skeath, J. B. and S. Thor (2003). "Genetic control of Drosophila nerve cord development." Curr Opin Neurobiol **13**(1): 8-15.

Son, O., S. Kim, Y. J. Shin, W. Y. Kim, H. J. Koh and C. I. Cheon (2015). "Identification of nucleosome assembly protein 1 (NAP1) as an interacting partner of plant ribosomal protein S6 (RPS6) and a positive regulator of rDNA transcription." Biochem Biophys Res Commun **465**(2): 200-205.

Sousa-Nunes, R., L. L. Yee and A. P. Gould (2011). "Fat cells reactivate quiescent neuroblasts via TOR and glial insulin relays in Drosophila." Nature **471**(7339): 508-512.

Southall, T. D. and A. H. Brand (2009). "Neural stem cell transcriptional networks highlight genes essential for nervous system development." EMBO J **28**(24): 3799-3807.

Spana, E. P., C. Kopczynski, C. S. Goodman and C. Q. Doe (1995). "Asymmetric localization of numb autonomously determines sibling neuron identity in the Drosophila CNS." Development **121**(11): 3489-3494.

St-Denis, N. A. and D. W. Litchfield (2009). "Protein kinase CK2 in health and disease: From birth to death: the role of protein kinase CK2 in the regulation of cell proliferation and survival." Cell Mol Life Sci **66**(11-12): 1817-1829.

Stenmark, H., R. Aasland, B. H. Toh and A. D'Arrigo (1996). "Endosomal localization of the autoantigen EEA1 is mediated by a zinc-binding FYVE finger." J Biol Chem **271**(39): 24048-24054.

Szebeni, A., K. Hingorani, S. Negi and M. O. Olson (2003). "Role of protein kinase CK2 phosphorylation in the molecular chaperone activity of nucleolar protein b23." J Biol Chem **278**(11): 9107-9115.

Tadros, W. and H. D. Lipshitz (2009). "The maternal-to-zygotic transition: a play in two acts." Development **136**(18): 3033-3042.

Tan, Y., M. Yamada-Mabuchi, R. Arya, S. St Pierre, W. Tang, M. Tosa, C. Brachmann and K. White (2011). "Coordinated expression of cell death genes regulates neuroblast apoptosis." Development **138**(11): 2197-2206.

Tang, W., W. You, F. Shi, T. Qi, L. Wang, Z. Djouder, W. Liu and X. Zeng (2009). "RNA helicase A acts as a bridging factor linking nuclear beta-actin with RNA polymerase II." Biochem J **420**(3): 421-428.

Technau, G. and M. Heisenberg (1982). "Neural reorganization during metamorphosis of the corpora pedunculata in Drosophila melanogaster." Nature **295**(5848): 405-407.

Teleman, A. A., Y. W. Chen and S. M. Cohen (2005). "4E-BP functions as a metabolic brake used under stress conditions but not during normal growth." Genes Dev **19**(16): 1844-1848.

Teleman, A. A., V. Hietakangas, A. C. Sayadian and S. M. Cohen (2008). "Nutritional control of protein biosynthetic capacity by insulin via Myc in Drosophila." Cell Metab **7**(1): 21-32.

Tettweiler, G., M. Miron, M. Jenkins, N. Sonenberg and P. F. Lasko (2005). "Starvation and oxidative stress resistance in Drosophila are mediated through the eIF4E-binding protein, d4E-BP." Genes Dev **19**(16): 1840-1843.

Thandapani, P., T. R. O'Connor, T. L. Bailey and S. Richard (2013). "Defining the RGG/RG motif." Mol Cell **50**(5): 613-623.

Tolwinski, N. S. (2017). "Introduction: Drosophila-A Model System for Developmental Biology." J Dev Biol **5**(3).

Tran, K. D. and C. Q. Doe (2008). "Pdm and Castor close successive temporal identity windows in the NB3-1 lineage." Development **135**(21): 3491-3499.

Truman, J. W. and M. Bate (1988). "Spatial and temporal patterns of neurogenesis in the central nervous system of Drosophila melanogaster." Dev Biol **125**(1): 145-157.

Tschochner, H. and E. Hurt (2003). "Pre-ribosomes on the road from the nucleolus to the cytoplasm." Trends Cell Biol **13**(5): 255-263.

Tsuji, T., E. Hasegawa and T. Isshiki (2008). "Neuroblast entry into quiescence is regulated intrinsically by the combined action of spatial Hox proteins and temporal identity factors." Development **135**(23): 3859-3869.

Urbach, R., R. Schnabel and G. M. Technau (2003). "The pattern of neuroblast formation, mitotic domains and proneural gene expression during early brain development in Drosophila." Development **130**(16): 3589-3606.

Urbach, R. and G. M. Technau (2003). "Molecular markers for identified neuroblasts in the developing brain of Drosophila." Development **130**(16): 3621-3637.

Urbach, R. and G. M. Technau (2003). "Segment polarity and DV patterning gene expression reveals segmental organization of the Drosophila brain." Development **130**(16): 3607-3620.

Urbach, R. and G. M. Technau (2004). "Neuroblast formation and patterning during early brain development in Drosophila." Bioessays **26**(7): 739-751.

Villares, R. and C. V. Cabrera (1987). "The achaete-scute gene complex of D. melanogaster: conserved domains in a subset of genes required for neurogenesis and their homology to myc." Cell **50**(3): 415-424.

Voigt, A., R. Pflanz, U. Schafer and H. Jackle (2002). "Perlecan participates in proliferation activation of quiescent Drosophila neuroblasts." Dev Dyn **224**(4): 403-412.

Wallace, K., T. H. Liu and H. Vaessin (2000). "The pan-neural bHLH proteins DEADPAN and ASENSE regulate mitotic activity and cdk inhibitor dacapo expression in the Drosophila larval optic lobes." Genesis **26**(1): 77-85.

Walsh, K. T. and C. Q. Doe (2017). "Drosophila embryonic type II neuroblasts: origin, temporal patterning, and contribution to the adult central complex." Development **144**(24): 4552-4562.

Wang, B., J. Goode, J. Best, J. Meltzer, P. E. Schilman, J. Chen, D. Garza, J. B. Thomas and M. Montminy (2008). "The insulin-regulated CREB coactivator TORC promotes stress resistance in Drosophila." Cell Metab **7**(5): 434-444.

Wang, H., Y. Ouyang, W. G. Somers, W. Chia and B. Lu (2007). "Polo inhibits progenitor self-renewal and regulates Numb asymmetry by phosphorylating Pon." Nature **449**(7158): 96-100.

Wang, H., G. W. Somers, A. Bashirullah, U. Heberlein, F. Yu and W. Chia (2006). "Aurora-A acts as a tumor suppressor and regulates self-renewal of Drosophila neuroblasts." Genes Dev **20**(24): 3453-3463.

Wei, H. M., H. H. Hu, G. Y. Chang, Y. J. Lee, Y. C. Li, H. H. Chang and C. Li (2014). "Arginine methylation of the cellular nucleic acid binding protein does not affect its subcellular localization but impedes RNA binding." FEBS Lett **588**(9): 1542-1548.

Weng, M., K. L. Golden and C. Y. Lee (2010). "dFezf/Earmuff maintains the restricted developmental potential of intermediate neural progenitors in Drosophila." Dev Cell **18**(1): 126-135.

White, K., M. E. Grether, J. M. Abrams, L. Young, K. Farrell and H. Steller (1994). "Genetic control of programmed cell death in Drosophila." Science **264**(5159): 677-683.

Wodarz, A., A. Ramrath, U. Kuchinke and E. Knust (1999). "Bazooka provides an apical cue for Inscuteable localization in Drosophila neuroblasts." Nature **402**(6761): 544-547.

Xue, S. and M. Barna (2012). "Specialized ribosomes: a new frontier in gene regulation and organismal biology." Nat Rev Mol Cell Biol **13**(6): 355-369.

Yamanaka, T., Y. Horikoshi, Y. Sugiyama, C. Ishiyama, A. Suzuki, T. Hirose, A. Iwamatsu, A. Shinohara and S. Ohno (2003). "Mammalian Lgl forms a protein complex with PAR-6 and aPKC independently of PAR-3 to regulate epithelial cell polarity." Curr Biol **13**(9): 734-743.

Yang, M., W. S. May and T. Ito (1999). "JAZ requires the double-stranded RNA-binding zinc finger motifs for nuclear localization." J Biol Chem **274**(39): 27399-27406.

Yang, Y., A. Hadjikyriacou, Z. Xia, S. Gayatri, D. Kim, C. Zurita-Lopez, R. Kelly, A. Guo, W. Li, S. G. Clarke and M. T. Bedford (2015). "PRMT9 is a type II methyltransferase that methylates the splicing factor SAP145." Nat Commun **6**: 6428.

Yasugi, T., D. Umetsu, S. Murakami, M. Sato and T. Tabata (2008). "Drosophila optic lobe neuroblasts triggered by a wave of proneural gene expression that is negatively regulated by JAK/STAT." Development **135**(8): 1471-1480.

Yoshiura, S., N. Ohta and F. Matsuzaki (2012). "Tre1 GPCR signaling orients stem cell divisions in the Drosophila central nervous system." Dev Cell **22**(1): 79-91.

Yu, F. and O. Schuldiner (2014). "Axon and dendrite pruning in Drosophila." Curr Opin Neurobiol **27**: 192-198.

Yu, M. C., F. Bachand, A. E. McBride, S. Komili, J. M. Casolari and P. A. Silver (2004). "Arginine methyltransferase affects interactions and recruitment of mRNA processing and export factors." Genes Dev **18**(16): 2024-2035.

Yusupova, G. and M. Yusupov (2014). "High-resolution structure of the eukaryotic 80S ribosome." <u>Annu Rev Biochem</u> **83**: 467-486.

Zars, T., M. Fischer, R. Schulz and M. Heisenberg (2000). "Localization of a short-term memory in Drosophila." <u>Science</u> **288**(5466): 672-675.

Zhang, Q., N. A. Shalaby and M. Buszczak (2014). "Changes in rRNA transcription influence proliferation and cell fate within a stem cell lineage." <u>Science</u> **343**(6168): 298-301.

Zhou, X., W. J. Liao, J. M. Liao, P. Liao and H. Lu (2015). "Ribosomal proteins: functions beyond the ribosome." <u>J Mol Cell Biol</u> **7**(2): 92-104.

Zhu, S., S. Barshow, J. Wildonger, L. Y. Jan and Y. N. Jan (2011). "Ets transcription factor Pointed promotes the generation of intermediate neural progenitors in Drosophila larval brains." <u>Proc Natl Acad Sci U S A</u> **108**(51): 20615-20620.

Zurita-Lopez, C. I., T. Sandberg, R. Kelly and S. G. Clarke (2012). "Human protein arginine methyltransferase 7 (PRMT7) is a type III enzyme forming omega-NG-monomethylated arginine residues." <u>J Biol Chem</u> **287**(11): 7859-7870.

10. Figures

11. Tables

Acknowledgments

Working on my Ph.D. thesis was a challenging experience and I would not have been successful without the support of several people to whom I would like to express my gratitude.

First and foremost, I want to thank my supervisor Prof. Dr. Thomas Raabe for giving me the opportunity to work in his lab and for all the support and good advice he gave me over the last couple of years. Thomas, working in your lab was a pleasure. Thank you!

Furthermore, I would like to thank Prof. Dr. Peter Gallant and Prof. Dr. Charlotte Förster for being my second and third supervisor and for the advice and helpful suggestions they provided me with.

I'm also very grateful to the other (former) members of our group, Dr. Stephanie Pütz, Dr. Anna Hovhanyan, Dr. Katherina Beck and Samantha Kretzler. And I would like to include Barbara Leibbrandt here, the former lab technician of our neighboring group in the old MSZ. They were always very supportive and helpful and made our lab a pleasant environment to work in.

Moreover, I would like to thank all members of the Department of Neurobiology and Genetics, who welcomed us warmly when we moved into our new lab in their direct neighborhood and had to use some of their infrastructure. A special thanks to the lab technicians and Sylwia Febecolon, who were always very helpful when I urgently needed something.

I would also like to thank my very good friend Dr. Sarah Keppler, who oftentimes supported me with suggestions and good advice and of course for just being there as a friend.

Last but not least, I want to say a huge THANK YOU to my parents. Since they do not speak English, I would like to say the last couple of words in German:

Mama, Paps, ich bin euch unendlich dankbar für die Unterstützung, die ihr mir all die Jahre habt zukommen lassen, ohne die vor allem mein Studium, aber somit letztlich auch meine Promotion nicht möglich gewesen wäre. Vielen, vielen Dank!

Abbreviations

&	and	dILP2/6	insulin-like peptides 2/6
~	approximately	Dlg1	Disc Large1
%	percent	DMSO	dimethyl sulfoxide
°C	degrees Celsius	DNA	deoxyribonucleic acid
ac/sc	*achaete-scute*	dNTP	deoxynucleotide triphosphate
AdOx	adenosine dialdehyde		
ALH	after larval hatching	Dpn	Deadpan
aPKC	atypical protein kinase C	DTT	dithiothreitol
Ase	Asense	*E. coli*	*Escherichia coli*
Baz	Bazooka	EDTA	ethylenediaminetetraacetic acid
C	cysteine		
Cas	Castor	EGF	epidermal growth factor
Cat. No.	catalogue number	Erm	Earmuff
CB	central brain	ETS	external transcribed spacer
CFD	cell fate determinants	FBS	fetal bovine serum
CLSM	confocal laser-scanning microscopy	FC	fibrillar center
CNS	central nervous system	fwd	forward
bp	base pairs	g	gram
BSA	bovine serum albumin	G	glycine
cDNA	complementary deoxyribonucleic acid	GC	granular component
		gDNA	genomic deoxyribonucleic acid
cm	centimeter(s)		
DART	*Drosophila* arginine methyltransferase	GMC	ganglion mother cell
DFC	dense fibrillar component	Grh	Grainyhead

h	hour(s)	mM	millimolar
Hb	Hunchback	µM	micromolar
hnRNP	heterogenous nuclear ribonucleoprotein	NaCl	sodium chloride
		$NaIO_4$	sodium periodate
IF	immunofluorescence	NB	neuroblast
INP	intermediate neural progenitor	NGS	normal goat serum
Insc	Inscutable	nm	nanometer
IP	immunoprecipitation	OD_{600}	optical density at a wavelength of 600 nm
ITS	internal transcribed spacer	OL	optic lobe
kb	kilobases	P	proline
KOAc	potassium acetate	PBS	phosphate buffered saline
Kr	Krüppel	PCR	polymerase chain reaction
LB^{Carb}	LB medium containing 100 µg/ml carbenicillin	Pins	Partner of Inscuteable
		PntP1	Pointed
LD	light dark cycle	Pol.	polymerase
Lgl	Lethal (2) of giant larvae	PRF	pre-ribosomal factor
MB	mushroom body	PRMT	protein arginine methyl transferase
MBNB	mushroom body neuroblasts		
Mbm	Mushroom body miniature	PSU	power supply unit
MeOH	methanol	R	arginine
mg	milligram	RBF	ribosome biogenesis factor
$MgCl_2$	magnesium chloride	rDNA	ribosomal deoxyribonucleic acid
$MgSO_4$	magnesium sulfate		
min	minute(s)	rev	reverse
Mir	Miranda	RNA	ribonucleic acid
µJ	microjoule	RP	ribosomal protein
µl	microliter(s)	RpL11	ribosomal protein L11
ml	milliliter	rpm	rounds per minute

RpS6	ribosomal protein S6
rRNA	ribosomal ribonucleic acid
RT	room temperature
S	serine
S6K	S6 kinase
SDS	sodium dodecyl sulfate
SFM	serum-free medium
SLIM	site-directed, ligase-independent mutagenesis
snoRNP	small nucleolar ribonucleoprotein
TBS	tris buffered saline
TBS-T	TBS with 0.1 % Tween® 20
TEMED	tetramethylethylenediamine
TOR	target of rapamycin
tris	tris(hydroxymethyl)-aminomethane
VNC	ventral nerve cord
WB	western blot
WT	wild-type
Y	tyrosine
ZnF	zinc-finger(s)